Journal of Climate

Atmospheric Response to a Collapse of the North Atlantic Circulation Under A Mid-Range Future Climate Scenario: A Regime Shift in Northern Hemisphere Dynamics

--Manuscript Draft--

Manuscript Number:	JCLI-D-22-0841
Full Title:	Atmospheric Response to a Collapse of the North Atlantic Circulation Under A Mid-Range Future Climate Scenario: A Regime Shift in Northern Hemisphere Dynamics
Article Type:	Article
Corresponding Author:	Clara Orbe, Ph.D NASA Goddard Institute for Space Studies Brooklyn, NY UNITED STATES
Corresponding Author's Institution:	NASA Goddard Institute for Space Studies
First Author:	Clara Orbe, Ph.D
Order of Authors:	Clara Orbe, Ph.D
	David Rind
	Ron Miller
	Larissa Nazarenko
	Anastasia Romanou
	Jeff Jonas
	Gary Russell
	Maxwell Kelley
	Gavin Schmidt
Abstract:	Climate models project a future weakening of the Atlantic Meridional Overturning Circulation (AMOC), but the impacts of this weakening on climate remain highly uncertain. A key challenge in quantifying the impact of an AMOC decline is in isolating its impact, relative to other changes related to increased greenhouse gases. Here we isolate the climate impacts of a weakened AMOC in the broader context of a warming climate using a unique ensemble of SSP 2-4.5 integrations that was performed using the CMIP6 version of the NASA Goddard Institute for Space Studies ModelE (E2.1). In these runs internal variability alone results in a spontaneous bifurcation of the ocean flow, wherein two out of ten ensemble members exhibit an entire AMOC collapse, while the other eight recover at various stages despite identical forcing of each ensemble member. We show that an AMOC collapse results in an abrupt northward shift and strengthening of the Northern Hemisphere (NH) Hadley Cell and intensification of the northern midlatitude jet. We then use a set of coupled atmosphere-ocean abrupt CO2 experiments spanning 1-8xCO2 to show that this response to an AMOC collapse results in a nonlinear shift in the NH circulation moving from 2- to 3xCO2. Slab-ocean versions of these experiments, by comparison, do not capture this nonlinear behavior. Our results suggest that changes in ocean heat flux convergences associated with an AMOC collapse can result in profound changes in the NH circulation and continued efforts to constrain the AMOC response to future climate change are needed.

National Aeronautics and Space Administration
Goddard Space Flight Center
Goddard Institute for Space Studies
2880 Broadway
New York, NY 10025

March 27, 2023

Dr. Stephen Yeager
Editor, Journal of Climate

Dear Dr. Yeager:

Thank you very much for your evaluation of the reviewers' assessments. We have modified the manuscript significantly after consideration of this feedback. A copy of the revised version of the manuscript indicating all changes in red text has also been included as reference material (the JCLI-D-22-0841_revision1_redchanges.pdf attachment) in order to assist the review process.

First, following your recommendation, along with that from Reviewer 3, we have recast all figures in terms of differences between the "collapsed" versus "recovered" SSP 2-4.5 ensemble members, rather than in terms of anomalies relative to the preindustrial control simulation. We hope that this makes the impacts of a weakened AMOC more transparent. Second, we also followed the recommendation of Reviewer 3 to first present the SSP 2-4.5 results, followed by the comparison with the $2xCO_2$ and $3xCO_2$ simulations, as reflected in the reorganization of Sections 3a1-3. Third, following the recommendation from both Reviewers 1 and 3 we now show the results from the full ten-member SSP 2-4.5 ensemble, as reflected in all (new) figures. As a result, the SSP 2-4.5 findings are now presented in terms of differences between the 8 "recovered" simulations and the 2 "collapsed" simulations, after year 2400. We believe that the incorporation of the full 10-member ensemble strongly supports the conclusions that were drawn in the previous version of the manuscript (which only featured two ensemble members), but now captures the statistical significance of these changes, supporting the robustness of our main findings. Fourth, we agree with all reviewers that the original manuscript was simply too long. To this end, we also agree with you and Reviewer 3 that the section describing the zonally varying response was the weakest part of the original manuscript and we have removed that entire section, only retaining now a passing reference to the zonally varying eddy kinetic energy responses, now shown in (new) Figure 5.

Overall, we feel that we have addressed all the reviewers concerns through a major reworking of the manuscript and figures, which now focus more on the robustness and implications of our key findings. We hope that the reviewers feel the same and we look forward to receiving their reviews on the revised manuscript.

Finally, we agree that is imperative that we provide the reviewers and you with a copy of the heavily referenced companion study entitled "Stochastic Bifurcation of the North Atlantic Circulation under a mid-range future climate scenario with the NASA-GISS ModelE," led by Dr. Anastasia Romanou (NASA GISS). We have now provided a draft (still under review) as reference material (see "AR2023.pdf").

Kind regards,

Dr. Clara Orbe
Research Physical Scientist
NASA GISS
clara.orbe@nasa.gov

Response to Reviewer 1

This paper quantifies the impact of internal variability in the AMOC response in the 21st century on the Northern Hemisphere (NH) large-scale atmospheric circulation using an ensemble of runs conducted with the same forcing in the same climate model (GISS E2.1). In two out of ten ensemble members, the AMOC collapses, which results in a northward shift and strengthening of the NH Hadley cell and a poleward shift of the NH midlatitude jet. The results are compared to runs with an abrupt quadrupling of CO2 and with slab ocean runs (which, by definition, do not capture this behavior).

Understanding the impact of AMOC collapse on the global atmospheric circulation is very important, and it's great that the authors have been able to isolate this in runs with identical forcing in the same model (which avoids complications of alternative methodologies used in past studies). The caveat is, of course, this is just from one model, but the authors have comprehensively compared their results with those from other studies using different models and methodologies.

I recommend publication after minor revisions. My main complaint about the paper in its present form is that it's too long, probably to its own detriment (as there are many internal inconsistencies within the text, as described below). The paper is comprehensive and well-written, but at times explores idiosyncrasies of the GISS model and the past literature that most readers would not care about and that get in the way of the central message. I would encourage the authors to be more concise and to eliminate text that is not centrally related to the key focus of the paper. Additionally, the analysis Section 3d (point #4 in conclusions) is not as carefully done as in the rest of the paper (see comments below) and could easily be removed or shortened (as many of the zonally asymmetries noted in Section 3d can easily be inferred from Figure 4).

We thank the reviewer for providing this very constructive feedback. We agree with her/him that the manuscript is too long and we have followed her/his recommendation to remove the more speculative material, most notably the entire section discussing the zonally varying responses. We agree that this section was handled with less care and we reserve more detailed examination of those results for future work. These changes have reduced the manuscript length by several pages which, coupled with removal of several of the appendix figures, results in a more concise and targeted story. We hope that the reviewer agrees.

Minor Revisions

Lines 21, 176-180, 688, 997-998: The midlatitude jet shifts, not strengthens. Please correct this to be consistent with the text on Lines 521-528.

As highlighted now in the new version of the manuscript, in which anomalies are now cast as "collapsed-recovered," the midlatitude jet does strengthen over the Atlantic (as it also extends eastward over Europe) while it mainly shifts poleward over the Pacific (new Fig. 3e). Therefore, while one could describe the zonal mean wind response (new Fig. 4b) as a poleward shift, the basin-specific response is more nuanced. We have revised this section in order to explain this structured response more carefully.

Lines 29-31: The direct radiative effects of increasing greenhouse gases can also change the circulation. It's not just modulated through the SSTs, although that is the biggest component. See Deser and Phillips (2009) and Grise and Polvani (2014).

Great point — we realize now that this sentence overlooks the direct radiative response of the circulation (as would be inferred from fixed SST experiments) which we agree with the reviewer can contribute

significantly to the total circulation response. We thank the reviewer for these references, which are now cited.

Lines 115-117: Why examine only one ensemble member for each? If you have multiple ensemble members, averaging over the two (for AMOC collapse) and eight (for non-AMOC collapse) would help to eliminate some of the noise due to internal variability among members. The similarity of ensemble member I to ensemble A for the AMOC collapse is addressed on lines 199-201/442-444, but how representative is ensemble member C of the other seven ensemble members without AMOC collapse? Are the eight ensemble members without AMOC collapse statistically distinguishable from the two with the AMOC collapse?

Another excellent point. We have now redone all analysis and figures contrasting the response among the 8 recovered ensemble members (now referred to more intuitively as SSP 2-4.5 R) and the 2 collapsed ensemble members (SSP 2-4.5 C). As the reviewer will now see, the equilibrated (i.e., year 2400-2500 averaged) responses among the recovered versus collapsed simulations are remarkably consistent, reinforcing the robustness of our conclusions. Note that statistical significance is also now denoted in all plots, where we have accounted for the different ensemble sizes of the recovered and collapsed (sub)ensembles. We thank the reviewer for encouraging us to pursue this analysis.

Lines 157-162, 358-364: These outlines of the paper do not actually correspond with what is shown in the results section in section 3. Please correct.

We apologize for this oversight and have fixed this in the manuscript.

Line 257: Correct citation here is Grise and Polvani (2017).

Thank you. This reference has been changed.

Line 323: I think you mean the largest eddy momentum flux convergence is co-located with the storm track. The largest eddy momentum fluxes are near the Hadley cell edge, as stated above.

Correct — we miswrote. This has been fixed.

Lines 427-430, 512-515, 529-531, 552-555: The sentences on these lines pose conflicting statements in my view. Some argue for a change in SH meridional temperature gradient due to AMOC collapse (i.e., that is more warming at SH high latitudes), and some argue for no change in SH meridional temperature gradient due to AMOC collapse. Please clarify this issue, and make the statements consistent throughout the paper.

We thank the reviewer for pointing out these conflicting statements and we have now taken care to more accurately describe these temperature gradient responses in the revised manuscript. Please note that these earlier sections have been significantly revised.

Lines 465-467: Here is a good example of extraneous information that is included that is tangential to the focus of this study on the atmospheric circulation.

Agreed. This material has been removed.

Line 479: I wouldn't describe this as a poleward shift. It's more of a strengthening of the eastern extension of the jet stream over Europe.

Agreed — we have revised the text to clarify that this is a strengthening and eastward extension of the jet over Europe. Please see the revised text.

Lines 488-494, 814-817: This text can be cut in my opinion. These details are parenthetical in nature and can be examined by the reader in Appendix figures if they so choose. The latter (lines 814-817) is also discussed later in more detail on lines 965-967, so there is no need to mention this twice.

Agreed — we have decided to cut all references to normalization by GMST as this is unnecessarily complicated and distracts from the central messages of the manuscript.

Line 501 (Figure 5): It would be helpful to have a difference figure in the appendix for this figure, as was done for the two previous figures (as in Fig. A2 and A3).

Agreed. At the recommendation of another reviewer, we have now cast all responses in terms of "collapsed-recovered" SSP 2-4.5 and "$3xCO_2$-$2xCO_2$" differences. Please see the new versions of Figures 3-7. We hope that this makes the AMOC "signal" more transparent.

Lines 529-531, 552-555: If anything, you would expect an equatorward jet shift due to a collapsed AMOC, due to the enhanced warming at SH high latitudes compared to the tropics. You can see this to some extent in the right column of Fig. 5b, as the poleward jet shift in the bottom panel is weaker than in the top panel.

Yes — we agree with the reviewer. We have added a brief clause to one of the sentences in this paragraph mentioning this possibility.

Lines 650-653: I question the close relationship between the latitude of max eddy momentum flux convergence (Fig. 7d) and the NH midlatitude dry static stability (Fig. 7e). Note the very different behaviors in the cyan lines in these two panels. The behavior of the static stability (Fig. 7e) much more closely matches that of the Hadley cell edge (Fig. 7a). Also, the latitude of max eddy momentum flux convergence resides in the midlatitudes and co-locates with the midlatitude jet. So, if the authors are interested in the Hadley cell edge, they should examine the latitude of maximum eddy momentum fluxes (not their convergence) as in Chemke and Polvani (2019) and Menzel et al. (2019).

Our apologies — we were completely inaccurate in our description of what we were plotting. Indeed, we *are* examining the latitude of maximum eddy momentum fluxes, not their convergences. We have removed all erroneous references to "momentum flux convergences" in the text.

Line 674, Figure 8c: How is baroclinic eddy kinetic energy generation defined? And, how is it calculated? Please include this methodology in the paper.

Apologies for the oversight — the baroclinic EKE generation term in the model dynamics, which refers to the lifting of heavy air, is $\sim -\alpha'\omega'$, where α is one over the density, and ω is the vertical velocity in pressure coordinates. We have clarified this in the text.

Lines 677-678: What is the proposed causal mechanism underlying Fig. 8? Changes in static stability will impact baroclinic eddies, which are closely related to the location of the Hadley cell edge. But, the Hadley cell edge and Hadley cell strength are not necessarily closely linked to one another (e.g., Menzel et al. 2019).

First, Menzel et al. (2019) did not make a direct statement about the coupling between HC edge and HC strength, but, rather, noted a strong disconnect between subtropical jet (STJ) strength and HC edge. It

seems, therefore, that the reviewer is assuming that HC strength and STJ strength are nearly interchangeable, but Figure 3 from Menzel et al. (2019) highlights that the two quantities are actually not that well correlated, especially during DJF in the NH (correlation 0.21). So, we begin by questioning the premise that the HC strength need necessarily be equated with the STJ strength.

Second, we note that the conclusions about HC strength and width made in that study were based on interannual variability and the response to $4xCO_2$ forcing. For both cases a HC expansion is always associated with a weakening of the HC strength. In response to a weakening of the AMOC, however, HC strength increases (a widely reported result). This strengthening of the Hadley Cell in the NH has often been linked in previous studies to a southward displacement of the ITCZ, which is evident in our figures in the precipitation changes (Fig. 3, Fig. 6) and is also a canonical response to a collapsed AMOC. As we do not wish to reinvent the wheel, we lean on previous studies which have shown that this displacement in the ITCZ and strengthening of the HC are coupled through ocean and atmosphere energy fluxes (note this was the argument presented in Orihuela-Pinto et al. (2022)) so we now note that this compensation is also operative in our model (see tropics region in (new) Figure 11). These ITCZ shifts were not explicitly considered in Menzel et al. (2019) and we suspect that different conclusions about the relationship between HC strength and HC edge changes may be therefore be drawn due to the different forcing scenarios considered in that study.

All of that said, we want to be clear that we are not attributing the Hadley Cell strength increases to the same northern midlatitude eddy changes that are linked to changes in static stability and midlatitude EKE. In this respect we agree with the reviews that our introduction of (new) Figure 10 is misleading and care must be taken to suggest that the HC strength changes are not necessarily mechanistically coupled to the changes in the fields shown in the other panels. It is certainly possible that midlatitude baroclinity changes over the Atlantic could drive a local intensification of the regional Hadley Cell in that region. This idea was proposed in Bradshaw et al. (2019) who used hosing experiments to show that in response to an AMOC collapse there is an enhancement of the NH subtropical jet in the region around 20ºN-30ºN and between 30ºW-10ºW (see their Figure 5). However, as we have removed much of the zonally varying HC analysis from the manuscript, we reserve further examination of that possibility to future work.

To summarize: we suspect that the apparent discrepancy with Menzel et al. (2019) relates to the different SST responses present in the different simulations, specifically in relation to the southward ITCZ shift that we find occurs in response to an AMOC collapse, but which is not necessarily captured in the models examined in Menzel et al. (2019). By now acknowledging that the HC strengthening is more directly related to regional SST anomalies associated with the ITCZ (and not midlatitude eddies) as has been reported in previous studies, we hope that this removes any apparent contradictions with the previous literature.

Brayshaw, David J., Tim Woollings, and Michael Vellinga. "Tropical and extratropical responses of the North Atlantic atmospheric circulation to a sustained weakening of the MOC." *Journal of Climate* 22, no. 11 (2009): 3146-3155.

Line 706: Approximately 1 PW, not exactly 1 PW

Noted. This has been changed.

Lines 756-758: This argument doesn't make sense to me. The top row shows stronger northward (not poleward) latent heat transport in the SH subtropics, but there is also stronger southward dry static energy transport in the same region compared to the bottom row.

We are talking about the fact that there is stronger southward oceanic transport in the SSP 2-4.5 collapsed runs, compared to the $3xCO_2$ run. This reflects differences in the degree of compensating northward latent heat and dry static energy transports, resulting in increased northward MSE in the SSP 2-4.5 collapsed runs, but decreased northward MSE in the $3xCO_2$ run. We hope this clarifies any confusion.

Line 768: What is the expectation from Held and Soden (2006)? This is not discussed elsewhere in the paper that I could find, so please be more specific here.

Yes, it is — see their section 6 and Figure 10 lines discussing the expectation that latent and sensible transports compensate.

Line 772, and hereafter (especially when describing Fig. 11): The manuscript uses the acronym DSE to refer to both dry static energy and dry static energy transport. When referring to transport, please say DSE transport to distinguish.

Thanks for the comment — we have fixed throughout. Note also that we have now removed (old) Figure 11 to help trim down the manuscript.

Line 778: Do you mean lower latitudes here? The poleward extent of the dry static energy changes in Fig. 10 is 40° latitude.

We have removed this section.

Line 820: How are the local Hadley circulations calculated? I didn't see this described anywhere. To do this correctly, you need to use the method of Schwendike et al. (2014), which uses the meridional component of the divergent wind (see also Staten et al. 2019). Otherwise, if the total meridional wind is used, rotational wind features can complicate the interpretation of the results (see Karnauskas and Ummenhofer 2014).

We agree. Note that we have now removed this section.

Line 824: Figure 12a is presumably reproduced from Fig. 5d, but the color scale must be changed. Yet, the color bar is identical in the two figures. Please reconcile.

Note that we have now removed this section.

Lines 824-827: The strengthening of the streamfunction above 200 hPa is the signature of the tropopause rising and the Hadley cell expanding upward in a warming climate.

We agree. Note that we have now removed this section.

Lines 830-832: The west Pacific (Fig. 12d) looks more like the zonal mean (Fig. 12a) than the east Pacific (Fig. 12c).

Note that we have now removed this section.

Lines 832-833: I don't follow the logic here. There are a number of theories for what governs Hadley cell strength (not just meridional SST gradients) (see Chemke and Polvani 2021), and it's unclear whether these same arguments would apply to the local Hadley circulation defined over a narrow longitude band. Furthermore, the meridional SST gradient also increases in the Atlantic, and the local Hadley cell does not strengthen there.

Note that we have now removed this section.

Lines 852-854: I don't follow the logic here, either. The Walker circulation should primarily affect vertical motion on the Equator, not at 20˚-30˚ latitude. Yet, the dominant differences seen in Figs. 12c-d are not on the Equator.

Note that we have now removed this section.

Lines 856-858: This might be a situation where the answer may depend on whether or not you normalize by the global-mean surface temperature change. This was already discussed above for the precipitation response in this region (lines 489-491).

We agree. Note that we have now removed this section.

Lines 867-869: What are the KE and P-K terms? These are not defined in this paper. This is an example of a detail that seems unnecessary to include unless you explain it fully.

Our apologies. P and K refer to the zonal mean available potential and kinetic energies, respectively. We agree that this detail is not that important, so we have removed it.

Lines 951-957: Here is another example of speculative text that could be deleted. These details are not understandable to the reader without being more fully explained.

Having trimmed down the text substantially we reserve the right to retain this text as we do think it is important to make the connection back to the results from Mitevski et al. (2021).

Line 962: Also over the west Pacific. See Figure 11.

Note that we have now removed this section.

Lines 1026-1029: I don't see how the Zurita-Gotor and Alvarez-Zapatero (2018) study is relevant here. Zonal mean dynamics cannot simply be applied to explain overturning cells confined to specific longitudes.

Note that we have now removed this bullet as we have removed the section describing the local circulation responses.

Typos

Lines 207, 252, 274, 537, 863: Section 3b

Thanks for noting. This has been fixed.

Line 253, 356, 959: Section 3c

Noted.

Line 364: Delete extra closed parenthesis.

Noted.

Line 404: El Niño

Noted

Line 639: Figure 4b

Noted.

Line 791: Section 3a

Noted.

Line 824: Figure 5d

Noted.

Line 947: Figure 5

Noted.

Line 976: a decrease

This section has been removed.

References

Thanks for these references. They have now been included (the ones that are relevant to the retained text).

Chemke, R., & Polvani, L. M. (2021). Elucidating the mechanisms responsible for Hadley cell weakening under 4 × CO2 forcing. Geophysical Research Letters, 48, e2020GL090348.

Deser, C., and A. S. Phillips (2009), Atmospheric circulation trends, 1950-200: The relative roles of sea surface temperature forcing and direct atmospheric radiative forcing, J. Clim., 22, 396-413.

Grise, K. M., and Polvani, L. M. (2014), The response of midlatitude jets to increased CO2: Distinguishing the roles of sea surface temperature and direct radiative forcing, Geophys. Res. Lett., 41, 6863- 6871, doi:10.1002/2014GL061638.

Grise, K. M., & Polvani, L. M. (2017). Understanding the Time Scales of the Tropospheric Circulation Response to Abrupt CO2 Forcing in the Southern Hemisphere: Seasonality and the Role of the Stratosphere, Journal of Climate, 30(21), 8497-8515.

Karnauskas, K. B., & Ummenhofer, C. C. (2014). On the dynamics of the Hadley circulation and subtropical drying. Climate Dynamics, 42(9-10), 2259-2269.

Schwendike, J., Govekar, P., Reeder, M. J., Wardle, R., Berry, G. J., & Jakob, C. (2014). Local partitioning of the overturning circulation in the tropics and the connection to the Hadley and Walker circulations. Journal of Geophysical Research: Atmospheres, 119, 1322-1339.

Staten, P. W., Grise, K. M., Davis, S. M., Karnauskas, K., & Davis, N. (2019). Regional widening of tropical overturning: Forced change, natural variability, and recent trends. Journal of Geophysical Research: Atmospheres, 124.

Response to Reviewer 2

This manuscript examines the differing impacts of collapsed vs. recovered AMOC on atmospheric circulation. The authors make use of two fully coupled simulations during the "extension" portion (beyond 2090) and four XxCO2 experiments ranging from 2-5xCO2 in both fully coupled and slab ocean model configurations. They address two central questions:

1) ***How does collapsed AMOC impact atmospheric circulation relative to recovered AMOC at the same forcing level and how does this compare with different abrupt CO2 forcing scenarios?***
2) ***How important are AMOC related impact and how do they scale with global mean surface temperature?***

To address these questions, the authors conduct a wide range of diagnostics looking at differences in simulations during time periods with either a collapsed or recovered AMOC state. The authors find a robust impact on the Hadley cell with a strengthening and Northward shift that is associated with a Bjerknes compensation, around 40N associated with impacts of AMOC on the storm track. They also show that the circulation response does not scale with equilibrium climate sensitivity.

Overall, the paper uses appropriate methodologies, logical arguments, and comes to impactful conclusions. The paper is well written, but I suspect is well beyond the word limit for the journal. My comments are all relatively minor and if addressed, I believe this manuscript will be suitable for publication.

We thank the reviewer for her/his constructive feedback and overall positive tone.

Comments

1- ***This manuscript is very well written and easy to follow, however in my estimation it might be over 1.5 x the maximum length. There are many instances where the authors refer to different subsections and summarize the results in subsections, both of which are symptoms of and contribute to the manuscript length. I would recommend working to trim down the manuscript for publication.***

We completely agree with the reviewer and have substantially trimmed down the manuscript by several pages, taking care to remove redundant passages, overly speculative statements, unnecessary appendix figures, etc. We hope that the reviewer thinks that this has contributed to a more readable study.

2- ***I think there could be some subtle but important differences in how the two SSP experiments are described.***

Although in this paper we only see two of the simulations, on line 104-107 the authors state "During this time period the authors show that internal variability alone results in a spontaneous bifurcation of the ocean flow, wherein two out of ten ensemble members exhibit an entire AMOC collapse, while the other eight recover at various stages". I believe the definition of collapse in the paper is ~5Sv (lines 234-235), but this is mentioned in the context of the time averaged and not in the first discussion of these two simulations, I would suggest including this earlier in the discussion.

At the request of Reviewer 2 as well another reviewer we now have included the results from the entire 10-member SSP 2-4.5 member, now contrasting the responses in the 2 "collapsed" simulations (more intuitively referred to as SSP 2-4.5 C) with the 8 "recovered" simulations (SSP 2-4.5), where "collapse" and "recovery" refer to the AMOC behavior beyond year 2400. To the point that the reviewer is making here, note that we have slightly altered our definition of the AMOC to reflect the maximum stream

function value at 48°N (earlier we were sampling at 900 m as well). The collapse (to 0 SV) is now more apparent and therefore does not need much explaining.

> ***On line 19-20 the authors state "We show that an AMOC collapse results in an abrupt northward shift and strengthening of the Northern Hemisphere Hadely Cell and intensification of the northern midlatitude jet". Another example is on line 987-988 "we have isolated the atmospheric response to a spontaneous collapse of the AMOC in the context of a warming climate". Focusing on the "collapse" gives the impression that there was an abrupt AMOC reduction in some of these simulations and this is what is being studied. When I look at the two simulations that are provided, I don't see a rapid AMOC collapse, I see a slow and steady continued decline in AMOC in SSP2-4.5 I and a recovery in SSP3-4.5C.***

Fair point. We have taken care to change references in the manuscript to "collapse" to "strong decline and eventual collapse" (and variations on this phrasing).

> ***I think small language changes could make it clearer that you are looking at the recovery period when GHG emissions are reduced. Given the time period of study and the forcing impacts, I think a better characterization of these simulations is the those with and without an AMOC recovery with reduced GHG emissions.***
>
> ***It is possible that this view point of focusing on the collapse in two members makes more sense given the mechanisms responsible that are outlined in AR2022, the manuscript under review, but without access to this manuscript or explanation in the current manuscript I can't be sure if this is true.***

We agree with the reviewer's concern that AR2022 was not made available for the initial submission. We have now supplied this material (referred to now as AR2023) and hope that this adds the context that the reviewer was seeking. We thank her/him for being patient.

3- ***Measures of statistical significance are missing from all the difference plots. These should be added.***

Excellent point. We have now added measures of statistical significance and a description of our methodology in Section 2.

4- ***When it comes to comparing the SOM to the FOM simulations, are differences in surface temperatures found only in the North Atlantic or are there generally higher SSTs in the SOM simulations. If so, how does that impact the interpretation of the results?***

Thank you very much for this comment as it has highlighted the fact that we did not mention an important detail when explaining the FOM and SOM comparisons. Indeed, another reviewer raised the same point! The reviewer here is correct in pointing out that the FOM and SOM setups do not produce the same warming at $2xCO_2$. In plotting these results we adjusted the SOM $2xCO_2$ simulation to match that of the FOM $2xCO_2$ results as we wanted to focus on the difference between their *scalings*, relative to CO_2 (and GMST). Again, thank you very much for highlighting this oversight, which we now clarify in the figure captions.

5- ***In general, I find it strange to conduct the analysis choosing only two ensemble members. However, I can appreciate that with the large amount of analysis that this choice might have been necessary. Why are the two ensemble members SSP 2-4.5 I and SSP 2-4.5 C given the***

letters "I" and "C"? Does this have any significance? If so, it would be good to mention it and if not, perhaps a nomenclature that allows a reader to recall which simulation exhibits which behavior might be better (e.g. "r" for recovery and "c" for collapse).

This is an excellent comment. As explained in our previous response, we now incorporate results from the entire 10-member SSP 2-4.5 ensemble and use the reviewer's suggested "R" and "C" to denote recovery and collapse, respectively.

Minor Comments:

Line 678-683: I don't understand this argument. Do you mean that other have argued that changes in the jet are simply an artifact of changes in the tropopause height but that here you do not see a change in the tropopause height? When you speak of the tropopause height how are you defining it, for example did you look at the dynamic tropopause on the 2PVU surface or the thermodynamic tropopause output from the model.

We mention this as previous studies have suggested a strong link between tropopause height changes (defined using the WMO thermal-based definition) and the response of the Hadley Cell. For example, Held (2000) claim that an increase in tropopause height should increase the critical shear necessary for baroclinity instability, thus pushing poleward the latitude where it is equal to the angular momentum conserving shear (Hadley Cell edge) (Lu et al. (2007)). However, this appears not to play out as predicted, as shown, for example, in the analysis presented in Section 4b in Chemke and Polvani (2019). Our results also confirm a weak relationship. We now reference these studies when motivating this brief discussion of the tropopause height changes.

Caption 10:
I believe "are shown in the left and right panels" should be "are shown in the upper and lower panels"

Thanks for catching this mistake! We have fixed this is in the manuscript.

Caption 12: For climatological values I'm assuming you have positive solid and negative dashed. This should be included in the caption.

This figure has now been removed.

Caption 13: A statement of the contour interval would be helpful.

This figure has now been modified and appears as Figure 5. We have now included a reference to the contour interval that is used.

Line 1022-1023: Watch the consistency in using the abbreviation HC for Hadley Cell.

Thanks. Noted.

Finally, this is more of a comment and not an item to address. The authors refer to a paper under review by Romanou et al. very frequently. Though it is not necessarily a problem to refer to a manuscript under review, it should be noted that it is challenging as a reviewer as we do not have access to this paper.

We are in complete agreement with the reviewer and have now included this as reference material for the reviewer.

Response to Reviewers 3 and 4

This manuscript discusses a series of experiments performed with the NASA GISS E2.1 climate model to characterise and understand the NH atmospheric response to an AMOC collapse. In this model, the AMOC collapses for a forcing equal to or exceeding 3xCO2, as well as in 2 out of 10 members forced by the extended SSP 2-4.5 scenario (corresponding to radiative forcing of about 2.5XCO2). By analysing one AMOC-collapsed (SSP 2-4.5 I) and one AMOC-recovered (SSP 2-4.5 C) member, the authors show that the AMOC collapse results in a shift in atmospheric circulation which, for a number of dynamical aspects, substantially exceeds the differences in circulation between 2xCO2 (AMOC recovers) and 3xCO2 (AMOC collapses). They show that an AMOC collapse completely disrupts the relationship between atmospheric circulation and global mean temperature change compared to simulations with a thermodynamic slab ocean version of the model. Specific examples include a wintertime strengthening and poleward shift of the NH jet stream, a strengthening of the Hadley cell, and a poleward shift of the NH Hadley cell edge. Such circulation changes are further placed in the context of changes in the meridional atmospheric and oceanic energy transports. The authors note that this is the first time the impact of an AMOC collapse under climate change is isolated within a single climate model and without adding an external freshwater forcing.

I found this study very interesting. This model shows a noise-induced bifurcation of the AMOC for the SSP 2-4.5 scenario which is fascinating and, regardless of the realism of the model, I fully agree with the authors that these experiments are extremely useful the examine the global climate and atmospheric circulation responses to an AMOC collapse. The proposed analyses are mostly sound, and this manuscript will be a very useful reference for any future study on the atmospheric response to an AMOC collapse. However, what this manuscript lacks is sufficient clarify in the discussion of some of the results. In particular, I have concerns regarding the choice of some of the displayed figures, which make really hard to follow the discussion in a few parts. Moreover, the manuscript is really long (about twice a standard J Clim paper). While I was initially skeptic about the need of such a long paper, I now overall feel that a longer than standard manuscript is justified to keep all the information in the same paper. Yet, I think some discussions and analysis are a bit redundant and I would suggest dropping them for the sake of conciseness. Finally, the authors mention a companion paper which is under review with supposedly a stronger oceanic flavour. I would appreciate receiving a copy of the manuscript to evaluate the presence of any major overlap. Overall, I have do doubt that this manuscript is suitable for publication in J. Climate with some revision.

We thank the reviewer for her/his very constructive feedback. While we appreciate that she/he is open to the possibility of retaining the longer format, we have decided to shorten the manuscript at the request of the editor and the other reviewers. This has involved removing much of the discussion of the zonally varying circulation response and several appendix figures. In the process of doing this we have also trimmed down several sections that were redundant and tried to be clearer in distilling the key messages. We hope that the reviewer agrees that the revised version is an improvement.

Main comments

1) The manuscript hardly ever shows spatial maps of the differences between the responses to the collapse and recovered AMOC experiments (either abrupt or SSP). The only cases where this is shown are supplementary Figure A1 and A3. This is probably motivated by the goal of comparing the full CO2 and SSP responses. However, I believe that communicating what the AMOC response is in the first place is a higher priority, and a number of discussions in the paper are really hard to follow without looking at the difference plot. Without the difference plot, the reader can only follow the discussion by mentally inferring the differences. This is quite tiring in the long term, especially for

such a long manuscript. For example, while reading the discussion of Fig 4, I had to look at Fig A3 all the time, The text was then clear to follow, but surely that shouldn't be the purpose of a figure in the Supplementary Material! Other figures (particularly, Fig 5, Fig 9, Fig 11 and Fig 12) didn't come with any difference plot and while I could follow most of the arguments, I cannot say it was straightforward. A related caveat of the current presentation, is that some figures consist in a very large number of small sub-sub-panels. Some of them, particularly Fig 4 and Fig 14, are really too small to be read.

We completely agree. We have now recast all anomalies in terms of "Collapsed-Recovered" SSP 2-4.5 and "$3xCO_2$-$2xCO_2$" differences, putting the former first (as requested by the reviewer) followed by comparisons with the latter. This has reduced the number of panels in each figure. We hope these changes have made the manuscript easier to follow.

I am not sure how the authors would like to address this, but it will probably require a moderate reshape of the presentation of the material, at least for the first part of the paper (Fig 4 and Fig 5). One option, certainly not the only one, would be to first answer what the response to the AMOC collapse is in the SSP runs (including the relevant difference plots in the main paper), and then ask how does this compare to the response to the AMOC collapse under 2xCO2 vs 3xCO2 (perhaps just for some variables).

This is a great suggestion – please see the revised Section 3a. As suggested, we now discuss the SSP 2-4.5 results and follow with a comparison with the $XxCO_2$ analysis. Please see the revised manuscript.

2) I think the authors could stress a bit more in the conclusions the important result that - for a number of variables - the impact of the AMOC collapse way exceeds that from having a 2x or 3xCO2 increase. I found this result remarkable, and I would suggest stressing it as much as possible.

We agree – indeed, this is a remarkable result. We have now tried to make this point clearer in the conclusions. For example, please see the revised first bullet in the conclusions. The other points have been modified as well, in order to better distill the key messages.

3) The manuscript is very long and very detailed. I liked it, but some parts felt redundant to the key messages conveyed. I have suggested specific parts that could be cut or removed in the specific comments below.

Agreed and thanks for these recommendations, which we have used when determining how to reduce the text.

4) The introduction does a very good job at convincing the reader that this is the first study in which the impact of an AMOC collapse is studied in a single model and without freshwater hosing. But then it would be nice if, in the conclusions, the authors could elaborate on this and explain whether their cleaner approach has revealed any potential caveat arising from studies that employ fresh water perturbations or analyses of the inter-model spread, or whether it mainly confirms previous studies.

The point that is being communicated is that this is truly a unique ensemble in which the different AMOC behavior among ensemble members arises entirely spontaneously. Furthermore, compared to previous studies we have identified new results (for example, the HC edge shift). We have tried to make this clearer throughout.

Specific comments:

L29-31: I had never heard the use of "direct response" to refer to the SST warming response without eddy feedback. Usually, the direct response refers to the response to radiative forcing before ocean warming, and the indirect response to that to SST warming (e.g. Shaw and Voigt, 2015). Please rephrase.

Agreed – another reviewer pointed out this sloppiness in our phrasing. We now distinguish between the direct radiative response and the slow vs. fast SST responses. Please see the revised text and added references.

l52: I think the poleward shift is only found for the zonal-mean NH jet stream. Please correct. The results of Liu et al. also suggest a strengthening of the NH zonal-mean jet at lower levels, though I agree that this is not found in Bellomo et al.

Agreed – we have taken care to distinguish between the zonal wind responses over the Atlantic (a strengthening and eastward extension) and over the Pacific (a poleward shift). This is an important point and we appreciate the reviewer for pointing this out.

l109: Do you mean that sea ice melting induces a regional cooling that decreases evaporation in ocean convective regions? Please be consistent with line 197, where you also mention a role for salinity changes.

At the request of another reviewer, we removed this material as it was tangential to the main points that we were making.

l133-135: I think referring to dynamical sensitivity is complicating the message, especially since it is not defined what it is meant. I think it could be simply phrased as to whether the circulation changes scale linearly or not with global-mean warming. I would postpone a discussion linking with the literature on dynamical sensitivity to the final discussion, and use a more readable language before.

We appreciate the reviewer's perspective, but we do not agree that we should reserve discussion until the end of the manuscript. Rather, we feel it is important to make a direct and clear link to these recent studies as they provide much of the motivation for examining the GMST and circulation responses that comprise Section 3. No changes to the manuscript.

l138: "it remains unclear": I agree this was never quantified, but, as far as I know, the proposed argument in the literature is always that the AMOC influences climate via changed T gradients / Bjerkness compensation. Please rephrase.

We do not agree that this is an obvious statement to the broader community, as reflected in the commonly used practice of pattern scaling (see the AR6 report). Therefore, while the reviewer may be right that the AMOC community may find this result obvious, we are seeking to broaden our reach here.

l169: Second part of Q1 is not clear. Please add: "response to an AMOC collapse induced by different CO2 forcing". It think it should be listed as a separate bullet point. I also think this second bullet could incorporate the first part of Q2.

Good points – we have rephrased Q1 and Q2 as suggested by the reviewer.

l172: It would be useful to make the second part of Q2 clearer, .e.g. is the impact of the AMOC mediated by GMST or by changes in temperature gradients? I would list this as a separate question.

Agreed – please see now the new questions Q1-Q3.

l241: I can't see any notable differences in the figure. Please clarify.

Agreed – the differences are too subtle to be significant. We have removed this sentence.

l262: I and C -> C and I

As we explain below, we have now incorporated the results of all ten members in the SSP 2-4.5 ensemble, defining now a "recovered" 8-member (sub) ensemble (SSP 2-4.5 R) and a "collapsed" 2-member ensemble (SSP 2-4.5 C). We feel that this has substantially reinforced the robustness of our results (and "R" and "C" are now more intuitive designations).

l265: ppb -> ppm

Thanks for catching this typo – it has been corrected.

l309: What is TropDMetricPSI?

This has now been removed.

l314: What is UAS?

As explained in the manuscript, UAS is a metric within the TropD package that uses the surface zonal wind to define the Hadley Cell edge (zero-crossing of the latitude of the surface zonal wind).

l318: These concepts were also mentioned in Schneider T, 2006.

Good point. This reference has now been added.

l323: "are closely collocated": collocation is not entirely correct; it would imply the stormtrack is located at the Hadley cell edge, but this is only true for seasons/regions with a merged subtropical and eddy driven jet. Please rephrase.

We inadvertently missed adding a "convergence" after the "momentum flux" – please see the revised text.

l326: It's not clear what cyclone tracking algorithm is adopted. Please clarify and provide some more details about previous studies that have employed this method.

In our attempt to trim the manuscript we have removed this section describing the zonally varying response (including the storm tracks).

l335: I understand you may want to keep consistency with the referenced paper, but I am just wondering whether T is the best variable to refer to fluxes, since T is also used to refer to temperature.

We agree that this may be confusing – however, we prefer to maintain as is to keep consistency with the referenced study.

l346: If you would like to use E2.1 as a short for GISS-E2-1-G, please specify it somewhere.

We already defined E2.1 when we introduced the model in Section 2. No change to the manuscript.

l365: The term "Equilibrated responses" in the section heading, and within the section, is misleading. The responses from the SSP simulations could be called quasi-equilibrium, but certainly not those from the Abrupt runs. Please correct.

We respectively disagree with the reviewer and lean on the large body of previous literature examining the abrupt $4xCO_2$ simulations, all of which designate the 100-150 year average response as the "equilibrated" response. While she/he is certainly true that the AMOC (and other circulation features) may end up behaving quite differently were these integrations to be extended to millennial timescales, we reserve the right to keep consistent with the previous literature.

L378: remove "more realistic".

Done. Please see the revised manuscript.

l390: The enhanced gradient at the gulf stream is difficult to see and the impact of temperature changes on the zonal temperature gradient depends on the latitude. Please clarify.

We agree and have removed this from the (significantly revised) section.

L397: stronger meridional SSTs compared to what?

Please note that this section has been significantly revised.

l404: it would be easier to appreciate the lack of ENSO response if the difference plots were showed.

Please see the revised Figures 3 and 6, which now show the differences. There is no ENSO response in each comparison.

l408-419: Does it have to be dynamical? Couldn't it not be due to the thermodynamic advection of colder North Atlantic air?

Good point – we now include a caveat in this sentence mentioning this possibility.

l421: I don't agree that NH SSTs adjust within the first 100 years. In the scenario with an AMOC collapse, NH temperatures keep evolving during the entire simulation (this is clear in the Appendix 1 I-C panel). Please clarify/rephrase.

We completely agree and thank the reviewer for pointing this out! Indeed, especially over the Pacific northern latitudes, this slower SST response results in some differences with the $3xCO_2$ simulation (where the jet not only accelerates, but also shifts poleward). Thank you very much for this comment – please see the revised manuscript.

l425: The reference to 2100-2200 is not consistent with the l 421. I would also say that the North Pacific Ocean adjustment takes longer than this. Please quantify/clarify.

Thanks. We have clarified this in the text.

Fig 4: these sub-subpanels are so small it's nearly impossible to see any detail.

We agree – the new figures are now much less cluttered as they now only show the "SSP 2-4.5C – SSP 2-4.5 R" and "$3xCO_2 – 2xCO_2$" anomalies.

l 479: Based on Fig A3, I see jet strengthening - with no poleward shift - in the North Atlantic at both 850 hPa and 500 hPa. The poleward shift seems to be confined in the North Pacific. Please modify. Regarding the presence of larger changes in the upper vs lower troposphere, it would be useful to examine whether this still holds in terms of percentage changes.

We completely agree and this point was also raised by the other reviewers. We have revised this text to reflect the different zonal wind response between the Atlantic and Pacific basins.

l483-494: this paragraph could be removed for the sake of space. KB2021 had to scale by mean warming to account for inter-model differences in climate sensitivity. In the SSP experiments, the differences in mean warming are due to the AMOC, so there is no particular point in scaling.

We agree – the normalization by GMST was making the discussion unnecessarily complicated. We have removed all related discussion.

l 532: KB2021 found a SH jet poleward shift. Could that be a consequence of the GMST normalisation too?

Good point. We now include a reference to this as another possible reason for the SH jet response in that study (in addition to the different simulation lengths).

l530: It is difficult to tell without looking at the difference plot, but based on Fig 5b the AMOC collapse seems to induce a reduction of the SH jet poleward shift found in SSP-C. This seems consistent with the amplified Antarctic warming found in SSP-I. It this correct?

Please see the new version of Figure 4. In the SH there is, if anything, a uniform weakening of the jet.

l 535: It's is unclear to me that the NH EKE change can be interpreted as a poleward shift, instead of a strengthening. Could you introduce some metrics to quantify this?

We agree – we have now rephrased to emphasize that these changes reflect a strengthening. While the maps do show some suggestion of a poleward shift over the Pacific in the $3xCO_2$-$2xCO_2$ comparison (Fig. 5b), it seem like the zonal mean response is dominated by a strengthening. Please see the revised manuscript.

l542-544: It is difficult to infer changes in Hadley cell edge based on Fig 5. Since the Hadley cell edge is discussed in detail in Fig 7, it might be useful to postpone this discussion.

We retain a passing reference to this change and clarify that this edge shift is most obvious in the lower troposphere for pressures greater than ~500-600 hPa. As this is evident in the zonal mean picture we do think it is important to mention here.

l547: I don't understand how shifts in the NAM would reinforce the Hadley/Ferrel cell coupling. Please clarify.

Agreed. We have removed this sentence.

l576: Fig 6 (and Fig 7): I am surprised by the 2XCO2 results. Are you saying that there is exactly the same mean warming and climate responses in the FOM and SOM setups? I would have expected at least some small differences to be present.

Thank you very much for this comment as it has highlighted the fact that we did not mention an important detail when making this figure. Indeed, the reviewer is correct in pointing out that the FOM and SOM setups do not produce the same warming at 2xCO2. In plotting these results we adjusted the SOM 2xCO_2 simulation to match that of the FOM results as we wanted to focus on the difference between their scalings, relative to CO_2 (and GMST). Again, thank you very much for highlighting this oversight, which we now clarify in the figure captions.

l588-591: I don't fully understand why the peak CO2 level is more relevant than the long-term level, especially considering that the temperature evolution is largely flat in the extended run. Please clarify.

We refer to the peak CO_2 level since the circulation will not necessarily scale with the long term (flat) GMST evolution, a point we have tried to highlight throughout.

l599: this is a very nice result. You could mention that the direction of the mismatch between the blue and cyan dots, for a given GMST, is consistent with the direct effect of GHGs, which tend to suppress global mean precipitation (see PDRMIP related papers, e.g. Samset et al., 2016).

This a very interesting point and one that we had failed to notice. Thank you very much for this observation, which we now note in the manuscript.

line 610: behaviour -> behaves

Thanks. This has been fixed.

line 615: suggests -> suggest

Thanks. This has been fixed.

line 617: simulations -> models

We actually mean “simulations” here, not models. No change to the manuscript.

line 650-652: I don't see how these results can demonstrate the causality between changes in static stability, eddy flux convergence and Hadley cell edge shifts induced by the AMOC collapse. Attributing whether the driving comes changes in static stability, rather than horizontal temperature gradients, is particularly difficult. Please rephrase or remove.

We agree that it is difficult to establish causality between these responses, but, as we do not seek to reinvent the wheel, we lean on the previous studies (particulary Chemke and Polvani (2019) and Menzel et al. (2019)) who showed that the changes in HC edge respond on a similar timescale as the latitude of maximum eddy momentum fluxes. Chemke and Polvani (2019) also used this to implicate static stability changes as a potential leading driver of the momentum flux changes.

Of course, none of this really proves causality, however, so we agree with the reviewer that more care must be taken to acknowledge this. We have tried softening our language when discussing this material.

line 658-664: this paragraph is unclear. Please clarify or remove for sake of space.

We agree. We have removed this paragraph.

line 673-683: I think this paragraph could be removed with little loss of content. I agree that these four dynamical quantities are related - and this is consistent with their similar time evolution - but showing this figure/discussion adds very little on their cause-effect driving.

We agree with the reviewer that this doesn't prove causality, but we reserve the right to show this figure because it does show a similar timescale of response between these variables, something which is highlighted even more now that we have included the results from the full ten-member SSP 2-4.5 ensemble. As the timescale of the response has been used to suggest that certain quantities are linked to others (see Chemke and Polvani (2019)) we feel that this adds some value. Hopefully the reviewer is open to retaining this figure, especially as we have significantly reduced the text and removed several of the appendix figures.

line 686: dynamical sensitivity -> atmospheric circulation

As explained earlier we wish to retain this language.

Line 692: I think Fig 8 can be removed for the sake of space. It adds little content in my view.

Please see our response to the previous related comment.

line 701: I would avoid using "abrupt" - here and in the following lines - to discuss the change between the 2xCO2 and 3xCO2 experiments, since these are two distinct experiments and there is no abruptness from a time evolution perspective.

Good point – we have replaced "abrupt" with "large".

line 733-744: this paragraph is confusing. It is not clear what net energy loss refers to. Are you referring to the reduced atmosphere+ocean poleward energy transport or to some change in the net globally-averaged energy balance, or to local imbalances in the North Atlantic? Please clarify and rephrase.

We are referring to the reduced atmosphere + ocean poleward energy transport (i.e. solid lines in (new) Figure 10). This has been clarified in the revised version of the manuscript.

line 757-758: Another reason of the possible cause of the difference in oceanic compensation may be the different length of the simulations, and hence their degree of equilibration. Especially considering that the differences between 3xCO2 and 5xCO2 are relatively small compared to those between SSP I vs C. Please discuss.

Excellent point – we now briefly mention this in the text.

line 779-788: for the sake of length, this paragraph may be sacrificed ... as the authors conclude: "these results are not too surprising".

Fair point, but we have chosen to retain this paragraph in light of the significant cuts that we have made to other sections of the manuscript. No changes made.

Line 794 and following: This section should be either removed or expanded. If kept, it would be useful to first analyse the contribution of transient vs stationary waves to the changes to the zonal-mean DSE transport. This cannot be inferred from Fig 11, since there is substantial compensation in the zonal direction associated with the stationary wave component. The discussion seems to assume that stationary waves are the dominant process, but this is not given.

This entire section has now been removed.

line 832-833: this sentence seems in contrast with the previous discussion of Fig 3, in which it was highlighted that the changes in temperature gradients were largest in the tropical Atlantic. Please clarify.

This entire section has now been removed.

line 851: It is hard to tell without the difference plot, but I would rather say the West Pacific seems entirely insensitive to the AMOC collapse.

This entire section has now been removed.

l853 and following: this seems a long discussion to just say that the AMOC weakening seems to have very little impact on the Walker cell. Please consider being more synthetic.

This entire section has now been removed.

Fig 14: It is nice to document storm track changes, but I am not sure this has added much information to the overall discussion. For sure, the figures are so small and full of detail that it is difficult to inform what the AMOC impact is.

Agreed. This entire section has now been removed.

l 879: Given the amount of spatial noise, could you please clarify whether the increase in the North Pacific storm intensity is statistically significant?

This entire section has now been removed.

l 889: for the sake of consistency, why not looking at members A and B for all the analyses in the paper then? Please explain.

Please note that now we have included the results from all ten members of the SSP 2-4.5 ensemble.

L 899: add: "sensitivity to greenhouse forcing"

Good point – this has been added.

l 925: what is an AMOC type freshwater forcing? please clarify.

Apologies – we realize this was obscure. We have replaced with “freshwater hosing forcing”.

l 933: I found that the goal of this discussion wasn't very clear. Could you try to spell out more clearly what is the question being discussed and why it is important? Are you asking why there is a compensation between LE and DSE changes in the tropics, but not in the NH extra-tropics?

We are asking why the compensation occurring in the NH extratropics is dominated by the DSE changes and not by the LE changes. We have tried to make this point clearer – please see the revised text.

l 934: as previously mentioned the term abrupt compensation does not seem appropriate to me.

As earlier, we have replaced "abrupt" with "large".

line 936: I would rather say the increase in DSE dominates northward of 20N. Please rephrase/clarify.

This has been fixed.

l941: it is not correct to say that changes in heat transport drive changes in dynamical aspects. If anything, it is the other way around, though there are mutual interactions. Please rephrase or clarify.

Good point – we have rephrased to remove any suggestions of causality. We now refer to "not fundamentally associated with" instead of "not fundamentally drive".

l958: Also in this section it would be nice if you could be clearer about what is the key question being discussed. Are you asking whether the atmospheric circulation changes might themselves contribute to reinforcing the AMOC weakening, via interactions along the gulf stream?

This section was removed.

l959: zonal --> zonally asymmetric

This section was removed.

l 959: 3e -> 3c

This section was removed.

l1010: what is ModelE?

Apologies – this is the encompassing term for all versions of the GISS model (including E2.1, E2.2, etc.). We have now replaced with "the GISS climate model."

l 1017: please add: "in presence of an AMOC collapse" after "does not scale GMST."

Done. Please see the revised text.

l 1017-1018: I find too simplistic saying that dynamic sensitivity does not scale with equilibrium climate sensitivity. For examples, based on the conceptual models of Grise and Polvani 2016 and Ceppi et al 2018, one would still expect that the doubling of the forcing leads to a doubling of the "equilibrated" circulation change. The current manuscript, and the cited papers, refer to very different situations: the present studies shows a real non-linearity in the amplitude of the forcing, while the others refer to (linear) superpositions of responses emerging on different time scales. Please rephrase or remove.

We have not "shown a real non-linearity in the amplitude of the forcing" – indeed, we never plotted the radiative forcing (as would be gauged from fixed SST experiments) as a function of CO_2. Rather, we

have shown that the large-scale circulation response does not scale with GMST (which contributes, in addition to radiative feedbacks, to equilibrium climate sensitivity). The previous studies have attempted to assess this relationship by, for example, correlating HC edge responses with GMST so we do not agree with the reviewer that the context of our presentation is very different from that of these studies.

l 1050: These results also seem very relevant for the purpose of developing storylines of atmospheric circulation change (e.g. Zappa and Shepherd, 2017)

Good point– this is now mentioned in the text.

References

We thank the reviewer for these references, which we now cite in the manuscript.

Shaw, T., Voigt, A. Tug of war on summertime circulation between radiative forcing and sea surface warming. Nature Geosci 8, 560-566 (2015).

Schneider, T., 2006. The general circulation of the atmosphere. Annual Review of Earth and Planetary Sciences, 34, pp.655-688.

Samset, B.H., Myhre, G., Forster, P.M., Hodnebrog, Ø., Andrews, T., Faluvegi, G., Flaeschner, D., Kasoar, M., Kharin, V., Kirkevåg, A. and Lamarque, J.F., 2016. Fast and slow precipitation responses to individual climate forcers: A PDRMIP multimodel study. Geophysical research letters, 43(6), pp.2782-2791.

Zappa, G. and Shepherd, T.G., 2017. Storylines of atmospheric circulation change for European regional climate impact assessment. Journal of Climate, 30(16), pp.6561-6577.

Atmospheric Response to a Collapse of the North Atlantic Circulation Under A Mid-Range Future Climate Scenario: A Regime Shift in Northern Hemisphere Dynamics

Clara Orbe[a,b], David Rind[a], Ron L. Miller[a], Larissa S. Nazarenko[a,c], Anastasia Romanou[a,b], Jeffrey Jonas[a,c], Gary L. Russell[a], Maxwell Kelley[a], and Gavin A. Schmidt[a]

[a] *NASA Goddard Institute for Space Studies, New York, NY*

[b] *Department of Applied Physics and Applied Mathematics, Columbia University, New York, NY*

[c] *Center for Climate Systems Research, Earth Institute, Columbia University, New York, NY*

Corresponding author: Clara Orbe, clara.orbe@nasa.gov

ABSTRACT: Climate models project a future weakening of the Atlantic Meridional Overturning Circulation (AMOC), but the impacts of this weakening on climate remain highly uncertain. A key challenge in quantifying the impact of an AMOC decline is in isolating its influence on climate, relative to other changes associated with increased greenhouse gases. Here we isolate the climate impacts of a weakened AMOC in the broader context of a warming climate using a unique ensemble of Shared Socioeconomic Pathway (SSP) 2-4.5 integrations that was performed using the Climate Model Intercomparison Project Phase 6 (CMIP6) version of the NASA Goddard Institute for Space Studies ModelE (E2.1). In these runs internal variability alone results in a spontaneous bifurcation of the ocean flow, wherein two out of ten ensemble members exhibit an entire AMOC collapse, while the other eight recover at various stages despite identical forcing of each ensemble member and with no externally prescribed freshwater perturbation. We show that an AMOC collapse results in an abrupt northward shift and strengthening of the Northern Hemisphere (NH) Hadley Cell and intensification of the northern midlatitude jet. We then use a set of coupled atmosphere-ocean abrupt CO_2 experiments spanning the range 1-5xCO_2 to show that this response to an AMOC collapse results in a nonlinear shift in the NH circulation moving from 2xCO_2 to 3xCO_2. Slab-ocean versions of these experiments, by comparison, do not capture this nonlinear behavior. Our results suggest that changes in ocean heat flux convergences associated with an AMOC collapse — while highly uncertain — can result in profound changes in the NH circulation and continued efforts to constrain the AMOC response to future climate change are needed.

1. Introduction

Future projections of the atmospheric circulation remain highly uncertain and reflect uncertainties in the direct radiative response to CO_2 forcing (Deser and Phillips (2009); Grise and Polvani (2014); Shaw and Voigt (2015); Ceppi et al. (2018)), as well as both the (direct) response to changes in sea surface temperatures (SSTs) and the (indirect) response to changes in eddy feedbacks (see Shepherd (2014) and references therein). Among the former, uncertainties in SST projections over the subpolar North Atlantic are particularly consequential, as they strongly influence the location and strength of the North Atlantic storm track, with profound downstream impacts on precipitation and wintertime weather over Europe and parts of Africa (e.g., Zhang and Delworth (2006), Smith et al. (2010), Woollings et al. (2012), O'Reilly et al. (2016)). In particular, while increases in greenhouse gases over the 21st century are expected to result in substantial warming over much of the North Atlantic, climate models project considerable cooling over midlatitudes resulting in a so-called "North Atlantic warming hole (NAWH)" (e.g., Josey et al. (2018), Drijfhout et al. (2012), Robson et al. (2016), Caesar et al. (2018)). While the drivers of this NAWH have been under considerable debate, recent detection-attribution analysis suggests that the anthropogenic signal of the NAWH has emerged from internal climate variability and, moreover, that this cooling can be attributed to declining northward oceanic heat flux over recent decades related to increased greenhouse gas emissions (Chemke et al. (2022)).

Among other mechanisms contributing to the development of the NAWH, the slowdown of the Atlantic Meridional Overturning Circulation (AMOC) has been invoked as one potential key driver (Cheng et al. (2013), Rahmstorf et al. (2015), Menary and Wood (2018)). Studies have long shown that changes in the strength of the AMOC can have widespread impacts not only on other components of the ocean circulation but, more generally, on the broader atmospheric climate system, resulting in a southward shift of the intertropical convergence zone (ITCZ) (e.g., Zhang and Delworth (2005), Vellinga and Wood (2008), Jackson et al. (2015)), a strengthening of the Walker circulation (e.g., Vial et al. (2018), Orihuela-Pinto et al. (2022)) and a northward shift of the Northern Hemisphere (NH) jet stream (e.g., Liu et al. (2020), Bellomo et al. (2021)). Understanding the global scale atmospheric response to changes in AMOC strength is important not only for projections of future climate, but also for understanding paleoclimate records and the dynamics of past Dansgaard-Oeschger events. In particular, while the future collapse of an

AMOC is still considered unlikely, the latest generation of coupled climate models project stronger weakening with future warming, compared to older generations of models (Weijer et al. (2020)).

In addition to its impacts on global precipitation, SST-related changes in the AMOC can change the baroclinicity of the atmosphere, which can result in changes in the storm tracks (Woollings et al. (2012)). However, the precise impacts of a weakened AMOC on atmospheric baroclinity are not well understood, largely because studies have used models that exhibit a wide diversity in the amplitude and spatial extent of the NAWH (Gervais et al. (2019), Haarsma et al. (2015), Menary and Wood (2018)). Nonetheless, despite these uncertainties in the drivers and extent of the NAWH, Woollings et al. (2012) showed that the response of the North Atlantic storm track to climate change was singularly shaped by changes in ocean-atmosphere coupling.

The role of the AMOC in future projections of the jet stream in the Climate Model Intercomparison Project Phase 5 (CMIP5) and Phase 6 (CMIP6) models was recently examined in Bellomo et al. (2021) (hereafter KB2021), who showed that changes in the AMOC play a primary role in determining the magnitude of the projected poleward displacement of the NH zonal mean jet stream. In particular, by stratifying models according to the strength of their projected AMOC weakening (in response to a quadrupling of CO_2), the authors showed that models with a larger AMOC decline (> 7 Sv, relative to preindustrial values) exhibit minimum warming over the North Atlantic, a southward displacement of the ITCZ and a poleward shift of the northern midlatitude jet. The results from KB2021 suggest that the AMOC is a major driver of intermodal uncertainty in future projections of the northern jet stream (and associated hydrological impacts).

A key challenge in quantifying the impact of AMOC uncertainties on future projections of the large-scale atmospheric circulation is in isolating its influence on climate, relative to other changes associated with increased greenhouse gases. Thus, while the results from KB2021 are compelling, that study drew conclusions based on the spread among models subject to the same abrupt $4xCO_2$ forcing and it is not clear if the models exhibiting greater AMOC weakening were also models that exhibit other characteristics that would independently impact the jet stream. At the same time, previous studies using more traditional freshwater flux perturbations to examine the jet (and other climate) responses to a weakened AMOC, have done so in the absence of other background changes related to increased CO_2 (e.g., Zhang and Delworth (2005), Jackson et al. (2015)). As such, these

studies may produce a circulation response to a weakened AMOC that is different than what might occur if other factors impacting atmospheric temperature gradients are included.

One recent attempt to isolate the climate impacts of a weakened AMOC in the broader context of a warming climate was performed in Liu et al. (2020). In that study, the authors compared fully coupled Representative Concentration Pathway (RCP) 8.5 simulations (Riahi et al. (2011)) using a full physics comprehensive model (CCSM4) with identically forced simulations in which a negative freshwater perturbation over the subpolar North Atlantic was added after year 1980 in order to maintain the AMOC strength (while preserving all other forcings). That study showed results that were generally consistent with KB2021, pointing to a major role of the AMOC in causing widespread cooling stretching from NH high latitudes to the tropics and a poleward displacement of the NH midlatitude jet.

While the results from Liu et al. (2020) represent an important step forward in isolating the impacts of the AMOC on the storm tracks in the context of a warming climate, it is not clear that prescribing a negative freshwater perturbation does not potentially interfere with nonlinear components of the AMOC response in a coupled system. To this end, here we present new results featuring an ensemble of Shared Socioeconomic Pathway (SSP) 2-4.5 integrations (Meinshausen et al. (2020)) that was performed using the CMIP6 version of the NASA Goddard Institute for Space Studies (GISS) ModelE (E2.1) (Kelley et al. (2020)). In particular, we show results from a subset of the runs documented in Romanou et al. (Under Review) (hereafter AR2023), in which the authors identified a tipping point in the SSP 2-4.5 ensemble occurring during the "extended" portion of the simulations (i.e. beyond year 2090, after which CO_2 emissions are ramped down). During this time period the authors show that internal variability alone results in a spontaneous bifurcation of the ocean flow, wherein two out of ten ensemble members exhibit an entire AMOC collapse, while the other eight recover at various stages (Figure 1a). Note that, in contrast to the aforementioned freshwater hosing studies, in which an AMOC collapse is induced by adding freshwater, in these experiments the AMOC collapse is caused by a reduction in evaporation from the ocean, mediated by sea ice melting (AR2023). As such, the atmospheric configuration that is used to produce this effect in an interactive mode is likely to be very different from an atmosphere which is simply responding to a prescribed freshwater flux perturbation.

Whereas AR2023 focused primarily on the oceanic conditions giving rise to this divergence in AMOC behavior among different ensemble members, here we focus on the subsequent impacts this has on the atmospheric large-scale circulation. In particular, we contrast the behavior between two and eight ensemble members in which the AMOC respectively collapses and recovers to historical values by year 2400 (red vs. green lines, Fig. 1a). As such, we isolate the impact of a weakened AMOC on the atmospheric circulation in the presence of increased greenhouse gas warming using a single model (unlike KB2021) and without any need to invoke negative freshwater perturbations (as in Liu et al. (2020)). To the best of our knowledge, this represents the first time that the AMOC imprint on the circulation has been isolated in the context of background increases in greenhouse gases using a fully coupled comprehensive model, absent any externally imposed freshwater perturbations that may potentially interfere with the model's internal dynamics.

As discussed in AR2023, the ensemble members in which the AMOC collapses are substantially cooler than those runs in which it recovers, with wintertime global mean surface temperature (GMST) differences of about 1°C by year 2400 (Fig. 1c). Therefore, in documenting the influence of the AMOC on the atmosphere in the different SSP 2-4.5 ensemble members it is natural to ask how the large-scale thermodynamic and dynamical circulations scale with these differences in GMST. Though perhaps naive, it is common practice to assume that the climate system scales linearly with GMST, as reflected in the use of so-called "global warming levels" in the recent IPCC AR6 report (James et al. (2017)) and the widely applied related practice of "pattern scaling" (e.g., Santer et al. (1990), Tebaldi and Arblaster (2014)). Recent studies, however, have shown that the climate's so-called "dynamical sensitivity" – in particular, circulation shifts associated with changes in the Hadley Cell and storm tracks - do not scale with equilibrium climate sensitivity (Grise and Polvani (2016), Ceppi et al. (2018)). As those studies, however, focused on large (CMIP5) multi-model ensembles, it is not clear if similar conclusions also apply to single models and to climate states in which the AMOC has undergone a substantial weakening. More precisely, it remains unclear how much of the circulation response to a weakened AMOC is related simply to changes in GMST or, rather, to changes in (free-tropospheric) meridional temperature gradients away from the surface.

To this end, in addition to reporting on the results from the SSP 2-4.5 ensemble we also examine a suite of abrupt 1-5xCO_2 experiments that were conducted using the same model version (Mitevski

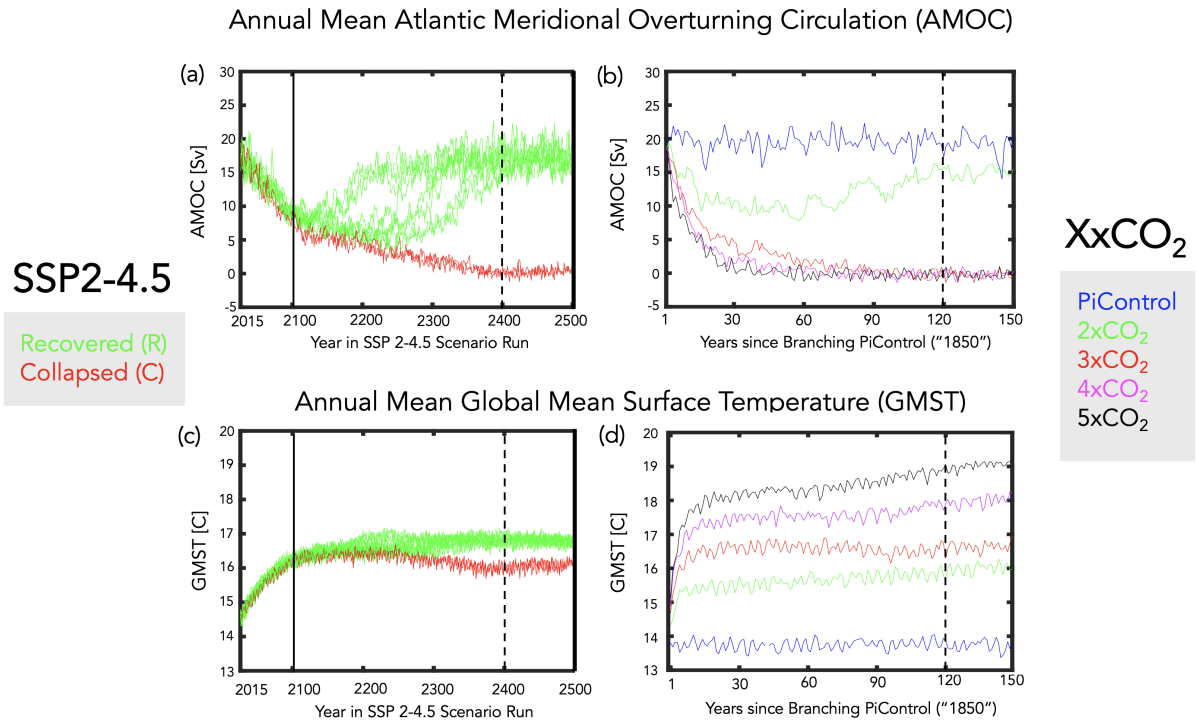

FIG. 1. Top: Evolution of the annual mean maximum overturning stream function in the Atlantic ocean, evaluated at 48°N, compared among the SSP 2-4.5 (8) recovered and (2) collapsed ensemble members (top, left) and among the abrupt $XxCO_2$ runs (top, right). Bottom: Same as top panels, except showing annual mean global surface temperature (GMST). Vertical solid lines mark the beginning of the "extension" portion of the SSP 2-4.5 scenario. Vertical dashed lines indicate the years after which climatological averages are evaluated (i.e., years 2400-2500 (left) and years 120-150 (right)).

et al. (2021)). In particular, we exploit the fact that between $2xCO_2$ and $3xCO_2$ abrupt forcing the AMOC respectively recovers and collapses by year 150 (Fig. 1b), behavior which is generally similar to the differences in AMOC responses between the recovered and collapsed members of the SSP 2-4.5 ensemble, hereafter referred to as SSP 2-4.5 R and SSP 2-4.5 C, respectively (Fig. 1a). However, by spanning a much broader range of GMST responses, compared to the SSP 2-4.5 ensemble – and assuming that the atmospheric responses to an AMOC collapse are similar between the $3xCO_2$ and SSP 2-4.5 collapsed ensemble members (a point which we examine in Section 3a3) – the broader set of $XxCO_2$ experiments affords a unique opportunity to investigate the relationship between dynamical and equilibrium climate sensitivity in the presence of a collapsed AMOC.

In Section 3 we begin by contrasting the large-scale atmospheric circulation responses between the SSP 2-4.5 R and C members in which the AMOC recovers and remains collapsed after year 2400 (Sections 3a1-2, Q1 below). We then compare this behavior with the circulation differences occurring in the 2xCO_2 and 3xCO_2 integrations (Section 3a3, Q2). After showing that the 3xCO_2 circulation changes in the NH are largely dominated by the behavior of the AMOC, we then use the broader set of 1-5xCO_2 abrupt experiments to examine how the collapse of the AMOC modulates the relationship between the NH dynamical circulation and GMST over a much broader range of CO_2 forcing (Section 3b, Q3). In addressing the latter we also use slab-ocean model integrations in order to examine if the behavior exhibited in the coupled atmosphere-ocean runs is reflected in simulations in which ocean heat flux convergence changes associated with an AMOC collapse are not allowed to occur.

The main goals of the manuscript are centered around addressing these three questions:

Q1) How does a collapse of the AMOC influence the atmospheric circulation in the presence of the same background CO_2 forcing (SSP 2-4.5 ensemble)?

Q2) How does this compare with the response to an AMOC collapse induced by different CO_2 forcing (2xCO_2 vs. 3xCO_2)?

Q3) Are AMOC-related circulation changes mediated primarily by GMST or by changes in atmospheric temperature gradients?

In addressing Q1-Q3 we show that the AMOC tipping point described in AR2023 results in a vastly different atmospheric response between ensemble members in which the AMOC collapses versus members in which the AMOC recovers. In particular, in our model the atmospheric response to an AMOC collapse (occurring on the timescales addressed in this study) reflects a regime shift between a climate state in which the NH Hadley Cell and midlatitude jet are substantially weaker and displaced further equatorward (strong AMOC) compared to a state in which they are substantially stronger and displaced poleward (weak AMOC).

2. Analysis/Methods

a. Models and Experiments

Here we use simulations from two sets of experiments produced using the GISS version E2.1 climate model (GISS-E2-1-G) (Kelley et al. (2020)), which consists of a 40-level atmospheric model with a horizontal resolution of 2° x 2.5° latitude/longitude coupled to the 1° horizontal resolution 40-level GISS Ocean v1 (GO1) model (for more details of GO1 see AR2023). Comprehensive reviews of this model's response to historical and future climate change simulations are provided in Miller et al. (2021) and Nazarenko et al. (2022), respectively.

We first examine results from the SSP 2-4.5 ensemble that contributed to the official submission of the NASA-GISS climate group to CMIP6. In particular, we contrast the behaviors of eight members in which the AMOC has recovered by year 2400 (SSP 2-4.5 R) with two members in which it has remained collapsed (SSP 2-4.5 C) (Fig. 1a). As discussed in AR2023, this contrasting behavior emerges during the "extension" portion following year 2090, beyond which CO_2 concentrations slow down in growth from 597 ppm to 643 ppm at year 2200 and decline thereafter (Meinshausen et al. (2020)). That study further showed that the divergence in the behavior of the AMOC results from stochastic variability associated with sea-ice transport and melting in the Irminger Sea that led to a reduction in evaporation and salinity. Note that, whereas AR2023 was primarily focused on identifying the mechanisms leading to different recovery times among the SSP 2-4.5 R, our interest is in quantifying the impact of an AMOC collapse on the large-scale circulation after year 2400 up to year 2500. To this end, we treat the SSP 2-4.5 R and C simulations as comprising two distinct "recovered" and "collapsed" ensembles.

To put the SSP 2-4.5 results in a broader context, we also examine the coupled atmosphere-ocean 1-5xCO_2 abrupt CO_2 experiments reported in Mitevski et al. (2021), which were performed using the same version of the model. We restrict our attention to a subset of the runs, focusing mainly on the 2xCO_2 and 3xCO_2 runs, but also including results from the 4xCO_2 and 5xCO_2 simulations when commenting on the linearity of the atmospheric circulation responses with respect to changes in GMST (Section 3b). As shown in Figure 1, the behavior of the AMOC by the end of the abrupt 2xCO_2 and 3xCO_2 runs is generally very similar to the AMOC behavior in the SSP 2-4.5 R and C ensemble members, respectively, past year 2400. This similar behavior also appears at

lower latitudes (26°N) (not shown), consistent with the findings in AR2023, who showed a strong correlation in AMOC strength at these two latitudes (0.97) within the broader SSP 2-4.5 ensemble.

In addition to the results from the fully coupled ocean-atmosphere model (hereafter FOM) SSP 2-4.5 and $XxCO_2$ integrations, we also show results from q-flux or slab-ocean model (SOM) integrations spanning the range 1-5xCO_2. In these experiments any changes in ocean horizontal heat transport and vertical heat uptake by the deep ocean are not included as the ocean heat flux convergences in the mixed layer ($-\nabla\cdot(vT)$, including both horizontal and vertical heat fluxes) are calculated using preindustrial control values. At the same time, the SOM experiments do capture the mixed layer temperature changes resulting from changes in the net surface heat fluxes (hereafter referred to as "thermodynamic" ocean coupling). As such, contrasting the responses in the FOM and SOM experiments isolates the role of dynamic (i.e. ocean heat flux convergence) coupling on the atmospheric responses in the FOM simulations, consistent with the presentation in Chemke et al. (2022). Note that this approach does not explicitly isolate the contribution of changes in SSTs to the atmospheric circulation response, as the SST response reflects both changes in thermodynamic and dynamic ocean-atmosphere coupling. However, robustly isolating the impact of SSTs can be tricky as previous studies utilizing prescribed SST "warming hole" patterns have shown large sensitivity to how these patterns are prescribed, particularly in relation to SST gradients (see discussion in Gervais et al. (2019)).

b. Temporal Averaging and Spatial Domains

To compare the atmospheric responses from the SSP 2-4.5 simulations with those from the abrupt CO_2 experiments we focus on climatological averaging periods during which the characteristics of the AMOC are similar, i.e., years when the AMOC has recovered in the 2xCO_2 and SSP 2-4.5 R runs, while the AMOC has remained collapsed in the 3xCO_2 and SSP 2-4.5 C experiments. As indicated in Figure 1 (dashed black vertical lines) this corresponds to years beyond which the maximum value of the overturning stream function at 48°N has reached nearly zero, corresponding to years 120-150 and 2400-2500 in the $XxCO_2$ and SSP 2-4.5 integrations, respectively. We refer to these periods hereafter as the "equilibrated" responses in the model, bearing in mind that the AMOC exhibits multi-centennial instability as was illustrated in an older version of the GISS

climate model (Rind et al. (2018)). Variations on these longer timescales are not addressed in this study.

We begin by presenting differences in climatological means between the SSP 2-4.5 R and C ensembles and between the 2xCO_2 and 3xCO_2 integrations. Statistical significance of the SSP 2-4.5 C-R differences is assessed using a Welch's t-test, given the unequal sample sizes represented by the 8-member R and two-member C ensembles. A two-sample Student's t-test is used when comparing the abrupt CO_2 responses. In addition, when putting the SSP 2-4.5 results in the context of the broader 1-to-5xCO_2 forcing range we define all responses relative to a 150-year average over the preindustrial control simulation from which the abrupt CO_2 experiments are "branched."

For the majority of the analysis considered here we focus on December-January-February (DJF) and over the NH. Our focus on DJF is consistent with the presentation in AR2023, while our focus on the NH is motivated by Mitevski et al. (2021), who showed that the AMOC collapse occurring between 2xCO_2 and 3xCO_2 results in a non-monotonic response in global mean surface temperature, driven primarily by changes occurring in the NH (more precisely, the North Atlantic). We deviate from this convention, however, at two different points in this study. First we use annual mean GMST when evaluating the dynamical sensitivity scaling in Section 3b; second, we present the energy budget analysis in Section 3c using annual means in order to facilitate comparison with previous studies. Some results about the Southern Hemisphere (SH) circulation response are also presented, but only discussed briefly.

Finally, while our main focus is on the "equilibrated" responses defined above, we are also interested in exploiting the evolution of the responses, as in Grise and Polvani (2017) and Chemke and Polvani (2019). As shown in those studies, consideration of the response timescales of different variables affords insight into possible mechanisms governing their evolution.

c. Scaling with Global Mean Surface Temperature (GMST)

We begin by comparing the absolute differences in the atmospheric "equilibrated" responses between the SSP 2-4.5 R and C members (Section 3a1-2) and between the 2-and 3xCO_2 simulations (Section 3a3). When interpreting these differences, however, it is important to note that these could partly be reflective of background differences in the CO_2 forcing. In particular, the CO_2 values in the SSP 2-4.5 extended experiments peak at 643 ppm, or roughly 2.4 times preindustrial values,

and decrease thereafter (Figure 1a in AR2023). It is perhaps not surprising, therefore, that this value of CO_2 lies in between the $2xCO_2$ and $3xCO_2$ levels identified in Mitevski et al. (2021) as the transition point between the AMOC recovering and collapsing under abrupt forcing (Fig. 1b).

Given these differences in CO_2 forcing (further exaggerated when considering the broader suite of 1-5xCO_2 experiments) it may seem most natural to compare the simulations with respect to their associated instantaneous radiative forcing (RF) as in Mitevski et al. (2021). However, another difference between the transient SSP 2-4.5 and abrupt 1-5xCO_2 experiments is the evolution of the forcing. As the AMOC is known to be sensitive to the time history of the forcing, this is important to take into consideration, and so we cast our scaling analysis in Section 3b (in which the SSP 2-4.5 results are compared against the broader 1-5xCO_2 suite) in terms of GMST. This approach is also more in spirit with Ceppi et al. (2018) as it directly addresses the extent to which the dynamical sensitivity captured in the simulations scales with equilibrium climate sensitivity (Q3).

Finally, a related but distinct approach is to normalize by annual mean GMST. KB2021 showed that doing so highlights large differences in temperature gradients and the zonal mean meridional circulation between models in which the AMOC weakens substantially (> 7 Sv), compared to models showing a limited AMOC response (< 7 Sv). However, while this approach is well suited to understanding the multi-model response to the same ($4xCO_2$) forcing, it does not directly afford insight into how dynamical sensitivity scales with GMST. As we have tried both normalizing and not normalizing in this study and draw generally very similar conclusions (not shown), we focus on the unnormalized results.

d. Analysis Approach

1) Hadley Cell and Storm Track Diagnostics

Whereas KB2021 focused on the latitude of the northern midlatitude jet, here we expand their analysis to also include measures of the Hadley Cell (HC) and the storm tracks. Figure 2a highlights how these measures of the HC and midlatitude jet are coupled through eddy momentum fluxes.

To quantify the characteristics of the Hadley Cell we use metrics calculated using the Tropical-width Diagnostics (TropD) code (Adam et al. (2018)) based on fields that were zonally and seasonally averaged before calculation of the metrics. The edge of the HC, ϕ_{UAS}, is defined as the zero-crossing latitude of the surface zonal wind (corresponds to UAS in TropD and is calculated

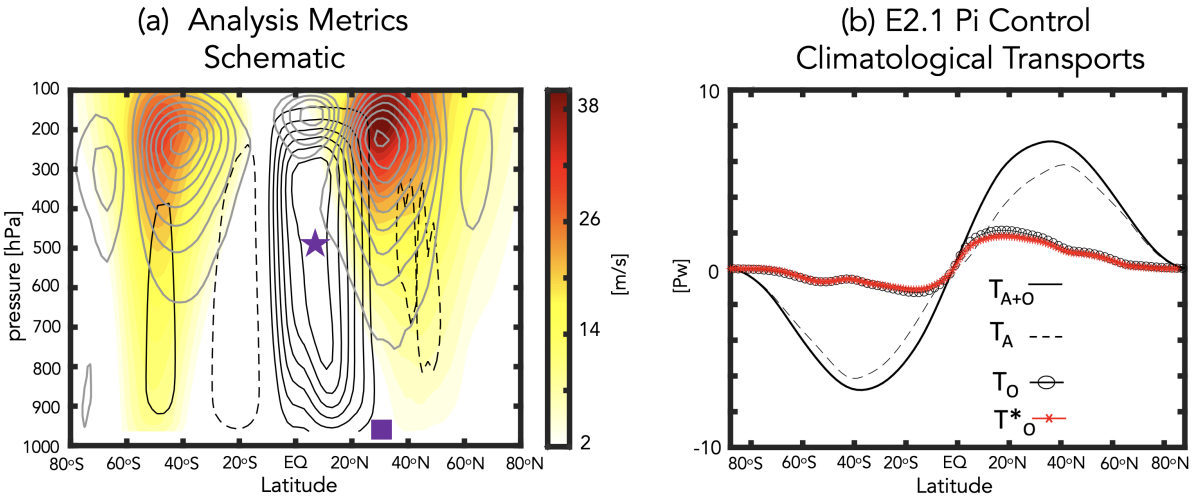

FIG. 2. (a): Schematic of the main zonal mean dynamical metrics considered in this study, illustrated using data from the preindustrial control simulation. The December-January-February (DJF) climatological mean meridional circulation is shown in black contours, with solid and dashed lines denoting clockwise and counterclockwise directions, respectively (contour interval: $3\text{x}10^{10}$ kg/s). The DJF zonally averaged zonal winds are shown in the filled colored contours (only positive values shown; contour interval: 2 m/s) and the DJF eddy momentum fluxes are shown in the grey contours (contour interval: 8 m^2/s^2). The purple star denotes the Northern Hemisphere (NH) Hadley Cell strength, or the maximum value of the mean meridional streamfunction at 500 hPa equatorward of where it crosses zero, while the edge is denoted by ϕ_{UAS} (purple square), or the zero-crossing latitude of the surface zonal wind. (b): Annual mean meridional distributions of the total atmospheric (T_A; black dashed line) and combined atmosphere-ocean ($\text{T}_{\text{A+O}}$; black solid line) northward energy transports for the preindustrial control simulation. The implied ocean heat transport (T_O; black circled line), calculated by subtracting T_A from $\text{T}_{\text{A+O}}$, exhibits good agreed with online calculations of the ocean transports (T^*_O; red starred line). For more details see Section 2.

using the "zero-crossing" method) (Fig. 2a, purple square). This measure of the HC was shown to correlate well with the latitude at which the mean meridional streamfunction at 500 hPa crosses 0 poleward of its tropical extremum (Waugh et al. (2018)). The value of that tropical extremum (Ψ_{500}) is also examined as a measure of HC strength (Fig. 2a, purple star).

In addition to looking at the Hadley Cell, we also examine its relation to the northern midlatitude jet via the eddy momentum fluxes. This is based on research showing a strong connection between the evolution of the Hadley Cell and the latitude of the maximum eddy momentum fluxes

(Schneider (2006); Chemke and Polvani (2019); Menzel et al. (2019)). The eddy momentum fluxes are calculated as in Chemke and Polvani (2019) as the time mean of [u'v'], where u and v are the zonal and meridional winds, respectively, and primes represent deviations from both the zonal and monthly means. In particular we are interested in the latitude where the eddy momentum flux maximizes (eddy momentum convergence = 0) (Fig. 2a, grey contours). As it is well known that the largest eddy momentum flux convergences are closely collocated with the extratropical storm tracks (e.g., Lau et al. (1978), Lim and Wallace (1991)), we also examine the vertically averaged eddy kinetic energy, calculated using daily output. Connections with static stability and baroclinic eddy generation are also made, where the latter is quantified using $\sim \alpha'\omega'$, where primes denote zonal deviations and α and ω refer to one over the density and vertical velocity in pressure coordinates, respectively.

2) Energetic Analysis

To put the results of the dynamical analysis in an energetic context we evaluate the total meridional heat transport of the coupled ocean-atmosphere transport system, further partitioned into its oceanic and atmospheric contributions. Following Magnusdottir and Saravannan (1999) we estimate the total vertically integrated atmospheric heat flux ($\mathrm{T_A}$) as:

$$\frac{\partial cos\phi}{acos\phi\partial\phi}\overline{[\mathrm{T_A}]} \equiv \frac{\partial cos\phi}{acos\phi\partial\phi}\int_1^0 \overline{(c_pT + gz + Lq)v\rho d\eta}$$

$$= \overline{[-\mathrm{F_T} - \mathrm{F_S} + \mathrm{SHF} + \mathrm{LHF}]} \qquad (1)$$

as well as the vertically integrated meridional heat flux in the combined atmosphere-ocean system ($\mathrm{T_{A+O}}$) as:

$$\frac{\partial cos\phi}{acos\phi\partial\phi}\overline{[\mathrm{T_{A+O}}]} \equiv \overline{[-\mathrm{F_T}]} \qquad (2)$$

where moist static energy density is the sum of dry static energy density ($c_pT + gz$) and the latent heat density (Lq), ρ and v refer to the mass density and horizontal velocity on η surfaces. Zonal averages and time averages are denoted by square brackets and overbars, respectively. The terms on the RHS of both equations refer to energy fluxes out of the top of the atmosphere and at the

surface: F_T (net upward flux of radiation at the top of the atmosphere, calculated as outgoing longwave radiation (OLR) minus the absorbed solar radiation (ASR)), F_S (net downward flux of radiation at the surface equal to the sum of net downward longwave (LWF) and shortwave (SWF) radiation), and the fluxes of latent and sensible heat at the surface (LHF and SHF).

The resulting annual mean meridional distributions of T_A and T_{A+O}, calculated using the E2.1 150-year preindustrial control simulation, is consistent with the climatological energy transports presented in other studies (e.g., Magnusdottir and Saravannan (1999), Held and Soden (2006)) (Figure 2b). Note that the implied ocean heat transport, calculated by subtracting the first from the second equation above (Fig. 2b, black circled line) is found to exhibit good agreement with online calculations of the ocean transports (Fig. 2b, red starred line). These northward ocean heat transports, simulated in historical integrations using E2.1, have been shown to agree well with 1992-2011 estimates from the ECCO ocean state estimate (Figure 23 in Kelley et al. (2020)). Finally, in addition to examining the compensation between atmospheric and oceanic poleward transports, we also further partition T_A into its moist versus dry contributions using online calculations of the vertically integrated dry static energy and latent heat northward transports (Section 3c).

3. Results

We begin by contrasting the regional SSP 2-4.5 C and R responses in sea surface temperature, sea level pressure, precipitation and zonal winds (Section 3a1) and in the large-scale zonal mean circulation (Section 3a2). Then we compare the SSP 2-4.5 C-R differences to the responses in the $2xCO_2$ and $3xCO_2$ simulations (Section 3a3), followed by a discussion of the full set of abrupt $1\text{-}5xCO_2$ experiments, which we use to examine how the changes in thermodynamics and the circulation scale with changes in global mean surface temperature (Section 3b). To interpret the dynamical scaling results we then examine the compensation that arises between the ocean and atmosphere in response to a decline and eventual collapse of the AMOC (Section 3c).

a. Equilibrated Responses

1) SSP 2-4.5 Collapsed vs. Recovered: Near-Surface Temperatures, Precipitation and Winds

Figure 1 (bottom panels) shows the evolution of annual global mean surface temperature in the SSP 2-4.5 C and R members (Fig. 1c) and the abrupt CO_2 experiments (Fig. 1d). Comparing the collapsed versus recovered SSP 2-4.5 ensemble members reveals global cooling associated with a sustained collapse of the AMOC such that by the time that the AMOC has recovered in the SSP 2-4.5 R members the annual mean global surface temperature is almost one degree warmer, relative to the SSP 2-4.5 C members. In the abrupt CO_2 simulations, the GMST change in the $3xCO_2$ experiment is only ~0.6^{o}C warmer than the $2xCO_2$ simulation, reflective of a clear flattening of the warming trend after years ~60-70. Overall, the changes in GMST are 2.2^{o}C, 2.8^{o}C, 3.0^{o}C, and 2.3^{o}C for the $2xCO_2$, $3xCO_2$ and SSP 2-4.5 recovered and SSP 2-4.5 collapsed ensembles, respectively.

That the cooling associated with a steady decline and eventual collapse of the AMOC acts to mitigate, and partially counteract, other components of the global surface temperature change is reflected in a non-monotonic change in equilibrium climate sensitivity that occurs between $2xCO_2$ and $3xCO_2$ over the broader range of experiments spanning 1-to-5xCO_2 (Figure 1 in Mitevski et al. (2021)). This counteracting of warming due to a weakening of the AMOC has also been shown to occur in 21st century warming simulations (Drijfhout et al. (2012), Caesar et al. (2018), Marshall et al. (2015)).

While the AMOC influence on the climate can occur via its changes in GMST, a reduction in AMOC strength can also influence sea surface temperature patterns. We examine this next, with a focus on DJF, and examine changes in SSTs and associated spatial gradients over the Atlantic and Pacific (Figure 3a). Note that a saturated color bar has been used in order to highlight the structure of SST changes outside of the North Atlantic region.

Examination of the North Atlantic reveals much more cooling in the SSP 2-4.5 collapsed simulations (Fig. 3a) over the subpolar North Atlantic (SPNA), consistent with the results from previous studies. This cooling within the SPNA region is also associated with a large increase in meridional SST gradients over the North Atlantic south of 40°N and enhanced zonal gradients between the

western and eastern Atlantic basins. There is also an indication of a slight increase in SST gradients in the tropics.

The cooler SSTs in the recovered simulations are not only confined to the Atlantic, but also span the Pacific (Fig. 3a), resulting in stronger meridional SST gradients, particularly over middle northern latitudes. Preliminary analysis of the evolution of the SST response (Appendix Figure 1) shows that this cooling over the extratropical Pacific occurs over several centuries and may be related to a deepening and poleward shift of the Aleutian Low (Fig. 3c), resulting in more advection of colder temperatures over the West Pacific (Wu et al. (2008)), although direct thermodynamic advection of colder North Atlantic air may also be occurring. By comparison, the changes in SSTs and associated gradients in the tropical Pacific are much smaller. Unlike some previous studies (Timmermann et al. (2007), Zhang and Delworth (2005)) we find no evidence of an El Niño like response to an AMOC weakening, although the robustness of this response has recently been questioned (KB2021).

In the SH, SSTs warm over the extratropics in the SSP 2-4.5 collapsed integrations, compared to the simulations in which the AMOC recovers. This warming takes several centuries to develop (Appendix Figure 1) and resembles the evolution of the SST pattern documented in Pedro et al. (2018) (their Figure 7). This delayed warming over the SH results in increased SST gradients over the South Atlantic (~60°S) in the SSP 2-4.5 C runs, relative to SSP 2-4.5 R, a feature which is not captured in the 3xCO_2 simulation (discussed more in Section 3a3).

In addition to the changes in SSTs, the response in precipitation in the SSP 2-4.5 collapsed simulations reflects large decreases over the North Atlantic subpolar region, reductions over the Amazon and suggestions of a southward shift of the ITCZ over both the Atlantic and East Pacific basins (Fig. 3b). By comparison, the increased precipitation in the West Pacific is not statistically significant, consistent with previous studies (Vellinga and Wood (2008), KB2021).

Moving next to more dynamical measures, we examine changes in sea level pressure and near-surface zonal winds (Fig. 3c,d). The changes in sea level pressure show differences over the North Atlantic indicative of enhanced (anticyclonic) high level pressure over the subpolar latitudes in the runs in which the AMOC collapses (Fig. 3c). In addition to these SLP changes over the Atlantic, there is also a pronounced dipole of increased and reduced sea level pressure values over the North Pacific middle and high latitudes. While this response was not discussed in KB2021, earlier studies

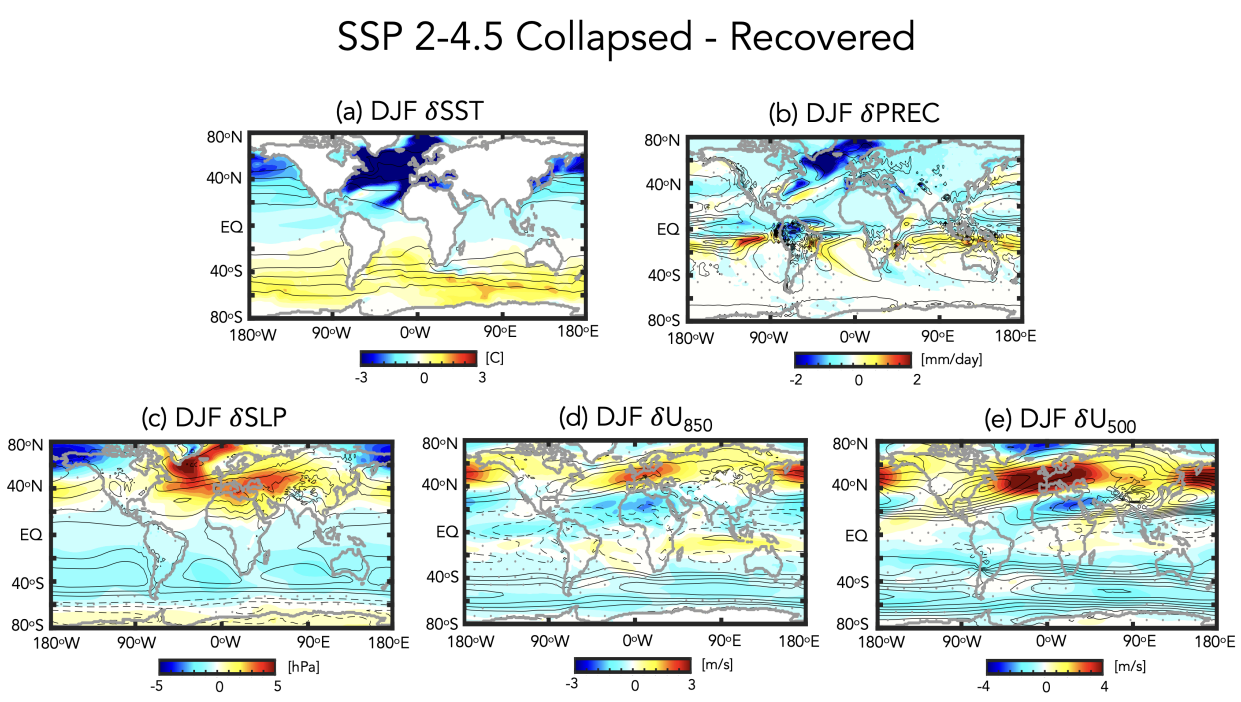

FIG. 3. The difference in the year DJF 2400-2500 climatological mean (a) sea surface temperatures (δSST), (b) precipitation (δPREC), (c) sea level pressure (δSLP), (d) 850 hPa zonal winds (δU_{850}) and (e) 500 hPa zonal winds (δU_{500}) between the SSP 2-4.5 collapsed (C) and recovered (R) ensemble members. Climatological mean values from the preindustrial control simulation are denoted in the black contours (contour intervals: (a) 5°C, (b) 2 mm/day, (c) 5 mb, (d) 3 m/s and (e) 3 m/s). Grey stippling denotes regions where the SSP 2-4.5 C-R differences are not statistically significant.

have shown that a weakening of the AMOC is associated with a deepening of the Aleutian Low (Wu et al. (2008), Liu et al. (2020)).

Consistent with the SLP changes over the North Pacific, there is a strong signature of a weakened AMOC in the near surface zonal winds (850 hPa) (Fig. 3d). These wind changes over the Pacific reflect a poleward shift of the midlatitude jet, whereas over the North Atlantic the jet mainly accelerates and extends further eastward over Europe. This acceleration over the North Atlantic is more pronounced in the mid-troposphere (Fig. 3e), as was also reported in KB2021, who identified a statistically significant strengthening of the midlatitude jet at 250 hPa, but not at 850 hPa, in models featuring a stronger AMOC decline. Finally, in contrast to the NH, there is a uniform weakening of the zonal winds over the SH extratropics. We discuss the vertical coherence of these wind changes in the next section.

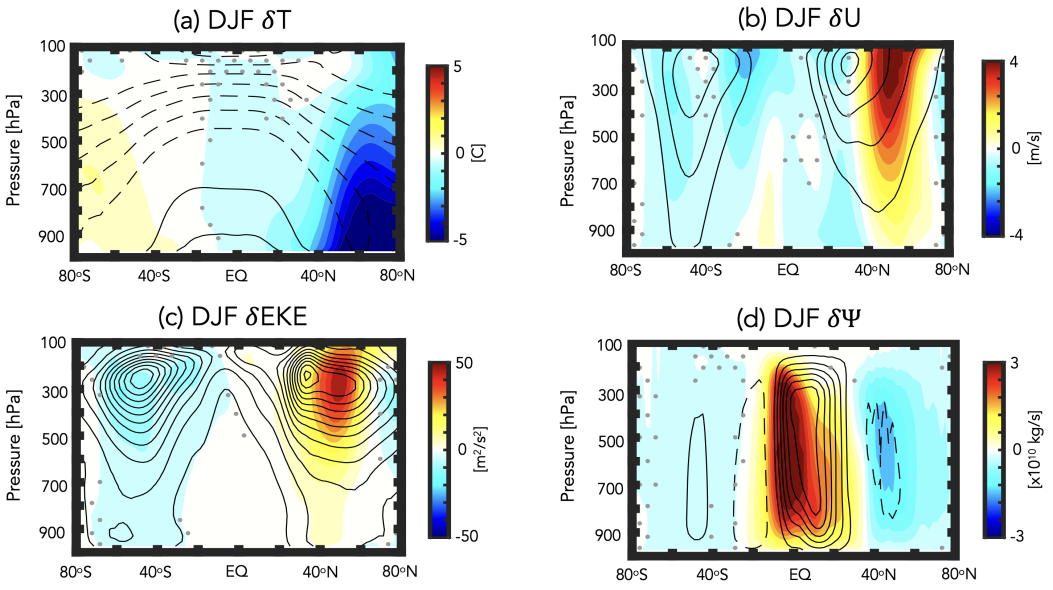

FIG. 4. The difference in the year DJF 2400-2500 climatological mean zonal mean (a) temperature (δT), (b) zonal wind (δU), (c) eddy kinetic energy (δEKE) and (d) Eulerian mean stream function ($\delta\Psi$) between the SSP 2-4.5 collapsed (C) and recovered (R) ensemble members. Climatological mean values from the preindustrial control simulation are denoted in the black contours (contour intervals: (a) 10°C, (b) 8 m/s, (c) 28 m^2/s^2 and (d) $3x10^{10}$ kg/s). Note that in (d) solid and dashed lines denoting clockwise and counterclockwise directions, respectively. Grey stippling denotes regions where the SSP 2-4.5 C-R differences are not statistically significant.

2) SSP 2-4.5 COLLAPSED VS. RECOVERED: VERTICAL STRUCTURE

In addition to its impacts on SSTs, changes in the AMOC impact the vertical structure of meridional temperature gradients in the atmosphere. To interpret the zonal wind changes shown in Figure 3 we therefore next examine the zonal mean changes in temperatures, zonal winds and eddy kinetic energy, as well as their coupling to responses in the tropical mean meridional circulation (Figure 4).

We begin by examining changes in temperature (Fig. 4a), which show much more cooling over the NH high latitude troposphere in the SSP 2-4.5 collapsed runs. A similar reduction in Arctic warming was reported in the "strongly" collapsed models examined in KB2021 (their Figure S5) and in Liu et al. (2020) (their Figure 6). In addition to the changes over the northern extratropics, we also find an indication of weak polar amplification characterized by warming throughout the

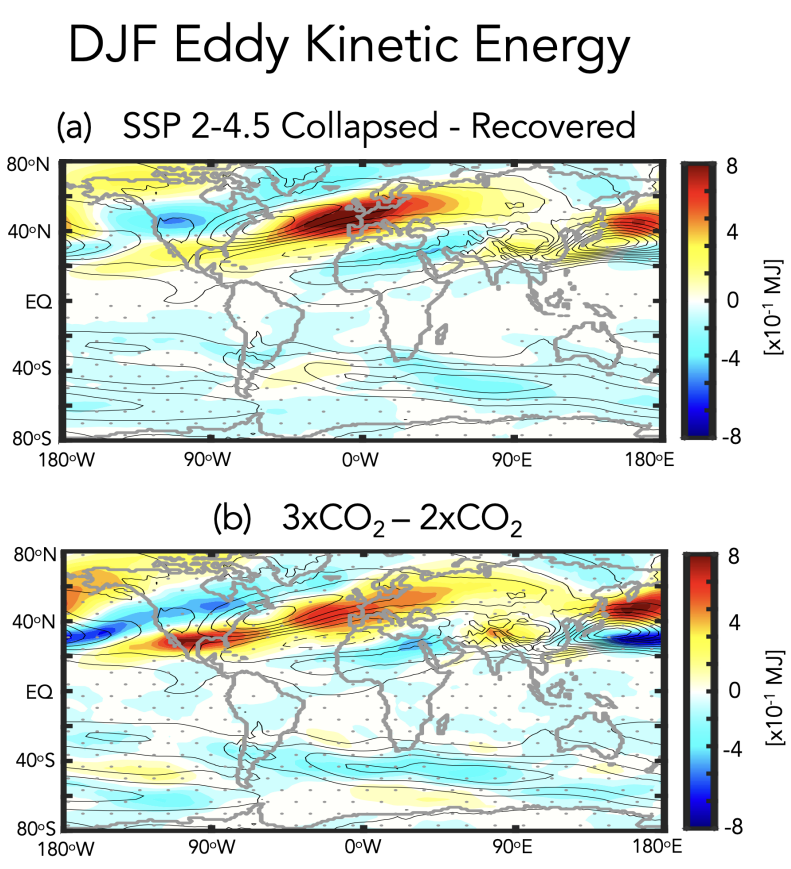

FIG. 5. (a) The difference in the year DJF 2400-2500 climatological mean vertically integrated eddy kinetic energy between the SSP 2-4.5 C and R ensembles. (b) Same as in (a), except showing the year 120-150 difference between the $3xCO_2$ and $2xCO_2$ integrations. Climatological mean values from the preindustrial control simulation are denoted in the black contours (contour interval: $5x10^{-1}$ MJ).

SH middle and high latitudes poleward of 40°S, also seen in the SST differences (Fig. 3a). This warming in the SH is consistent with Liu et al. (2020) (their Figure 6), but inconsistent with KB2021, which likely reflects their focus on shorter (100-150 year) timescales. In addition, KB2021 also identified more warming in the tropical upper troposphere, a feature that is also not evident in the SSP 2-4.5 collapsed runs. Normalization of our results by GMST (not shown) produces an anomalous upper tropical tropospheric warming, suggesting that the results reported in KB2021 are reflective of the normalization performed in that study, not of absolute temperature differences.

Moving next to the zonal winds (Fig. 4b) we find that the reduced warming over NH high latitudes is associated with enhanced meridional temperature gradients, which result in a poleward

shift of the zonal mean northern midlatitude jet in response to a decline and eventual collapse of the AMOC. A similar poleward shift in the NH jet was documented in KB2021 (their Figure 4) and in Liu et al. (2020). In the SH the zonal winds weaken and, if anything shift equatorward, in the SSP 2-4.5 C ensemble members, consistent with the weak polar amplification in that region (Fig. 4a). Again, this wind response is highly consistent with Liu et al. (2020), but opposite to that shown in KB2021, who identified a poleward shift of the SH jet. As that study did not propose a testable mechanism for the SH jet changes, it is not entirely clear what is the driver of the differences between their results and those presented here and in Liu et al. (2020), although both the normalization by GMST as well as the differing integration lengths likely contribute.

In concert with the changes in the zonal winds, the changes in eddy kinetic energy (EKE) over the NH feature increases north of 40°N (Fig. 4c). Note that there is no statistically significant response in the subtropics and only the wind (and EKE) changes poleward of 40°N are robust. Zonally, the increases in EKE are concentrated over the North Atlantic and extend eastward over Europe, as well as over the West Pacific (Fig. 5a), strongly resembling the zonal wind changes at 500 hPa (Fig. 3e). Comparisons with the changes in EKE associated with an AMOC collapse in another model (the Community Earth System Model (CESM-LE)) examined in Mitevski et al. (2021) show very similar anomalies (not shown). Furthermore, a spectral decomposition of these NH EKE changes show increased wave energy over wavenumbers 1-6 in the collapsed SSP 2-4.5 members, relative to the recovered members (also not shown).

Finally, the changes in the mean meridional stream function indicate an overall strengthening of the wintertime NH Hadley circulation in the collaped SSP 2-4.5 simulations (Fig. 4d). This intensification of the NH Hadley circulation in response to an AMOC shutdown has been reported in previous studies (Zhang and Delworth (2005), Orihuela-Pinto et al. (2022)) and generally associated with a southward displacement of the ITCZ, although Brayshaw et al. (2009) also identify a zonally localized enhancement of the Hadley Cell region over the subtropical Atlantic, which they associate with increased meridional SST gradients in that region. Compared to those studies, however, our results also show a poleward displacement of the northern Hadley Cell edge in the lower troposphere (>500 hPa), a result which has not been directly commented on in the literature. These stream function anomalies over the NH extratropical lower troposphere appear to be coupled to a slight strengthening and poleward displacement of the northern Ferrel cell.

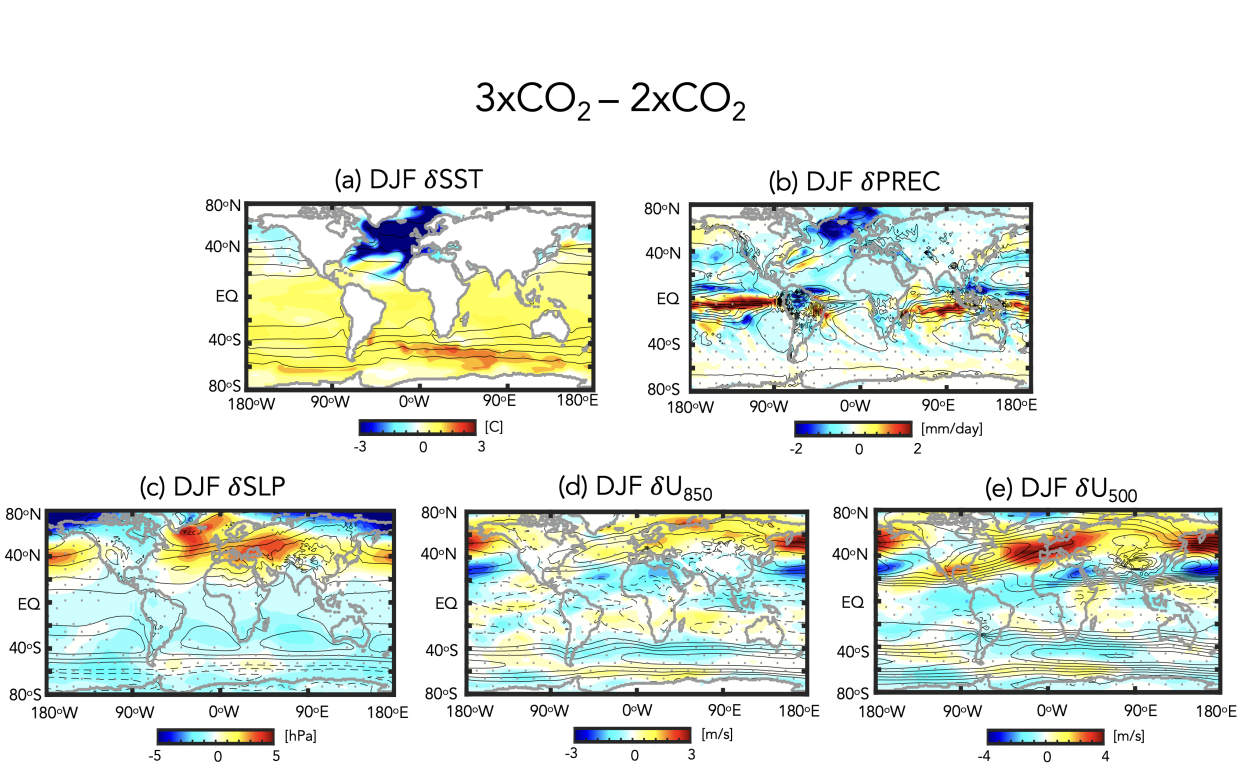

499 FIG. 6. Same as Figure 3, except showing the difference between the year 120-150 climatological mean 3xCO$_2$
500 and 2xCO$_2$ responses.

512 ### 3) COMPARISON WITH 2xCO$_2$ VS 3xCO$_2$

513 Comparisons of the surface and lower tropospheric impacts associated with an AMOC collapse
514 in the SSP 2-4.5 ensemble (Fig. 3) are highly consistent with the responses moving from 2xCO$_2$
515 to 3xCO$_2$ (Fig. 6). In particular, over the North Atlantic the changes moving from 2xCO$_2$ to
516 3xCO$_2$ reflect cooler SSTs (Fig. 6a), reduced precipitation (Fig. 6b) and an anomalous anticylonic
517 circulation over the North Atlantic subpolar gyre region (Fig. 6c), as well as a strengthening and
518 eastward extension of the North Atlantic jet over Europe (Fig. 6d, 6e). The magnitudes of the
519 3xCO$_2$ changes are also similar to the responses in the SSP 2-4.5 collapsed ensemble members,
520 albeit somewhat smaller (Fig. 3).

521 Though the overall responses in the surface temperatures and winds are very similar, there are
522 some important differences worth noting. First, the SSTs in the 3xCO$_2$ simulation show much less
523 cooling over the Pacific northern midlatitudes (> 40°N) compared to the SSP 2-4.5 C simulations,
524 which likely reflects differences in the length of these integrations as this cooling takes centuries
525 to equilibrate (Appendix Figure 1). Second, in response to 3xCO$_2$ there is more warming over the

NH subtropics and tropics, consistent with the higher CO_2 forcing in that simulation. Thus, unlike what happens in the SSP 2-4.5 C ensemble members, there is no SH polar amplification occurring at $3xCO_2$.

The different SST gradients over the northern high latitude Pacific and tropics and SH occurring at $3xCO_2$ have implications for the jet and precipitation changes in these regions. In particular, over the Pacific northern midlatitudes, where there is much less cooling compared to the SSP 2-4.5 C integrations, the jet response resembles more of a poleward shift, characterized not only by an acceleration north of 40°N, but also reduced winds ~20°N; in the tropical Pacific there is also a much stronger increase in precipitation, relative to the AMOC SSP 2-4.5 C ensemble.

Even over the North Atlantic the SST cooling is slightly weaker and less expansive and the jet response at 850 hPa is not statistically significant at $3xCO_2$, in contrast to the SSP 2-4.5 collapsed ensemble members. In the SH, there is also a suggestion of a poleward shift of the midlatitude jet at $3xCO_2$, not evident in the SSP 2-4.5 C integrations, although these changes are not statistically significant. These subtle differences aside, however, the overall similarities between Figures 3 and 6 are remarkable and suggest that the climate response that occurs moving from $2xCO_2$ to $3xCO_2$ is, to first order, determined by the changes in AMOC strength.

Strong consistency is also found when comparing the vertical response of the large-scale circulation between the AMOC SSP 2-4.5 collapsed ensemble (Fig. 4) and the $3xCO_2$ integration (Fig. 7). That is, in concert with stronger cooling over the Arctic (Fig. 7a), the $3xCO_2$ simulation features a stronger poleward shift of the NH zonal mean jet (Fig. 7b), increased EKE northward of 40°N (Fig. 7c) and a strengthened Hadley Cell (Fig. 7d).

One difference in vertical structure occurs over the Arctic, where the cooling that occurs at $3xCO_2$ (Fig. 7a) is much smaller than in the collapsed SSP 2-4.5 ensemble (Fig. 4a), reflecting the higher CO_2 forcing in that simulation. There is also stronger warming occurring within the tropics and over southern latitudes. Despite these differences in absolute temperature, however, the increase in meridional temperature gradients that occurs is similar to what happens when comparing the SSP 2-4.5 C and R ensemble members. As such, the zonal mean NH jet response is quite similar in the $3xCO_2$ simulation (Fig. 7b) compared to SSP 2-4.5 C (Fig. 4b) and is also coupled to an EKE increase on the poleward flank of the jet (Fig. 7c). Maps of the EKE response show that at $3xCO_2$ much of this increased EKE reflects changes over the Atlantic (Fig. 5b), as in the SSP 2-4.5 C en-

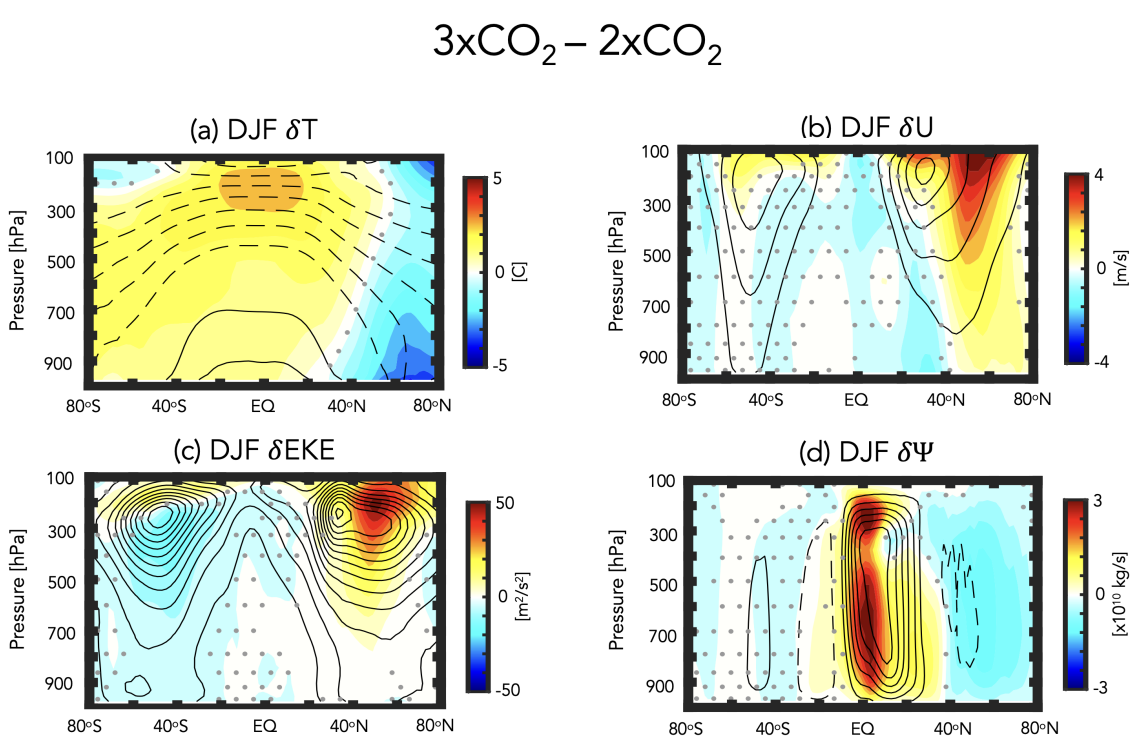

FIG. 7. Same as Figure 4, except showing the difference between the year 120-150 climatological mean 3xCO$_2$ and 2xCO$_2$ responses.

semble (Fig. 5a), although there is also increased EKE over the western Pacific and North America.

To summarize: In response to a collapse of the AMOC, our results show widespread cooling over the Arctic and stronger meridional temperature gradients over the NH. This increase in temperature gradients is associated with a poleward shift of the midlatitude jet (and associated eddy energy) as well as a strengthening of the NH Hadley Cell. In the lower troposphere (> 600 hPa) the NH Hadley cell is displaced poleward.

Over the Northern Hemisphere the response to an increase from 2xCO$_2$ to 3xCO$_2$ is remarkably similar to the differences between the SSP 2-4.5 R and C simulations, in terms of both the magnitude and spatial patterns of these changes. Some exceptions, however, include the near surface (850 hPa) wind response over the North Atlantic, which is not statisically significant at 3xCO$_2$, as well as in the tropics, where precipitation increases strongly over the Pacific. There is also more warming in the tropical upper troposphere and SH in the 3xCO$_2$ simulation. Overall, this close

correspondence suggests that the collapse of the AMOC is the dominant driver of the large-scale circulation changes moving from 2xCO_2 to 3xCO_2 in our model.

b. Scaling of Equilibrated Thermodynamic and Dynamic Responses with Global Mean Surface Temperature (GMST)

One question (Q3) not addressed in the previous sections relates to how changes in the climate response to an eventual collapse of the AMOC scale with changes in GMST. To this end, here we expand our analysis to include the results of additional (4xCO_2 and 5xCO_2) FOM abrupt CO_2 runs, as well as the results from the SOM abrupt CO_2 integrations.

1) Global Thermodynamic Changes

Figure 8a shows the annual global mean surface temperature response among all of the simulations, plotted as a function of associated instantaneous radiative forcing (RF), where RF is calculated from the expression 5.35ln (N x CO_2/1x CO_2) (Byrne and Goldblatt (2014)) and, for each run, N is the CO_2 multiple of the PI value (2.4, for the case of all SSP 2-4.5 ensemble members). The changes in GMST across this broader range of CO_2 forcing show the nonlinear behavior between the 2xCO_2 and 3xCO_2 FOM simulations (blue circles) that was first identified in Mitevski et al. (2021) (their Figure 1). By comparison, the results from the SOM experiments (aqua circles) show no evidence of a nonlinearity. This result was also documented in Mitevski et al. (2021) and suggests that the changes in ocean horizontal and vertical heat fluxes not included in the q-flux experiments are primarily responsible for the nonlinear changes in GMST occurring in the FOM experiments.

Building on Mitevski et al. (2021), here we also include the results from the SSP 2-4.5 R and C ensemble members (red circles, cyan and blue outlines) which are seen to align respectively with the SOM (solid cyan) and FOM (solid blue) scalings. This suggests that the GMST differences between the collapsed (C) versus recovered (R) SSP 2-4.5 ensemble members are primarily associated with the changes in ocean heat convergence occurring in the former. Note that the SSP 2-4.5 results are plotted with respect to the peak CO_2 level achieved (i.e. 643 ppm), which occurs at year 2200 (not at the values occurring during years 2400-2500, which are lower (579-598 ppm)) (Meinshausen et al. (2020)).

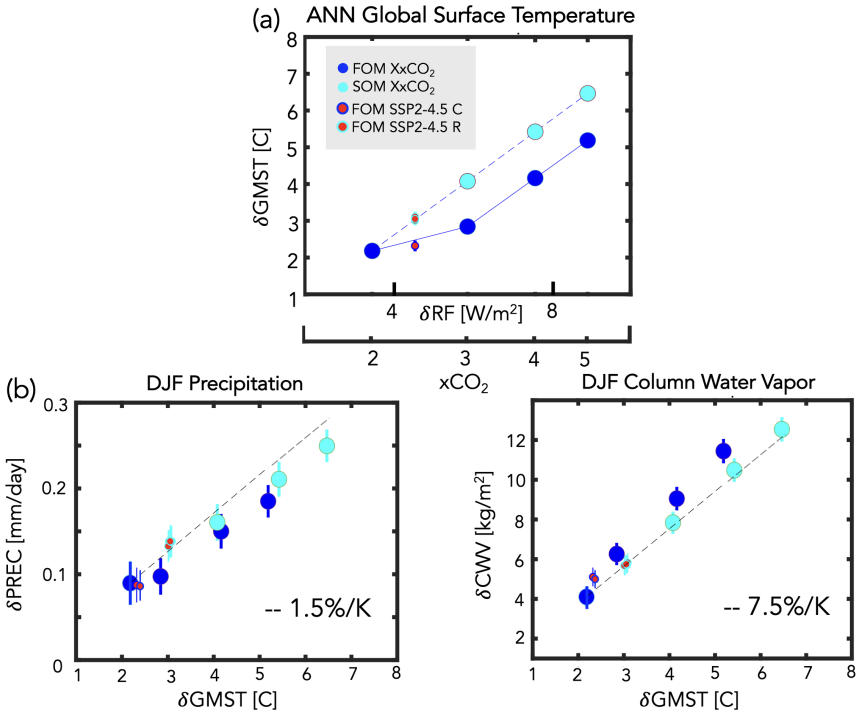

591 FIG. 8. Top: Changes in annual mean global mean surface temperature (GMST), plotted as a function of the
592 associated radiative forcing (RF), calculated from the expression 5.35ln ($NxCO_2/1xCO_2$) (Byrne and Goldblatt
593 (2014)) where, for each run, N is the CO_2 multiple of the PI value (2.4, for the case of the SSP 2-4.5 ensemble
594 members), consistent with the presentation in Mitevski et al. (2021). Bottom: Changes in DJF global mean
595 precipitation (left) and atmospheric column water vapor (right). Changes in precipitation and column water
596 vapor are plotted relative to the annual mean GMST changes in (a). Results from the abrupt 2-5xCO_2 fully
597 coupled atmosphere-ocean model (FOM) and slab ocean model (SOM) results are shown in the blue and cyan
598 filled circles. The FOM SSP 2-4.5 recovered (R) and collapsed (C) results are also shown in the red circles
599 (cyan and blue outlines, respectively). Interannual variability for each metric is indicated by the vertical bars.
600 Note that in all panels the SOM 2xCO_2 results have been adjusted to match the FOM 2xCO_2 results in order to
601 facilitate comparison of the FOM and SOM scalings with CO_2 and GMST, not on the absolute magnitude of the
602 responses.

611 Next we examine how changes in first-order thermodynamic variables scale with these (nonlinear)
612 changes in GMST. As with GMST, the changes in global mean precipitation and integrated column
613 water vapor (CWV) also vary nonlinearly with respect to radiative forcing in the FOM simulations
614 moving from 2xCO_2 to 3xCO_2 (Appendix Figure 2). As expected from the GMST changes, this

behavior is absent in the SOM integrations and the SSP 2-4.5 C and R members again align with the FOM and SOM scalings, respectively.

However, plotting the precipitation and CWV DJF changes relative to annual mean GMST, reveals that the nonlinear scaling with RF more-or-less disappears (Fig. 8b). This demonstrates that, while the first order global scale hydrological cycle is sensitive to the collapse of the AMOC, this sensitivity occurs primarily through changes in GMST. It is also interesting to note that the lower precipitation values occurring in the SOM integrations, for a given values of GMST, are consistent with the direct effect of greenhouse gases, which tend to suppress global mean precipitation (Samset et al. (2016)).

Finally, we note that the scaling of precipitation and CWV with GMST roughly follow the predictions from Held and Soden (2006), who identified a Clausius-Clapeyron (CC) scaling of integrated column water vapor (dashed black line denoting 7.5%/K, Fig. 8b, right) and a significantly sub-CC scaling of global mean precipitation (1.5%/K, Fig. 8b, left). While some additional nonlinearity in precipitation is also evident at higher CO_2 levels, as this is not immediately relevant to the SSP 2-4.5 ensemble, we reserve further discussion for future work.

2) Northern Hemisphere Dynamical Changes: A Regime Shift

Moving next to the dynamical response, we find that several measures of the NH DJF zonal mean dynamical circulation behave nonlinearly (and even non-monotonically) with respect to radiative forcing in the FOM simulations (Appendix Figure 3). Unlike precipitation and CWV, however, this non-linear behavior in the NH surface wind-based Hadley cell edge (Fig. 9a), Hadley Cell strength (Fig. 9b), northern midlatitude EKE (Fig. 9c), latitude of maximum eddy momentum fluxes (Fig. 9d) and northern midlatitude static stability (Fig. 9e) also occurs after plotting as a function of GMST. Overall, these results suggest that there is no clear (certainly not linear) relationship between the northern Hadley Cell (strength and lower tropospheric edge) and midlatitude jet behavior with GMST in simulations ((¿)3xCO_2 and SSP 2-4.5 C) in which the AMOC eventually collapses.

Rather, the changes in both the NH Hadley Cell edge and strength reflect an abrupt poleward shift and increase, respectively, moving from 2xCO_2 to 3xCO_2 and between the SSP 2-4.5 R and SSP 2-4.5 C ensemble members. This abrupt poleward shift and strengthening saturates at 3xCO_2 and even decreases at higher CO_2 values for certain metrics, despite continued increases in GMST (Fig.

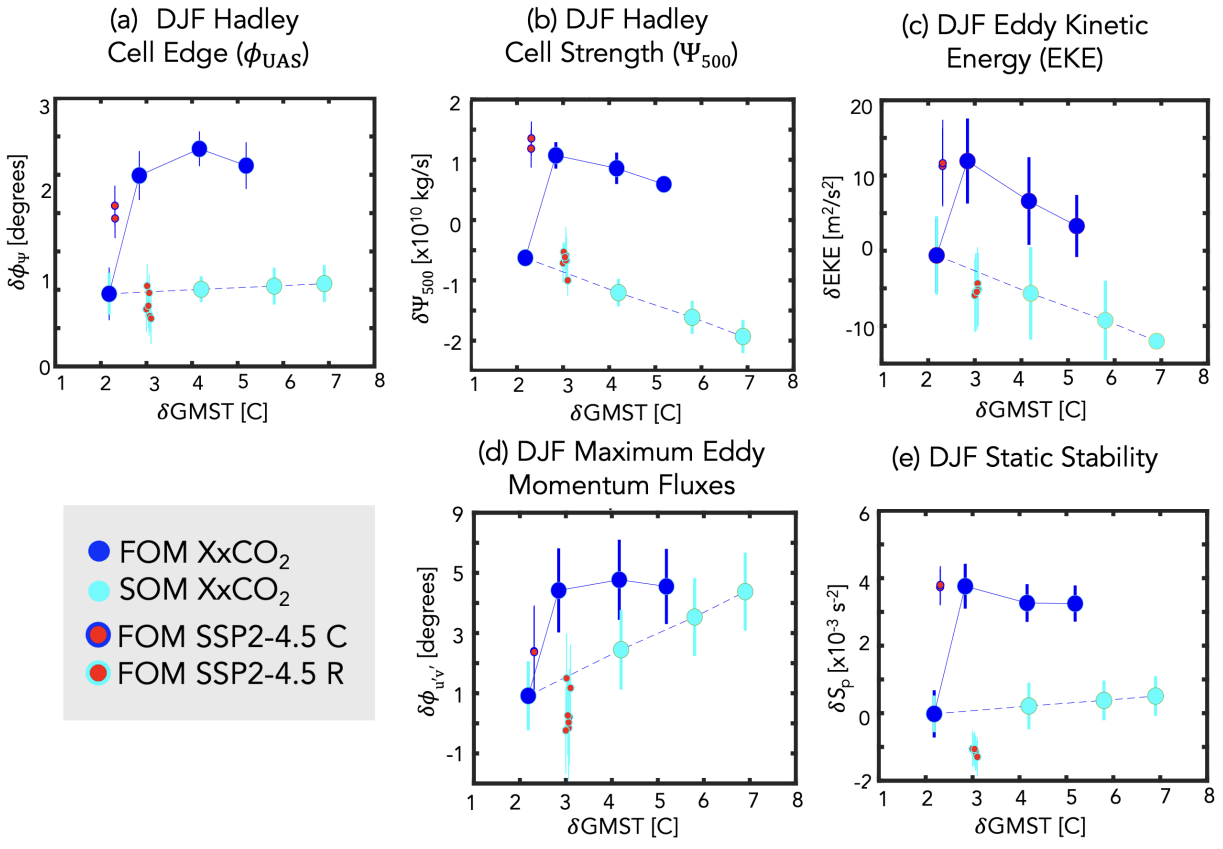

FIG. 9. Changes in various DJF Northern Hemisphere (NH) dynamical metrics, plotted as a function of GMST. Specifically, shown are the Hadley Cell edge (ϕ_{UAS}) (a), Hadley Cell strength (Ψ_{500}) (b), NH column eddy kinetic energy (EKE) (c), latitude of the maximum NH eddy momentum fluxes (d) and NH midlatitude dry static stability (e). The quantities in (a), (b) and (d) are defined in Section 2, while the zonally averaged EKE and static stability changes have both been averaged over 300-1000 hPa and 30°N-60°N. Results from the abrupt 2-5xCO$_2$ fully coupled atmosphere-ocean model (FOM) and slab ocean model (SOM) results are shown in the blue and cyan filled circles. The FOM SSP 2-4.5 recovered (R) and collapsed (C) ensemble members are shown in the red circles (cyan and blue outlines, respectively). Interannual variability for each metric is indicated by the vertical bars. As in Figure 8 the SOM 2xCO$_2$ results have been adjusted to match the FOM 2xCO$_2$ results.

9b, 9c). As such, this saturation in the NH circulation is indicative of a "regime" shift in our model, consistent with the use of the term in Caballero and Langen (2005), albeit for the low-gradient, high temperature regime identified in their study using a more idealized model (see discussion in Section 4). In particular, our results suggest that the AMOC collapse is associated with a regime shift in our model between a climate state in which the Hadley Cell is substantially weaker and

displaced equatorward (strong AMOC) and a state in which the Hadley Cell and midlatitude EKE is stronger and displaced poleward (weak AMOC).

Note that, while the increases in Hadley Cell strength (Fig. 9b) have been well documented, the poleward shift in the northern Hadley Cell edge has been less examined (Fig. 9a). Our examination of the Hadley Cell edge, as gauged using the surface zonal winds, is partly motivated by the results presented in Figure 3d, which show increased SLP over the North Pacific and Atlantic high latitudes. That is, the SLP increases over the North Atlantic extend as far south as 40°N and thus, together with the Pacific response, reflect a pattern which is consistent with the SLP pressure signature of an expanded northern edge of the Hadley cell (Schmidt and Grise (2017)). Another motivation comes from KB2021, who suggest that, in addition to reduced warming over the Arctic, stronger tropical heating and a related expansion of the HC may contribute to the poleward shift of the northern jet, although this was never explicitly shown.

The fact that changes in the Hadley Cell and midlatitude eddy-driven jet are linked is consistent with recent studies showing that the HC edge is strongly linked to the latitude of maximum eddy momentum fluxes, such that a poleward shift of the jet is associated with HC expansion (Chemke and Polvani (2019), Waugh et al. (2018), Menzel et al. (2019)). As discussed in those studies, this connection is likely associated with changes in the latitude of the maximum eddy momentum fluxes and the vertical potential temperature gradient (i.e., the static stability, $S_p = -(\frac{T}{\Theta})(\frac{\partial \Theta}{\partial P})$) over northern midlatitudes, which also exhibit regime shifts in the NH (Fig. 9 d-e). The sensitivity of the extratropical tropospheric eddy response to even modest changes in isentropic slope, resulting both from changes in baroclinicity and static stability, is well known (Thompson and Birner (2012)) and previous studies have shown that increases in static stability at higher CO_2 forcing can increase subtropical baroclinicity, causing the HC edge and subtropical eddy fields to shift poleward (Chemke and Polvani (2019); Menzel et al. (2019)). Note that the changes in EKE and static stability are shown averaged over 300-1000 hPa and over 30°N-60°N; similar results are found averaging over the entire hemisphere poleward of 20°N.

Another interesting feature highlighted in Figure 9 is that for some variables even the *sign* of the response is different than would otherwise be predicted from the SOM experiments which ignore changes in ocean heat convergence. This applies both to the changes in Hadley Cell strength (Fig. 9b) and tropospheric column averaged EKE (Fig. 9c) which otherwise decrease in response to

increasing CO_2. This role of the ocean in the behavior of projected changes in northern EKE is consistent with Chemke et al. (2022), who showed that changes in ocean heat convergence are essential for correctly capturing the sign of the projected response in future storm track changes over the North Atlantic.

To further relate the changes in the Hadley Cell to the changes in midlatitude eddies, Figure 10 shows the evolution of the response in northern HC strength (a), EKE (b), baroclinic eddy generation (c), and midlatitude static stability (d). While the HC strengthening may be more directly linked to the southward shift of the ITCZ as proposed in previous studies (Zhang et al. (2010)), the increases in dry static stability in the 3xCO_2 and SSP 2-4.5 C simulations evolve on a similar time scale as the changes in northern midlatitude tropospheric baroclinic eddies. The similar behavior among those variables suggests that they are mechanistically related. Furthermore, while changes in tropopause height have also been invoked to interpret future changes in the midlatitude jet stream (Cronin and Jansen (2016), Held (1993), Vallis et al. (2015)) and edge of the Hadley Cell (Lu et al. (2007)), we do not observe a consistent response in tropopause height between the 3xCO_2 and SSP 2-4.5 C integrations (not shown), suggesting that tropopause height changes alone are not the primary drivers of the Hadley Cell and jet behaviors exhibited in these runs.

Note that the similar evolution of the HC strength and midlatitude eddy changes suggested in Figure 10 may seem at odds with the findings in Menzel et al. (2019), who showed a strong disconnect between the strength of the subtropical jet and the edge of the Hadley Cell. However, there are some subtle differences in the evolution of those responses; furthermore, that study inferred this disconnect based on interannual variability and the response to an abrupt 4xCO_2 forcing, which both yield a weakening and poleward shift of the Hadley Cell. By comparison, in connection with a southward shifted ITCZ a collapse of the AMOC is associated with a strengthened Hadley Cell (Zhang and Delworth (2005); Orihuela-Pinto et al. (2022)).

c. Energetic Analysis: Bjerknes Compensation in Response to an AMOC Shutdown

The previous section showed that, unlike the global mean thermodynamic response, several measures of NH dynamical sensitivity do not scale linearly with changes in global mean surface temperature. Rather, a collapsed AMOC in our model is accompanied by an abrupt strengthening and northward shift of the Hadley Cell and northern midlatitude jet. To better understand why these

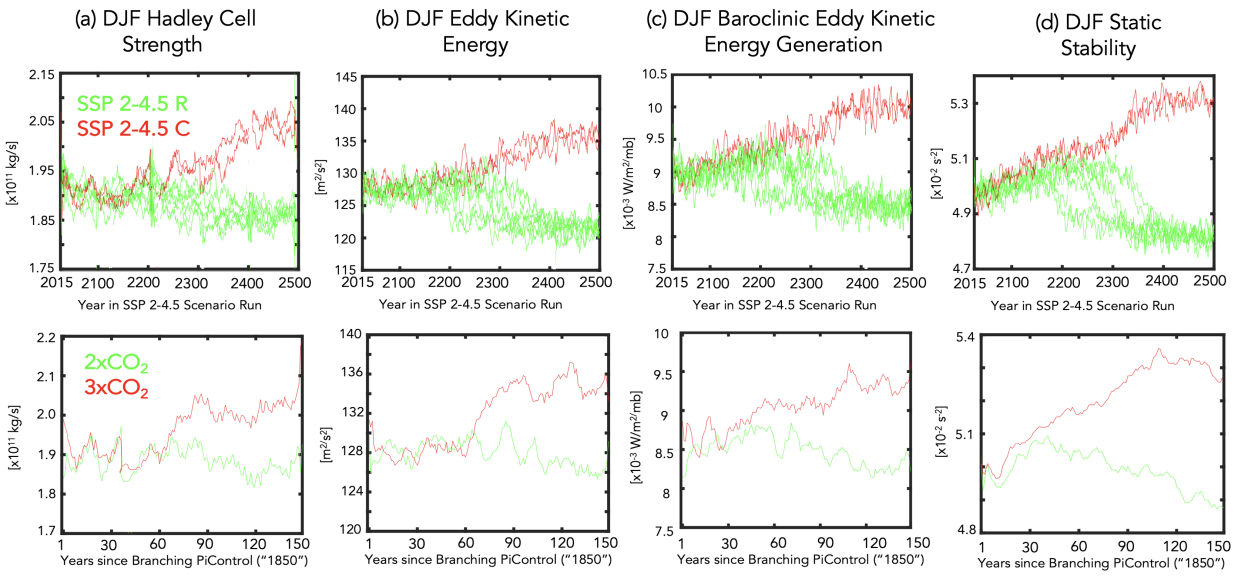

720 FIG. 10. Evolution of DJF Northern Hemisphere Hadley Cell strength (a), eddy kinetic energy (b), baroclinic
721 eddy kinetic energy generation (c) and midlatitude dry static stability (d). The baroclinic eddy generation has been
722 averaged over the same region (300-1000 hPa, 30°N-60°N) as the EKE and static stability fields, consistent with
723 Figure 9. Comparisons among the SSP 2-4.5 recovered (R) and collapsed (C) ensemble members (top panels)
724 and between the 2xCO_2 and 3xCO_2 runs (bottom panels) are shown in the green and red lines, respectively. A
725 5-year moving average has been applied to all time series.

717 variables exhibit this regime shift we examine the changes in energetics – and their partitioning
718 between the atmosphere and ocean – that arise moving from 2xCO_2 to 3xCO_2 and between the
719 SSP 2-4.5 R and SSP 2-4.5 C members.

726 ### 1) Ocean and Atmosphere Compensation

727 Figure 11 shows the response in the annual mean northward total (atmosphere + ocean), oceanic
728 and atmospheric transports, relative to the preindustrial control simulation. Between 2xCO_2 and
729 3xCO_2 and between the SSP 2-4.5 R and SSP 2-4.5 C members there is a large decrease/increase
730 in T_O/T_A over northern latitudes with a peak located at ~30-40°N. This behavior is reflective of an
731 abrupt Bjerknes compensation that emerges in the model, wherein large anomalies in heat trans-
732 ported by the atmosphere increase to approximately balance large reductions in northward ocean
733 transport (Bjerknes (1964)). More precisely, the reduction in northward ocean heat transport in
734 the SSP 2-4.5 C ensemble members and at 3xCO_2 is approximately 1 PW (Fig. 11), representing

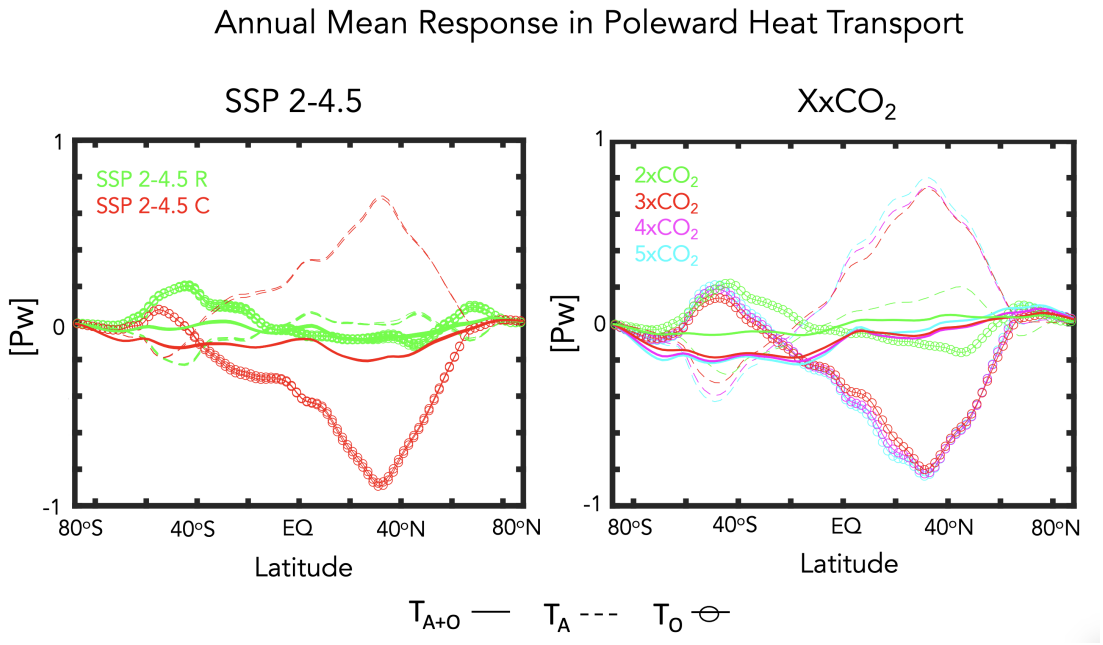

741 FIG. 11. Changes in the annual mean atmospheric (T_A), oceanic (T_O) and total (atmospheric + oceanic, T_{A+O})
742 northward energy transport, relative to the preindustrial control simulation. Results from the SSP 2-4.5 ensemble
743 members and the 2-5xCO_2 simulations are shown in the left and right panels. The simulations in which the
744 AMOC collapses (3xCO_2, SSP 2-4.5 C) versus recovers (2xCO_2, SSP 2-4.5 R) are highlighted in the red and
745 green lines, respectively.

735 a ~50% decrease relative to preindustrial values (Fig. 2b). Magnusdottir and Saravannan (1999)
736 attributed this compensatory response in the atmosphere to high dynamical efficiency of atmo-
737 spheric eddy transport. Note that the annual mean is shown here to facilitate comparison with the
738 annual mean results presented in previous studies (e.g., Figure 1 in Zhang and Delworth (2005)
739 and Figure 5 in Zhang et al. (2010)). We note in passing that the responses in the boreal winter
740 transports look very similar (not shown).

746 What Figure 11 makes clear is that the changes in ocean heat transport are dominated by the
747 changes in the AMOC, as reflected in the magnitude of the compensation occurring at 3xCO_2
748 (similar to the compensation occurring in the SSP 2-4.5 C ensemble) which saturates, despite
749 further increases in CO_2 (and GMST). This helps to explain the behavior of the dynamical indices
750 discussed in the previous section (Fig. 9), which also saturate at 3xCO_2 and do not increase
751 (rather, decrease) moving to higher CO_2 forcings. A dramatic reduction in poleward ocean heat

transport at ~30-40°N was also noted in the CMIP5 historical models in association with strong air-sea interactions within the midlatitude storm tracks (Outten et al. (2018)) and in several future climate integrations performed using the CMIP5 version of the GISS climate model (E2) Rind et al. (2018). In the latter case, however, the near cessation of the AMOC severely limited, but did not entirely shut off, poleward heat transport, which was partly maintained through the ocean subtropical gyre contribution. Our results also show stronger compensation occurring over SH high latitudes poleward of 40°S.

While the changes in T_O and T_A reflect near entire compensation, this compensation is nonetheless not perfect and slightly negative, resulting in a net reduction in the total northward combined atmospheric and oceanic energy transport. This reduction in net poleward energy transport was also found in Liu et al. (2020), who showed that a weakened AMOC caused a larger energy change at the Earth's surface than at the TOA (their Figure S.5). In particular, over the NAWH region they found that more energy was taken from the atmosphere through surface turbulent heat fluxes, resulting in a situation where the NH atmosphere loses more energy at the surface compared to the energy that is gained at the TOA (through reduced OLR). In the GISS model we also find that there is more energy loss at the surface compared to changes at the TOA and that these are primarily associated with reduced latent heat fluxes (Appendix Figure 4). The reductions in surface latent heat fluxes occur over the North Atlantic and are strongly shaped by changes in evaporation (not shown). The exact extent and nature of this compensation, however, is likely shaped strongly by cloud feedbacks (Zhang et al. (2010)) as discussed more in Section 4b.

2) Moist vs. Dry Atmospheric Transports

To better understand the nature of the compensation occurring in the GISS model, Figure 12 further decomposes the changes in T_A into changes in the northward transports of latent heat (Fig. 12a) and dry static energy (Fig. 12b). Over the SH the changes in dry and moist static energy nearly compensate in all simulations, resulting in weakly negative northward atmospheric transports poleward of ~40°S in both the $XxCO_2$ and SSP 2-4.5 runs. Equatorward of ~40°S, however, this behavior transitions in the SSP 2-4.5 C members to net positive northward atmospheric transport from the SH subtropics towards and across the equator (which compensates the reduction in oceanic equatorward heat transport in that region evident in Figure 11). This behavior over the SH

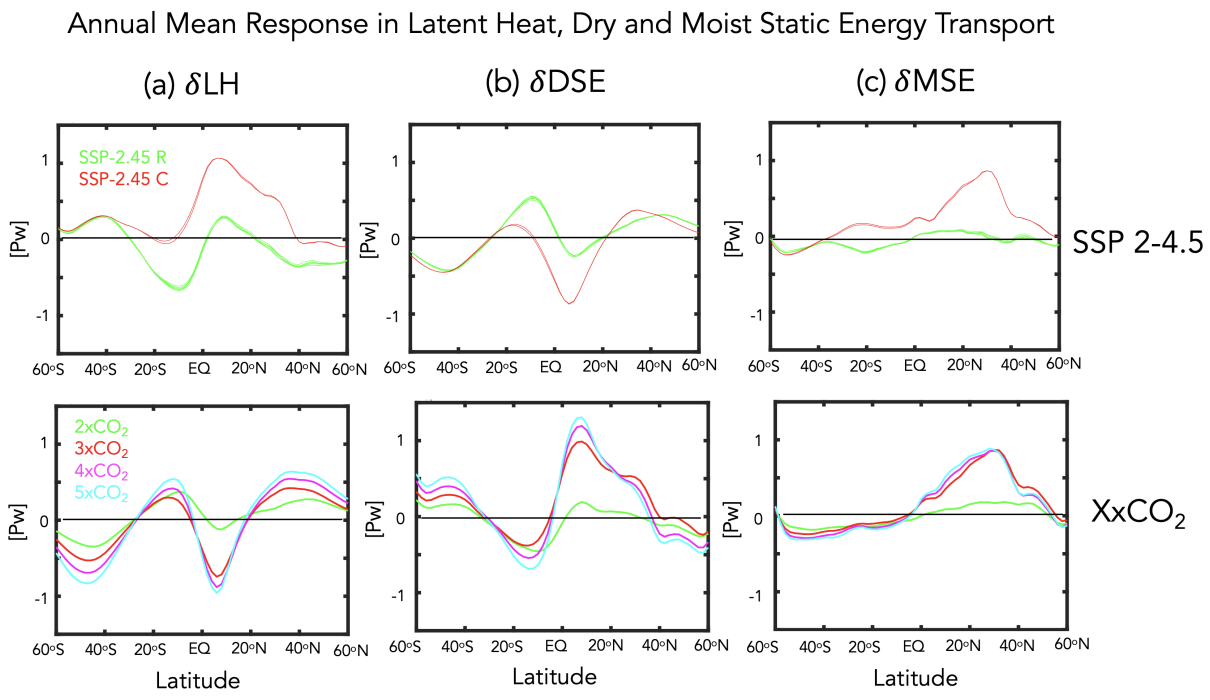

FIG. 12. Changes in the annual mean atmospheric latent heat (a), dry static energy (b) and total moist static energy (c) northward transports, relative to the preindustrial control simulation. Results from the SSP 2-4.5 ensemble members and the 2-5xCO_2 simulations are shown in the top and bottom panels. The simulations in which the AMOC collapses (3xCO_2, SSP 2-4.5 C) versus recovers (2xCO_2, SSP 2-4.5 R) are highlighted in the red and green lines, respectively.

subtropics is distinct from what occurs in the XxCO_2 simulations, in which there is overall reduced northward atmospheric transport (and less compensation by the oceanic transports). The fact that the oceanic compensation in this region is weaker at 3xCO_2 (relative to the SSP 2-4.5 C members) may reflect the differences in simulation length between the abrupt CO_2 and SSP 2-4.5 integrations or the fact that at 3xCO_2 there is increased water vapor in the atmosphere in the warmer climate and hence increased poleward latent heat transport. Notably, however, the AMOC response in all runs has little effect on extratropical latent heat transport over the Southern Hemisphere extratropics.

Aside from the subtle differences between the 3xCO_2 and SSP 2-4.5 C runs that occur over the SH subtropics, the fact that the changes in dry static energy (DSE) and latent heat transport nearly compensate over southern and tropical latitudes in all runs is consistent with the expectation from Held and Soden (2006). Interestingly, however, this compensation does not occur over northern latitudes spanning ~10°N to ~40°N, resulting in a net increase in poleward moist static energy

transport (Fig. 12c). Over these latitudes the increased atmospheric energy transport resulting from an AMOC collapse is almost entirely due to changes in dry static energy, not latent heat transport. In particular, DSE transport exhibits a "jump" between $2xCO_2$ and $3xCO_2$ (also evident in the differences between the SSP 2-4.5 C and SSP 2-4.5 R members) (Fig. 12b); a similar jump is only evident in the latent heat transports equatorward of 20°N (which, if anything, enhances energy transport equatorward, not poleward). The jump in DSE transport over the northern extratropics saturates for forcings greater than $3xCO_2$. Further analysis of the evolution of the dry static energy transports at different latitudes in the northern hemisphere (not shown) reveals that these changes in DSE transport first emerge between 30°N-40°N and propagate thereafter to higher latitudes.

The fact that the abrupt increase in atmospheric poleward transport derives primarily from changes in DSE transport helps in interpreting why a similar shift emerges in the Hadley Cell and eddy-driven jet, since the Hadley cell fluxes dry static energy poleward (Frierson et al. (2007)). Indeed, previous energetic definitions of the storm track have appealed directly to DSE (e.g. latitude of maximum vertically-integrated dry static energy flux (Hoskins and Valdes (1990)). More recently, Lachmy and Shaw (2018) show that the vertically integrated eddy potential energy flux shifts in same sense as the vertically integrated eddy DSE flux. They then use the Eliassen-Palm flux relation to connect these changes in energy fluxes to changes in the eddy momentum fluxes. Therefore, the fact that these features all shift in concert with each other in our runs should perhaps not be too surprising.

4. Discussion

a. Caveats Concerning Model Biases

One important caveat with our results relates to known biases in vertical mixing in the ocean component of the GISS model, as discussed in Miller et al. (2021). This biased mixing is likely related to why E2.1 exhibits a more sensitive AMOC response to a quadrupling of CO_2, compared to some other CMIP6 models (KB2021). In addition, Rind et al. (2020) showed that the parameterization of rainfall evaporation associated with moist convective precipitation has a strong influence on the AMOC sensitivity to greenhouse gas forcing in the E2.1 (and higher top E2.2) models, likely via its effect on moisture loading in the atmosphere. Thus, in addition to oceanic processes, atmospheric parameterizations could also be influencing this result.

Along with biases in vertical mixing, the ocean component of E2.1 is also low resolution (one degree). This likely has direct implications for the stability of the AMOC, as discussed in AR2023 (see references therein). In particular, the stability of the AMOC will differ between low resolution climate models, which exhibit a negative salt-advection feedback (leading to salinification of the subpolar gyre and AMOC recovery), and eddy-permitting models, which tend to exhibit a stable AMOC-off state. We emphasize here, however, that throughout we have focused on the response of the atmospheric circulation given a collapse in the AMOC. Thus, while the particular mechanisms by which the AMOC is weakened (and subsequently recovers) in E2.1 may be model-specific, our focus has been on quantifying the atmospheric changes. We also note that Mitevski et al. (2021) showed that the behavior of the AMOC in E2.1 was similar to the response in CESM-LE; furthermore that model also featured a nonlinear response in GMST related to a collapse of the AMOC, albeit one occurring at the transition between $3xCO_2$ and $4xCO_2$.

b. Bjerknes Compensation: Cloud Feedbacks and Dry Versus Moist Energy Transports

A key result from our study is that a collapse of the AMOC results in a regime shift in various components of the NH large-scale circulation and this shift is reflective of an abrupt Bjerknes compensation that emerges at $3xCO_2$ and in the SSP 2-4.5 C ensemble members. There are several aspects of this compensation, however, that require closer examination. Among others, these include:

1) Influence of Cloud Feedbacks

Mitevski et al. (2022) showed that nonlinearity in ECS occurring between $2xCO_2$ and $3xCO_2$ in our model was related to nonlinear variations in the atmospheric feedback parameter and not to changes in radiative forcing. At the same time, the strength of the Bjerknes compensation in our model will likely depend on cloud feedbacks, as the right-hand-side of Equation (1) makes clear (via the F_T and F_S terms). For example, Zhang et al. (2010) showed a strong sensitivity of the tropical climates' response to a freshwater hosing forcing to changes in cloud feedbacks, showing that in a model with no cloud feedbacks the tropical response to the weakening of the AMOC (including its southward ITCZ shift) was much smaller. Thus, while the overall Bjerknes compensation occurring in our model is generally consistent (in its meridional distribution and

amplitude) with the results from other similar studies, the exact details of how compensation occurs is likely to be sensitive to local climate feedbacks which may be model-dependent and/or poorly constrained by observations. Future work will focus on better understanding how changes in cloud feedbacks modulate the response of the atmosphere to a weakened AMOC in our model.

2) Atmospheric Dry vs. Moist Compensation

One interesting result from this study is that the large compensation in poleward atmospheric transport that occurs as the AMOC collapses is primarily related to increases in the northward transport of dry static energy poleward of 20°N (coincident with the edge of the non-monotonically shifting HC edge) (Fig. 12). This result is initially surprising as it downplays the compensation that occurs through changes in latent heat transport over northern midlatitudes. Thus, while our results do show a compensatory latent heat transport occurring in the tropics, this does not occur over the NH extratropics and is therefore not fundamentally associated with the non-monotonic behavior in the NH Hadley Cell edge and midlatitude eddy-driven jet.

The diminished importance of the latent heat transports over northern midlatitudes is initially surprising, given that warming in response to increased CO_2 results in an overall increase in atmospheric water vapor. Upon further reflection, however, this effect of enhanced global warming needs to be considered in the context of both the reduced Arctic warming and poleward shifted EKE evident in Figure 4. The former can, via cooling, reduce the total moisture available for northward transport, while the latter would impact the efficiency with which subtropical moisture is transported poleward to higher latitudes. In our results it appears that these changes compensate, resulting in no net AMOC imprint on the latent heat transports over northern extratropical latitudes (Fig. 10a, bottom). While disentangling these contributions is beyond the scope of this study, we do comment on the consistent results shown in Figure S5 of Mitevski et al. (2021), who identified a much stronger non-monotonicity present in the edge of the dry zone (P-E) compared to NH specific humidity. While this suggests that the circulation changes are themselves responsible for the behavior of the latent heat transports (and not vice versa), more work is needed to understand the underlying mechanism present in our model and whether this behavior is also exhibited in other models (or the real atmosphere).

5. Conclusions

Here we have documented the atmospheric response to a CO_2-induced AMOC collapse using the CMIP6 version of the NASA GISS climate model (E2.1). Using simulations from an identically forced (SSP 2-4.5) ensemble in which the AMOC collapses and recovers in two and eight members, respectively, we have isolated the atmospheric response to a spontaneous collapse of the AMOC in the context of a warming climate, absent any external perturbations that may interfere with the model's internal dynamics. By comparison, previous studies have all needed to employ (negative) freshwater flux perturbations or similar AMOC "locking" methods (Liu et al. (2020), Orihuela-Pinto et al. (2022)). We then placed the atmospheric response in the SSP 2-4.5 simulations in the broader context of a set of integrations in which CO_2 is abruptly increased, run both using fully coupled atmosphere-ocean (FOM) and slab-ocean (SOM) configurations, in which changes in ocean heat flux convergences are respectively included and neglected.

Our main results are as follows:

- In our model a sustained decline and eventual collapse of the AMOC results in a strengthening of the NH Hadley cell and the northern midlatitude jet, as well as an abrupt northward shift of the Hadley Cell edge in the lower troposphere. Quite remarkably, these features dominate the large-scale atmospheric circulation response that occurs in the NH moving from 2xCO_2 to 3xCO_2.

- For certain variables (i.e., HC strength, EKE) an ultimate collapse of the AMOC produces changes that are *opposite* in sign to the response to increased CO_2 forcing occurring in the absence of ocean circulation changes.

- The regime shift in the NH large-scale circulation reflects an abrupt Bjerknes compensation that emerges in the 3xCO_2 and collapsed SSP 2-4.5 C simulations. This compensation is located further south (~40°N) of what is often considered to be the main region of maximum ocean-atmosphere compensation (70°N) (Shaffrey and Sutton (2006)) and reflects a key role for the midlatitude storm tracks in the coupled system's response to a warmer climate.

- The impact of the AMOC on the large-scale NH circulation occurs mainly through its influence on mean free-tropospheric temperature gradients, not GMST. This finding reinforces growing evidence that the climate's "dynamical sensitivity" does not scale with equilibrium climate sensitivity (Grise and Polvani (2016), Ceppi et al. (2018)), particularly in the presence of a collapsed AMOC .

The regime shift in NH dynamics resulting from an AMOC collapse in our model is, to the best of our knowledge, the first time that such behavior has been documented for a CMIP class model. While previous studies have also reported nonlinear behaviors in Hadley Cell strength (Levine and Schneider (2011), O'Reilly et al. (2016)) these studies have employed mainly idealized models. In addition to the changes in the Hadley Cell we also identify a regime shift in the behavior of the northern storm tracks. This result brings to mind the findings from Caballero and Langen (2005), who showed that poleward energy transport increases over a range of increasing surface temperature but saturates in the low-gradient, high temperature regime. As in our study, they attribute this "low-gradient" paradox to increasing tropospheric static stability and the poleward migration of the storm tracks. However, they too employed a highly idealized (aquaplanet) model and find that this saturation in storm track behavior is related to a saturation of latent heat transport. Our results, by comparison, highlight the role of compensatory dry static energy transports and suggests that studies accounting for dynamic ocean-atmospheric coupling (i.e., changes in vertical and horizontal ocean heat fluxes) may come to different conclusions about the nature of compensation in the atmosphere.

In addition to contributing to improved understanding of the coupled atmosphere-ocean response to a weakening of the AMOC, our results also have a practical implication for the purpose of developing storylines of atmospheric circulation changes (Zappa and Shepherd (2017)) and for interpreting model differences in projected storm tracks. In particular, while the use of "global warming levels" applied throughout the IPCC AR6 report may suffice for understanding the global hydrological cycle (Hausfather et al. (2022)) here we have shown that this does not hold true for projections of the NH jet stream and Hadley Cell edge. This underscores the need to understand the direct impact of the AMOC on meridional temperature gradients and not only on surface temperature.

Finally, preliminary analysis of the high-top GISS climate model (E2.2 (Rind et al. (2020), Orbe et al. (2020)) suggests a different sensitivity of the AMOC compared to E2.1 (occurring between $3xCO_2$ and $4xCO_2$). Understanding these differences and how they are reflected in different Bjerknes compensations will be described in a follow-up paper.

Acknowledgments. C.O. thanks Ivan Mitevski for processing the zonally varying eddy kinetic energy fields that were used as part of this analysis. Climate modeling at GISS is supported by the NASA Modeling, Analysis and Prediction program, and resources supporting this work were provided by the NASA High-End Computing (HEC) Program through the NASA Center for Climate Simulation (NCCS) at Goddard Space Flight Center.

Data availability statement. The CMIP6 SSP 2-4.5 data used in this study is available from the Earth System Grid Federation (ESGF) (`https://esgf-node.llnl.gov/search/cmip6/`) or from the NASA Center for Climate Simulations (NCCS) (`https://portal.nccs.nasa.gov/datashare/giss/cmip6/`). The specific simulations used here are a subset of the historical r[1-10]i1p1f2 (`doi:87010.22033/ESGF/CMIP6.7127`) and SSP 2-4.5 r[1-10]i1p1f2 (`doi:10.22033/ESGF/CMIP6.7415`) runs. The $XxCO_2$ data used to produce the figures in the study is publicly available in a Zenodo repository at `https://doi.org/10.5281/zenodo.3901624`. The authors acknowledge the World Climate Research Programme's Working Group on Coupled Modeling and we thank all climate modeling groups for making available their model output. All GISS ModelE components are open source and available at `https://www.giss.nasa.gov/tools/modelE/`.

APPENDIX

Appendix Figures

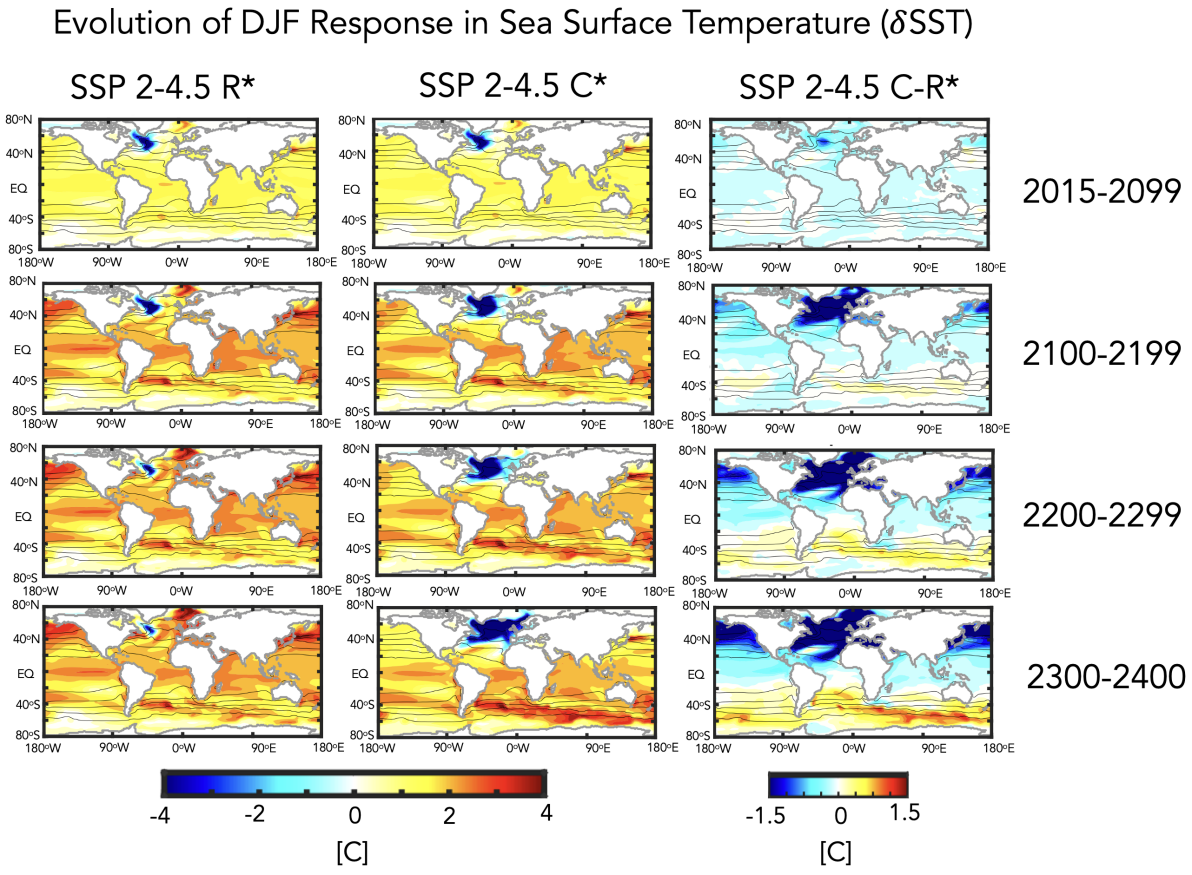

962 FIG. A1. The evolution of the DJF sea surface temperature difference, relative to the preindustrial control
963 simulation, in one of the SSP 2-4.5 recovered (R) (left) and collapsed (C) ensemble members (middle). The
964 difference between the SSP 2-4.5 recovered and collapsed ensemble members is also shown (right). Note that
965 only one ensemble member is used due to the different recovery times of the AMOC among the "recovered"
966 ensemble members prior to year 2400. Climatological mean values from the preindustrial control simulation are
967 denoted in the black contours.

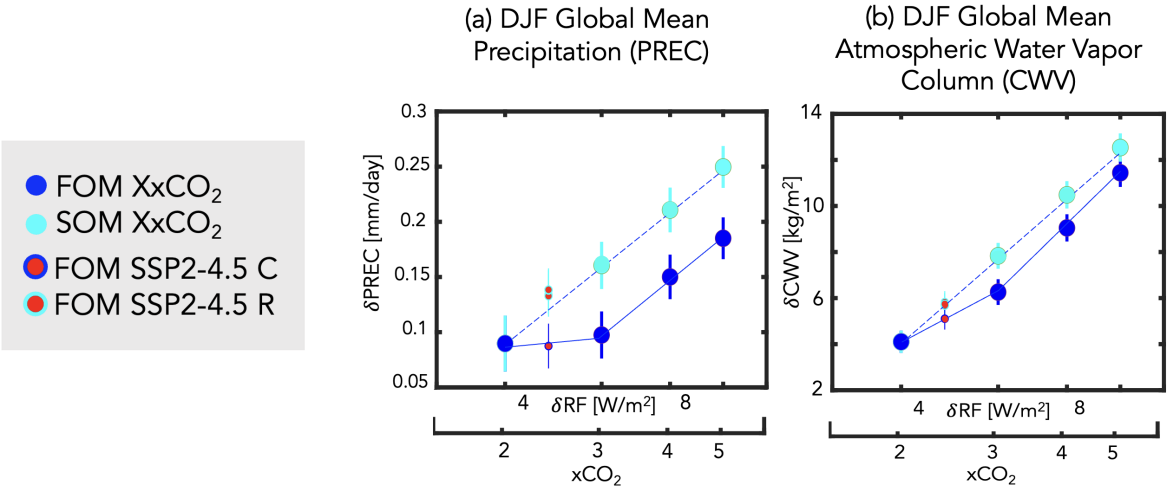

FIG. A2. Changes in DJF global mean precipitation (a) and atmospheric column water vapor (b), plotted as a function of the associated radiative forcing (RF), calculated from the expression 5.35ln ($NxCO_2/1xCO_2$) (Byrne and Goldblatt (2014)) where, for each run, N is the CO_2 multiple of the PI value (2.4, for the case of the SSP 2-4.5 ensemble members). Results from the abrupt 2-5xCO_2 fully coupled atmosphere-ocean model (FOM) and slab ocean model (SOM) results are shown in the blue and cyan filled circles. The FOM SSP 2-4.5 recovered and collapsed ensemble members are also shown in the red circles (cyan and blue outlines, respectively). Interannual variability for each metric is indicated by the vertical bars.

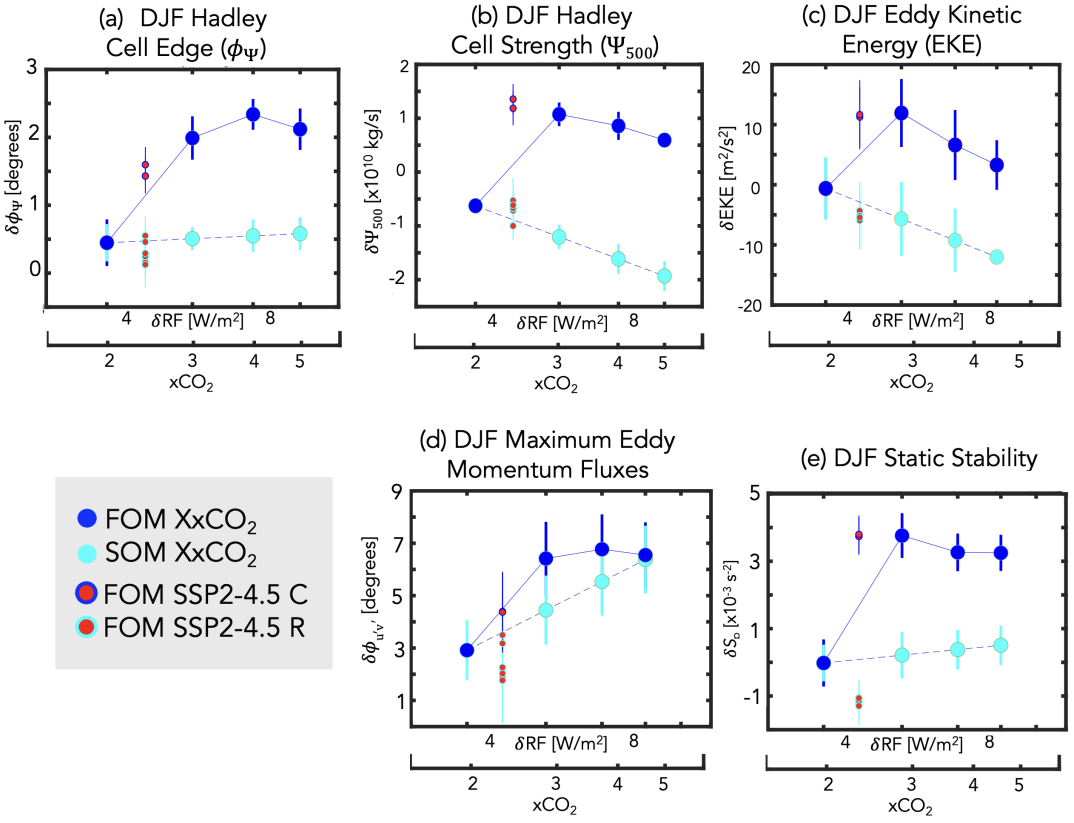

FIG. A3. Changes in various DJF Northern Hemisphere (NH) dynamical metrics, plotted as a function of associated radiative forcing. Specifically, shown are the Hadley Cell edge (ϕ_{UAS}) (a), Hadley Cell strength (Ψ_{500}) (b), NH column eddy kinetic energy (EKE) (c), latitude of the maximum NH eddy momentum fluxes (d) and NH midlatitude dry static stability (e). The quantities in (a), (b) and (d) are defined in Section 2, while the zonally averaged EKE and static stability changes have both been averaged over 300-1000 hPa and 30°N-60°N. Results from the abrupt 2-5xCO_2 fully coupled atmosphere-ocean model (FOM) and slab ocean model (SOM) results are shown in the blue and cyan filled circles. The FOM SSP 2-4.5 recovered and collapsed ensemble members are shown in the red circles (cyan and blue outlines, respectively). Interannual variability for each metric is indicated by the vertical bars.

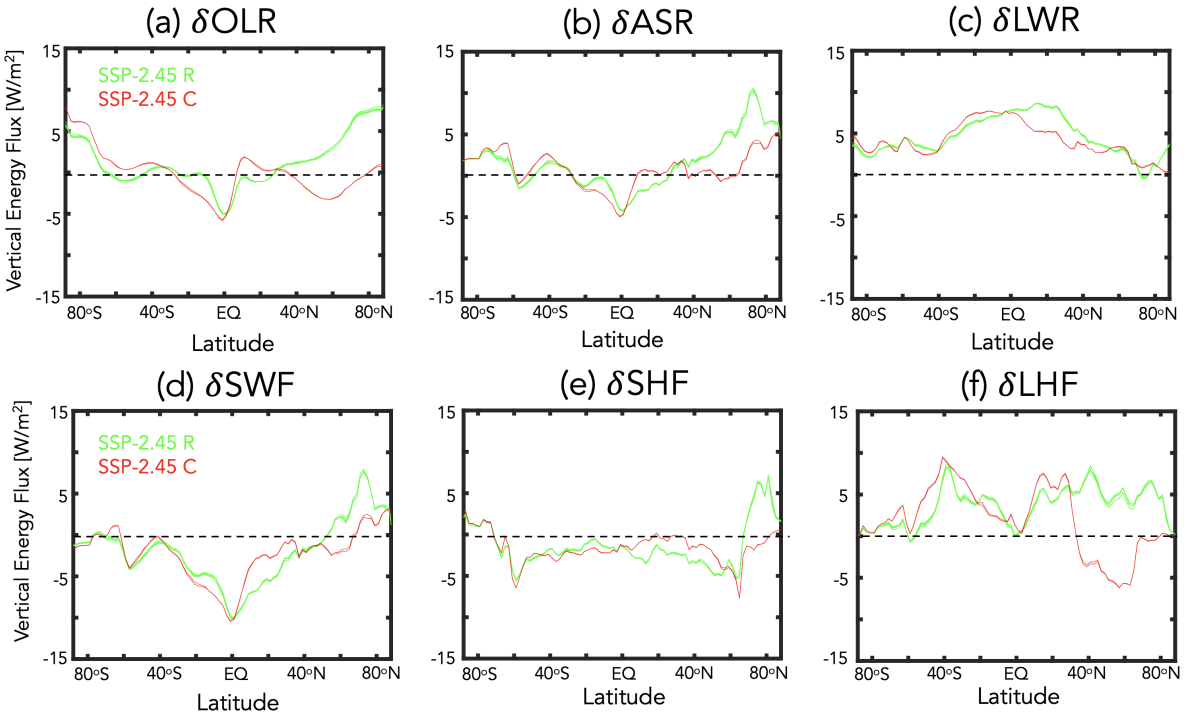

FIG. A4. Changes in the annual mean top of the atmosphere outgoing longwave radiation (OLR) (a) and absorbed shortwave radiation (ASR) (b) and the downward fluxes of radiation at the surface, decomposed into longwave (LWF) (c) and shortwave (SWF) (d) components. The fluxes of latent and sensible heat at the surface (LHF and SHF) are shown in (e) and (f), respectively. All changes are shown for the SSP 2-4.5 collapsed (C) (red) and SSP 2-4.5 recovered (R) (green) ensemble members and are defined relative to the preindustrial control simulation.

References

Adam, O., and Coauthors, 2018: The TropD software package (v1): standardized methods for calculating tropical-width diagnostics. *Geoscientific Model Development*, **11 (10)**, 4339–4357.

Bellomo, K., M. Angeloni, S. Corti, and J. von Hardenberg, 2021: Future climate change shaped by inter-model differences in Atlantic meridional overturning circulation response. *Nature Communications*, **12 (1)**, 1–10.

Bjerknes, J., 1964: Atlantic air-sea interaction. *Advances in geophysics*, Vol. 10, Elsevier, 1–82.

Brayshaw, D. J., T. Woollings, and M. Vellinga, 2009: Tropical and extratropical responses of the North Atlantic atmospheric circulation to a sustained weakening of the MOC. *Journal of Climate*, **22 (11)**, 3146–3155.

Byrne, B., and C. Goldblatt, 2014: Radiative forcing at high concentrations of well-mixed greenhouse gases. *Geophysical Research Letters*, **41 (1)**, 152–160.

Caballero, R., and P. L. Langen, 2005: The dynamic range of poleward energy transport in an atmospheric general circulation model. *Geophysical Research Letters*, **32 (2)**.

Caesar, L., S. Rahmstorf, A. Robinson, G. Feulner, and V. Saba, 2018: Observed fingerprint of a weakening Atlantic ocean overturning circulation. *Nature*, **556 (7700)**, 191–196.

Ceppi, P., G. Zappa, T. G. Shepherd, and J. M. Gregory, 2018: Fast and slow components of the extratropical atmospheric circulation response to CO_2 forcing. *Journal of Climate*, **31 (3)**, 1091–1105.

Chemke, R., and L. M. Polvani, 2019: Exploiting the abrupt $4\times$ CO_2 scenario to elucidate tropical expansion mechanisms. *Journal of Climate*, **32 (3)**, 859–875.

Chemke, R., L. Zanna, C. Orbe, L. T. Sentman, and L. M. Polvani, 2022: The future intensification of the North Atlantic winter storm track: the key role of dynamic ocean coupling. *Journal of Climate*, **35 (8)**, 2407–2421.

Cheng, W., J. C. Chiang, and D. Zhang, 2013: Atlantic meridional overturning circulation (AMOC) in CMIP5 models: RCP and historical simulations. *Journal of Climate*, **26 (18)**, 7187–7197.

Cronin, T. W., and M. F. Jansen, 2016: Analytic radiative-advective equilibrium as a model for high-latitude climate. *Geophysical Research Letters*, **43 (1)**, 449–457.

Deser, C., and A. S. Phillips, 2009: Atmospheric circulation trends, 1950–2000: The relative roles of sea surface temperature forcing and direct atmospheric radiative forcing. *Journal of Climate*, **22 (2)**, 396–413.

Drijfhout, S., G. J. Van Oldenborgh, and A. Cimatoribus, 2012: Is a decline of AMOC causing the warming hole above the North Atlantic in observed and modeled warming patterns? *Journal of Climate*, **25 (24)**, 8373–8379.

Frierson, D. M., I. M. Held, and P. Zurita-Gotor, 2007: A gray-radiation aquaplanet moist GCM. Part II: Energy transports in altered climates. *Journal of the Atmospheric Sciences*, **64 (5)**, 1680–1693.

Gervais, M., J. Shaman, and Y. Kushnir, 2019: Impacts of the North Atlantic warming hole in future climate projections: Mean atmospheric circulation and the North Atlantic jet. *Journal of Climate*, **32 (10)**, 2673–2689.

Grise, K. M., and L. M. Polvani, 2014: The response of midlatitude jets to increased co2: Distinguishing the roles of sea surface temperature and direct radiative forcing. *Geophysical Research Letters*, **41 (19)**, 6863–6871.

Grise, K. M., and L. M. Polvani, 2016: Is climate sensitivity related to dynamical sensitivity? *Journal of Geophysical Research: Atmospheres*, **121 (10)**, 5159–5176.

Grise, K. M., and L. M. Polvani, 2017: Understanding the time scales of the tropospheric circulation response to abrupt co2 forcing in the southern hemisphere: Seasonality and the role of the stratosphere. *Journal of Climate*, **30 (21)**, 8497–8515.

Haarsma, R., F. Selten, and S. Drijfhout, 2015: Decelerating Atlantic meridional overturning circulation main cause of future west european summer circulation changes. *Environmental Research Letters*, **10 (9)**.

Hausfather, Z., K. Marvel, G. A. Schmidt, J. W. Nielsen-Gammon, and M. Zelinka, 2022: Climate simulations: Recognize the 'hot model'problem. Nature Publishing Group.

Held, I. M., 1993: Large-scale dynamics and global warming. *Bulletin of the American Meteorological Society*, **74 (2)**, 228–242.

Held, I. M., and B. J. Soden, 2006: Robust responses of the hydrological cycle to global warming. *Journal of climate*, **19 (21)**, 5686–5699.

Hoskins, B. J., and P. J. Valdes, 1990: On the existence of storm-tracks. *Journal of Atmospheric Sciences*, **47 (15)**, 1854–1864.

Jackson, L., R. Kahana, T. Graham, M. Ringer, T. Woollings, J. Mecking, and R. Wood, 2015: Global and european climate impacts of a slowdown of the AMOC in a high resolution GCM. *Climate Dynamics*, **45 (11)**, 3299–3316.

James, R., R. Washington, C.-F. Schleussner, J. Rogelj, and D. Conway, 2017: Characterizing half-a-degree difference: a review of methods for identifying regional climate responses to global warming targets. *Wiley Interdisciplinary Reviews: Climate Change*, **8 (2)**, e457.

Josey, S. A., J. J.-M. Hirschi, B. Sinha, A. Duchez, J. P. Grist, and R. Marsh, 2018: The recent Atlantic cold anomaly: Causes, consequences, and related phenomena. *Annual Review of Marine Science*, **10**, 475–501.

Kelley, M., and Coauthors, 2020: GISS-E2. 1: Configurations and climatology. *Journal of Advances in Modeling Earth Systems*, **12 (8)**, e2019MS002 025.

Lachmy, O., and T. Shaw, 2018: Connecting the energy and momentum flux response to climate change using the Eliassen-Palm relation. *Journal of Climate*, **31 (18)**, 7401–7416.

Lau, N.-C., H. Tennekes, and J. M. Wallace, 1978: Maintenance of the momentum flux by transient eddies in the upper troposphere. *Journal of Atmospheric Sciences*, **35 (1)**, 139–147.

Levine, X. J., and T. Schneider, 2011: Response of the Hadley circulation to climate change in an aquaplanet GCM coupled to a simple representation of ocean heat transport. *Journal of the Atmospheric Sciences*, **68 (4)**, 769–783.

Lim, G. H., and J. M. Wallace, 1991: Structure and evolution of baroclinic waves as inferred from regression analysis. *Journal of Atmospheric Sciences*, **48 (15)**, 1718–1732.

Liu, W., A. V. Fedorov, S.-P. Xie, and S. Hu, 2020: Climate impacts of a weakened Atlantic Meridional Overturning Circulation in a warming climate. *Science Advances*, **6 (26)**, eaaz4876.

Lu, J., G. A. Vecchi, and T. Reichler, 2007: Expansion of the Hadley cell under global warming. *Geophysical Research Letters*, **34 (6)**.

Magnusdottir, G., and R. Saravannan, 1999: The response of atmospheric heat transport to zonally-averaged SST trends. *Tellus A: Dynamic Meteorology and Oceanography*, **51 (5)**, 815–832.

Marshall, J., J. R. Scott, K. C. Armour, J.-M. Campin, M. Kelley, and A. Romanou, 2015: The ocean's role in the transient response of climate to abrupt greenhouse gas forcing. *Climate Dynamics*, **44 (7)**, 2287–2299.

Meinshausen, M., and Coauthors, 2020: The shared socio-economic pathway (SSP) greenhouse gas concentrations and their extensions to 2500. *Geoscientific Model Development*, **13 (8)**, 3571–3605.

Menary, M. B., and R. A. Wood, 2018: An anatomy of the projected North Atlantic warming hole in CMIP5 models. *Climate Dynamics*, **50 (7)**, 3063–3080.

Menzel, M. E., D. Waugh, and K. Grise, 2019: Disconnect between Hadley cell and subtropical jet variability and response to increased CO_2. *Geophysical Research Letters*, **46 (12)**, 7045–7053.

Miller, R. L., and Coauthors, 2021: CMIP6 historical simulations (1850–2014) with GISS-E2. 1. *Journal of Advances in Modeling Earth Systems*, **13 (1)**, e2019MS002 034.

Mitevski, I., C. Orbe, R. Chemke, L. Nazarenko, and L. M. Polvani, 2021: Non-monotonic response of the climate system to abrupt CO_2 forcing. *Geophysical Research Letters*, **48 (6)**, e2020GL090 861.

Mitevski, I., L. M. Polvani, and C. Orbe, 2022: Asymmetric warming/cooling response to CO_2 increase/decrease mainly due to non-logarithmic forcing, not feedbacks. *Geophysical Research Letters*, **49 (5)**, e2021GL097 133.

Nazarenko, L. S., and Coauthors, 2022: Future climate change under SSP emission scenarios with GISS-E2. 1. *Journal of Advances in Modeling Earth Systems*, e2021MS002871.

Orbe, C., and Coauthors, 2020: GISS model E2. 2: A climate model optimized for the middle atmosphere—2. Validation of large-scale transport and evaluation of climate response. *Journal of Geophysical Research: Atmospheres*, **125 (24)**, e2020JD033 151.

O'Reilly, C. H., M. Huber, T. Woollings, and L. Zanna, 2016: The signature of low-frequency oceanic forcing in the Atlantic Multidecadal Oscillation. *Geophysical Research Letters*, **43 (6)**, 2810–2818.

Orihuela-Pinto, B., M. H. England, and A. S. Taschetto, 2022: Interbasin and interhemispheric impacts of a collapsed Atlantic Overturning Circulation. *Nature Climate Change*, 1–8.

Outten, S., I. Esau, and O. H. Otterå, 2018: Bjerknes compensation in the CMIP5 climate models. *Journal of Climate*, **31 (21)**, 8745–8760.

Pedro, J. B., M. Jochum, C. Buizert, F. He, S. Barker, and S. O. Rasmussen, 2018: Beyond the bipolar seesaw: Toward a process understanding of interhemispheric coupling. *Quaternary Science Reviews*, **192**, 27–46.

Rahmstorf, S., J. E. Box, G. Feulner, M. E. Mann, A. Robinson, S. Rutherford, and E. J. Schaffernicht, 2015: Exceptional twentieth-century slowdown in Atlantic Ocean overturning circulation. *Nature climate change*, **5 (5)**, 475–480.

Riahi, K., and Coauthors, 2011: RCP 8.5—A scenario of comparatively high greenhouse gas emissions. *Climatic Change*, **109**, 33–57.

Rind, D., G. A. Schmidt, J. Jonas, R. Miller, L. Nazarenko, M. Kelley, and J. Romanski, 2018: Multicentury instability of the Atlantic meridional circulation in rapid warming simulations with GISS ModelE2. *Journal of Geophysical Research: Atmospheres*, **123 (12)**, 6331–6355.

Rind, D., and Coauthors, 2020: GISS Model E2. 2: A climate model optimized for the middle atmosphere—Model structure, climatology, variability, and climate sensitivity. *Journal of Geophysical Research: Atmospheres*, **125 (10)**, e2019JD032 204.

Robson, J., P. Ortega, and R. Sutton, 2016: A reversal of climatic trends in the North Atlantic since 2005. *Nature Geoscience*, **9 (7)**, 513–517.

Romanou, A., and Coauthors, Under Review: Stochastic bifurcation of the North Atlantic circulation under a mid-range future climate scenario with the NASA-GISS ModelE. *Journal of Climate*.

Samset, B., and Coauthors, 2016: Fast and slow precipitation responses to individual climate forcers: A PDRMIP multimodel study. *Geophysical Research Letters*, **43 (6)**, 2782–2791.

Santer, B. D., T. M. Wigley, M. E. Schlesinger, and J. F. Mitchell, 1990: Developing climate scenarios from equilibrium GCM results.

Schmidt, D. F., and K. M. Grise, 2017: The response of local precipitation and sea level pressure to Hadley cell expansion. *Geophysical Research Letters*, **44 (20)**, 10–573.

Schneider, T., 2006: The general circulation of the atmosphere. *Annu. Rev. Earth Planet. Sci.*, **34**, 655–688.

Shaffrey, L., and R. Sutton, 2006: Bjerknes compensation and the decadal variability of the energy transports in a coupled climate model. *Journal of Climate*, **19 (7)**, 1167–1181.

Shaw, T., and A. Voigt, 2015: Tug of war on summertime circulation between radiative forcing and sea surface warming. *Nature Geoscience*, **8 (7)**, 560–566.

Shepherd, T. G., 2014: Atmospheric circulation as a source of uncertainty in climate change projections. *Nature Geoscience*, **7 (10)**, 703–708.

Smith, D. M., R. Eade, N. J. Dunstone, D. Fereday, J. M. Murphy, H. Pohlmann, and A. A. Scaife, 2010: Skilful multi-year predictions of Atlantic hurricane frequency. *Nature Geoscience*, **3 (12)**, 846–849.

Tebaldi, C., and J. M. Arblaster, 2014: Pattern scaling: Its strengths and limitations, and an update on the latest model simulations. *Climatic Change*, **122 (3)**, 459–471.

Thompson, D. W., and T. Birner, 2012: On the linkages between the tropospheric isentropic slope and eddy fluxes of heat during Northern Hemisphere winter. *Journal of the Atmospheric Sciences*, **69 (6)**, 1811–1823.

Timmermann, A., and Coauthors, 2007: The influence of a weakening of the Atlantic meridional overturning circulation on ENSO. *Journal of Climate*, **20 (19)**, 4899–4919.

Vallis, G. K., P. Zurita-Gotor, C. Cairns, and J. Kidston, 2015: Response of the large-scale structure of the atmosphere to global warming. *Quarterly Journal of the Royal Meteorological Society*, **141 (690)**, 1479–1501.

Vellinga, M., and R. A. Wood, 2008: Impacts of thermohaline circulation shutdown in the twenty-first century. *Climatic Change*, **91 (1)**, 43–63.

Vial, J., C. Cassou, F. Codron, S. Bony, and Y. Ruprich-Robert, 2018: Influence of the Atlantic meridional overturning circulation on the tropical climate response to CO_2 forcing. *Geophysical Research Letters*, **45 (16)**, 8519–8528.

Waugh, D. W., and Coauthors, 2018: Revisiting the relationship among metrics of tropical expansion. *Journal of Climate*, **31 (18)**, 7565–7581.

Weijer, W., W. Cheng, O. A. Garuba, A. Hu, and B. Nadiga, 2020: CMIP6 models predict significant 21st century decline of the Atlantic meridional overturning circulation. *Geophysical Research Letters*, **47 (12)**, e2019GL086 075.

Woollings, T., J. M. Gregory, J. G. Pinto, M. Reyers, and D. J. Brayshaw, 2012: Response of the North Atlantic storm track to climate change shaped by ocean–atmosphere coupling. *Nature Geoscience*, **5 (5)**, 313–317.

Wu, L., C. Li, C. Yang, and S.-P. Xie, 2008: Global teleconnections in response to a shutdown of the Atlantic meridional overturning circulation. *Journal of Climate*, **21 (12)**, 3002–3019.

Zappa, G., and T. G. Shepherd, 2017: Storylines of atmospheric circulation change for european regional climate impact assessment. *Journal of Climate*, **30 (16)**, 6561–6577.

Zhang, R., and T. L. Delworth, 2005: Simulated tropical response to a substantial weakening of the Atlantic thermohaline circulation. *Journal of Climate*, **18 (12)**, 1853–1860.

Zhang, R., and T. L. Delworth, 2006: Impact of Atlantic multidecadal oscillations on India/Sahel rainfall and Atlantic hurricanes. *Geophysical Research Letters*, **33 (17)**.

Zhang, R., S. M. Kang, and I. M. Held, 2010: Sensitivity of climate change induced by the weakening of the Atlantic meridional overturning circulation to cloud feedback. *Journal of Climate*, **23 (2)**, 378–389.

Atmospheric Response to a Collapse of the North Atlantic Circulation Under A Mid-Range Future Climate Scenario: A Regime Shift in Northern Hemisphere Dynamics

Clara Orbe[a,b], David Rind[a], Ron L. Miller[a], Larissa S. Nazarenko[a,c], Anastasia Romanou[a,b], Jeffrey Jonas[a,c], Gary L. Russell[a], Maxwell Kelley[a], and Gavin A. Schmidt[a]

[a] *NASA Goddard Institute for Space Studies, New York, NY*

[b] *Department of Applied Physics and Applied Mathematics, Columbia University, New York, NY*

[c] *Center for Climate Systems Research, Earth Institute, Columbia University, New York, NY*

Corresponding author: Clara Orbe, clara.orbe@nasa.gov

ABSTRACT: Climate models project a future weakening of the Atlantic Meridional Overturning Circulation (AMOC), but the impacts of this weakening on climate remain highly uncertain. A key challenge in quantifying the impact of an AMOC decline is in isolating its influence on climate, relative to other changes associated with increased greenhouse gases. Here we isolate the climate impacts of a weakened AMOC in the broader context of a warming climate using a unique ensemble of Shared Socioeconomic Pathway (SSP) 2-4.5 integrations that was performed using the Climate Model Intercomparison Project Phase 6 (CMIP6) version of the NASA Goddard Institute for Space Studies ModelE (E2.1). In these runs internal variability alone results in a spontaneous bifurcation of the ocean flow, wherein two out of ten ensemble members exhibit an entire AMOC collapse, while the other eight recover at various stages despite identical forcing of each ensemble member and with no externally prescribed freshwater perturbation. We show that an AMOC collapse results in an abrupt northward shift and strengthening of the Northern Hemisphere (NH) Hadley Cell and intensification of the northern midlatitude jet. We then use a set of coupled atmosphere-ocean abrupt CO_2 experiments spanning the range 1-5xCO_2 to show that this response to an AMOC collapse results in a nonlinear shift in the NH circulation moving from 2xCO_2 to 3xCO_2. Slab-ocean versions of these experiments, by comparison, do not capture this nonlinear behavior. Our results suggest that changes in ocean heat flux convergences associated with an AMOC collapse — while highly uncertain — can result in profound changes in the NH circulation and continued efforts to constrain the AMOC response to future climate change are needed.

1. Introduction

Future projections of the atmospheric circulation remain highly uncertain and reflect uncertainties in the direct radiative response to CO_2 forcing (Deser and Phillips (2009); Grise and Polvani (2014); Shaw and Voigt (2015); Ceppi et al. (2018)), as well as both the (direct) response to changes in sea surface temperatures (SSTs) and the (indirect) response to changes in eddy feedbacks (see Shepherd (2014) and references therein). Among the former, uncertainties in SST projections over the subpolar North Atlantic are particularly consequential, as they strongly influence the location and strength of the North Atlantic storm track, with profound downstream impacts on precipitation and wintertime weather over Europe and parts of Africa (e.g., Zhang and Delworth (2006), Smith et al. (2010), Woollings et al. (2012), O'Reilly et al. (2016)). In particular, while increases in greenhouse gases over the 21st century are expected to result in substantial warming over much of the North Atlantic, climate models project considerable cooling over midlatitudes resulting in a so-called "North Atlantic warming hole (NAWH)" (e.g., Josey et al. (2018), Drijfhout et al. (2012), Robson et al. (2016), Caesar et al. (2018)). While the drivers of this NAWH have been under considerable debate, recent detection-attribution analysis suggests that the anthropogenic signal of the NAWH has emerged from internal climate variability and, moreover, that this cooling can be attributed to declining northward oceanic heat flux over recent decades related to increased greenhouse gas emissions (Chemke et al. (2022)).

Among other mechanisms contributing to the development of the NAWH, the slowdown of the Atlantic Meridional Overturning Circulation (AMOC) has been invoked as one potential key driver (Cheng et al. (2013), Rahmstorf et al. (2015), Menary and Wood (2018)). Studies have long shown that changes in the strength of the AMOC can have widespread impacts not only on other components of the ocean circulation but, more generally, on the broader atmospheric climate system, resulting in a southward shift of the intertropical convergence zone (ITCZ) (e.g., Zhang and Delworth (2005), Vellinga and Wood (2008), Jackson et al. (2015)), a strengthening of the Walker circulation (e.g., Vial et al. (2018), Orihuela-Pinto et al. (2022)) and a northward shift of the Northern Hemisphere (NH) jet stream (e.g., Liu et al. (2020), Bellomo et al. (2021)). Understanding the global scale atmospheric response to changes in AMOC strength is important not only for projections of future climate, but also for understanding paleoclimate records and the dynamics of past Dansgaard-Oeschger events. In particular, while the future collapse of an

AMOC is still considered unlikely, the latest generation of coupled climate models project stronger weakening with future warming, compared to older generations of models (Weijer et al. (2020)).

In addition to its impacts on global precipitation, SST-related changes in the AMOC can change the baroclinicity of the atmosphere, which can result in changes in the storm tracks (Woollings et al. (2012)). However, the precise impacts of a weakened AMOC on atmospheric baroclinity are not well understood, largely because studies have used models that exhibit a wide diversity in the amplitude and spatial extent of the NAWH (Gervais et al. (2019), Haarsma et al. (2015), Menary and Wood (2018)). Nonetheless, despite these uncertainties in the drivers and extent of the NAWH, Woollings et al. (2012) showed that the response of the North Atlantic storm track to climate change was singularly shaped by changes in ocean-atmosphere coupling.

The role of the AMOC in future projections of the jet stream in the Climate Model Intercomparison Project Phase 5 (CMIP5) and Phase 6 (CMIP6) models was recently examined in Bellomo et al. (2021) (hereafter KB2021), who showed that changes in the AMOC play a primary role in determining the magnitude of the projected poleward displacement of the NH zonal mean jet stream. In particular, by stratifying models according to the strength of their projected AMOC weakening (in response to a quadrupling of CO_2), the authors showed that models with a larger AMOC decline (> 7 Sv, relative to preindustrial values) exhibit minimum warming over the North Atlantic, a southward displacement of the ITCZ and a poleward shift of the northern midlatitude jet. The results from KB2021 suggest that the AMOC is a major driver of intermodal uncertainty in future projections of the northern jet stream (and associated hydrological impacts).

A key challenge in quantifying the impact of AMOC uncertainties on future projections of the large-scale atmospheric circulation is in isolating its influence on climate, relative to other changes associated with increased greenhouse gases. Thus, while the results from KB2021 are compelling, that study drew conclusions based on the spread among models subject to the same abrupt $4xCO_2$ forcing and it is not clear if the models exhibiting greater AMOC weakening were also models that exhibit other characteristics that would independently impact the jet stream. At the same time, previous studies using more traditional freshwater flux perturbations to examine the jet (and other climate) responses to a weakened AMOC, have done so in the absence of other background changes related to increased CO_2 (e.g., Zhang and Delworth (2005), Jackson et al. (2015)). As such, these

studies may produce a circulation response to a weakened AMOC that is different than what might occur if other factors impacting atmospheric temperature gradients are included.

One recent attempt to isolate the climate impacts of a weakened AMOC in the broader context of a warming climate was performed in Liu et al. (2020). In that study, the authors compared fully coupled Representative Concentration Pathway (RCP) 8.5 simulations (Riahi et al. (2011)) using a full physics comprehensive model (CCSM4) with identically forced simulations in which a negative freshwater perturbation over the subpolar North Atlantic was added after year 1980 in order to maintain the AMOC strength (while preserving all other forcings). That study showed results that were generally consistent with KB2021, pointing to a major role of the AMOC in causing widespread cooling stretching from NH high latitudes to the tropics and a poleward displacement of the NH midlatitude jet.

While the results from Liu et al. (2020) represent an important step forward in isolating the impacts of the AMOC on the storm tracks in the context of a warming climate, it is not clear that prescribing a negative freshwater perturbation does not potentially interfere with nonlinear components of the AMOC response in a coupled system. To this end, here we present new results featuring an ensemble of Shared Socioeconomic Pathway (SSP) 2-4.5 integrations (Meinshausen et al. (2020)) that was performed using the CMIP6 version of the NASA Goddard Institute for Space Studies (GISS) ModelE (E2.1) (Kelley et al. (2020)). In particular, we show results from a subset of the runs documented in Romanou et al. (Under Review) (hereafter AR2023), in which the authors identified a tipping point in the SSP 2-4.5 ensemble occurring during the "extended" portion of the simulations (i.e. beyond year 2090, after which CO_2 emissions are ramped down). During this time period the authors show that internal variability alone results in a spontaneous bifurcation of the ocean flow, wherein two out of ten ensemble members exhibit an entire AMOC collapse, while the other eight recover at various stages (Figure 1a). Note that, in contrast to the aforementioned freshwater hosing studies, in which an AMOC collapse is induced by adding freshwater, in these experiments the AMOC collapse is caused by a reduction in evaporation from the ocean, mediated by sea ice melting (AR2023). As such, the atmospheric configuration that is used to produce this effect in an interactive mode is likely to be very different from an atmosphere which is simply responding to a prescribed freshwater flux perturbation.

Whereas AR2023 focused primarily on the oceanic conditions giving rise to this divergence in AMOC behavior among different ensemble members, here we focus on the subsequent impacts this has on the atmospheric large-scale circulation. In particular, we contrast the behavior between two and eight ensemble members in which the AMOC respectively collapses and recovers to historical values by year 2400 (red vs. green lines, Fig. 1a). As such, we isolate the impact of a weakened AMOC on the atmospheric circulation in the presence of increased greenhouse gas warming using a single model (unlike KB2021) and without any need to invoke negative freshwater perturbations (as in Liu et al. (2020)). To the best of our knowledge, this represents the first time that the AMOC imprint on the circulation has been isolated in the context of background increases in greenhouse gases using a fully coupled comprehensive model, absent any externally imposed freshwater perturbations that may potentially interfere with the model's internal dynamics.

As discussed in AR2023, the ensemble members in which the AMOC collapses are substantially cooler than those runs in which it recovers, with wintertime global mean surface temperature (GMST) differences of about 1°C by year 2400 (Fig. 1c). Therefore, in documenting the influence of the AMOC on the atmosphere in the different SSP 2-4.5 ensemble members it is natural to ask how the large-scale thermodynamic and dynamical circulations scale with these differences in GMST. Though perhaps naive, it is common practice to assume that the climate system scales linearly with GMST, as reflected in the use of so-called "global warming levels" in the recent IPCC AR6 report (James et al. (2017)) and the widely applied related practice of "pattern scaling" (e.g., Santer et al. (1990), Tebaldi and Arblaster (2014)). Recent studies, however, have shown that the climate's so-called "dynamical sensitivity" – in particular, circulation shifts associated with changes in the Hadley Cell and storm tracks - do not scale with equilibrium climate sensitivity (Grise and Polvani (2016), Ceppi et al. (2018)). As those studies, however, focused on large (CMIP5) multi-model ensembles, it is not clear if similar conclusions also apply to single models and to climate states in which the AMOC has undergone a substantial weakening. More precisely, it remains unclear how much of the circulation response to a weakened AMOC is related simply to changes in GMST or, rather, to changes in (free-tropospheric) meridional temperature gradients away from the surface.

To this end, in addition to reporting on the results from the SSP 2-4.5 ensemble we also examine a suite of abrupt 1-5xCO_2 experiments that were conducted using the same model version (Mitevski

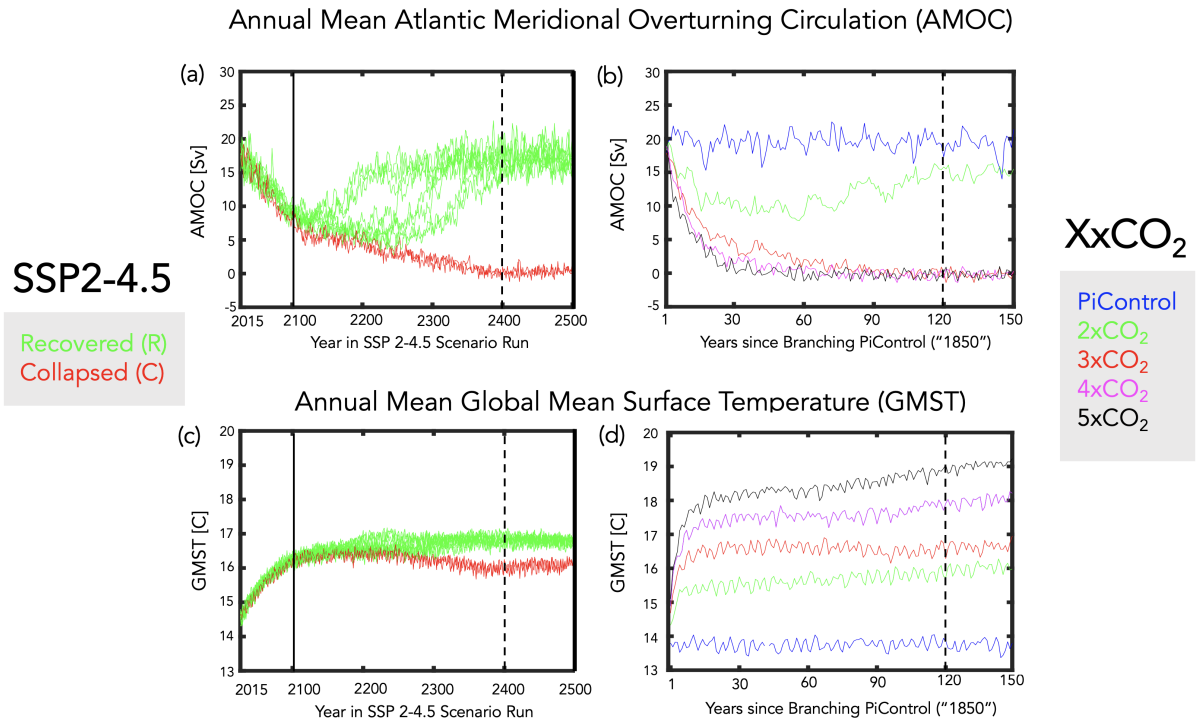

FIG. 1. Top: Evolution of the annual mean maximum overturning stream function in the Atlantic ocean, evaluated at 48°N, compared among the SSP 2-4.5 (8) recovered and (2) collapsed ensemble members (top, left) and among the abrupt $XxCO_2$ runs (top, right). Bottom: Same as top panels, except showing annual mean global surface temperature (GMST). Vertical solid lines mark the beginning of the "extension" portion of the SSP 2-4.5 scenario. Vertical dashed lines indicate the years after which climatological averages are evaluated (i.e., years 2400-2500 (left) and years 120-150 (right)).

et al. (2021)). In particular, we exploit the fact that between $2xCO_2$ and $3xCO_2$ abrupt forcing the AMOC respectively recovers and collapses by year 150 (Fig. 1b), behavior which is generally similar to the differences in AMOC responses between the recovered and collapsed members of the SSP 2-4.5 ensemble, hereafter referred to as SSP 2-4.5 R and SSP 2-4.5 C, respectively (Fig. 1a). However, by spanning a much broader range of GMST responses, compared to the SSP 2-4.5 ensemble – and assuming that the atmospheric responses to an AMOC collapse are similar between the $3xCO_2$ and SSP 2-4.5 collapsed ensemble members (a point which we examine in Section 3a3) – the broader set of $XxCO_2$ experiments affords a unique opportunity to investigate the relationship between dynamical and equilibrium climate sensitivity in the presence of a collapsed AMOC.

In Section 3 we begin by contrasting the large-scale atmospheric circulation responses between the SSP 2-4.5 R and C members in which the AMOC recovers and remains collapsed after year 2400 (Sections 3a1-2, Q1 below). We then compare this behavior with the circulation differences occurring in the 2xCO_2 and 3xCO_2 integrations (Section 3a3, Q2). After showing that the 3xCO_2 circulation changes in the NH are largely dominated by the behavior of the AMOC, we then use the broader set of 1-5xCO_2 abrupt experiments to examine how the collapse of the AMOC modulates the relationship between the NH dynamical circulation and GMST over a much broader range of CO_2 forcing (Section 3b, Q3). In addressing the latter we also use slab-ocean model integrations in order to examine if the behavior exhibited in the coupled atmosphere-ocean runs is reflected in simulations in which ocean heat flux convergence changes associated with an AMOC collapse are not allowed to occur.

The main goals of the manuscript are centered around addressing these three questions:

Q1) How does a collapse of the AMOC influence the atmospheric circulation in the presence of the same background CO_2 forcing (SSP 2-4.5 ensemble)?

Q2) How does this compare with the response to an AMOC collapse induced by different CO_2 forcing (2xCO_2 vs. 3xCO_2)?

Q3) Are AMOC-related circulation changes mediated primarily by GMST or by changes in atmospheric temperature gradients?

In addressing Q1-Q3 we show that the AMOC tipping point described in AR2023 results in a vastly different atmospheric response between ensemble members in which the AMOC collapses versus members in which the AMOC recovers. In particular, in our model the atmospheric response to an AMOC collapse (occurring on the timescales addressed in this study) reflects a regime shift between a climate state in which the NH Hadley Cell and midlatitude jet are substantially weaker and displaced further equatorward (strong AMOC) compared to a state in which they are substantially stronger and displaced poleward (weak AMOC).

2. Analysis/Methods

a. Models and Experiments

Here we use simulations from two sets of experiments produced using the GISS version E2.1 climate model (GISS-E2-1-G) (Kelley et al. (2020)), which consists of a 40-level atmospheric model with a horizontal resolution of 2^o x 2.5^o latitude/longitude coupled to the 1^o horizontal resolution 40-level GISS Ocean v1 (GO1) model (for more details of GO1 see AR2023). Comprehensive reviews of this model's response to historical and future climate change simulations are provided in Miller et al. (2021) and Nazarenko et al. (2022), respectively.

We first examine results from the SSP 2-4.5 ensemble that contributed to the official submission of the NASA-GISS climate group to CMIP6. In particular, we contrast the behaviors of eight members in which the AMOC has recovered by year 2400 (SSP 2-4.5 R) with two members in which it has remained collapsed (SSP 2-4.5 C) (Fig. 1a). As discussed in AR2023, this contrasting behavior emerges during the "extension" portion following year 2090, beyond which CO_2 concentrations slow down in growth from 597 ppm to 643 ppm at year 2200 and decline thereafter (Meinshausen et al. (2020)). That study further showed that the divergence in the behavior of the AMOC results from stochastic variability associated with sea-ice transport and melting in the Irminger Sea that led to a reduction in evaporation and salinity. Note that, whereas AR2023 was primarily focused on identifying the mechanisms leading to different recovery times among the SSP 2-4.5 R, our interest is in quantifying the impact of an AMOC collapse on the large-scale circulation after year 2400 up to year 2500. To this end, we treat the SSP 2-4.5 R and C simulations as comprising two distinct "recovered" and "collapsed" ensembles.

To put the SSP 2-4.5 results in a broader context, we also examine the coupled atmosphere-ocean 1-5xCO_2 abrupt CO_2 experiments reported in Mitevski et al. (2021), which were performed using the same version of the model. We restrict our attention to a subset of the runs, focusing mainly on the 2xCO_2 and 3xCO_2 runs, but also including results from the 4xCO_2 and 5xCO_2 simulations when commenting on the linearity of the atmospheric circulation responses with respect to changes in GMST (Section 3b). As shown in Figure 1, the behavior of the AMOC by the end of the abrupt 2xCO_2 and 3xCO_2 runs is generally very similar to the AMOC behavior in the SSP 2-4.5 R and C ensemble members, respectively, past year 2400. This similar behavior also appears at

lower latitudes (26^{o}N) (not shown), consistent with the findings in AR2023, who showed a strong correlation in AMOC strength at these two latitudes (0.97) within the broader SSP 2-4.5 ensemble.

In addition to the results from the fully coupled ocean-atmosphere model (hereafter FOM) SSP 2-4.5 and X$\times CO_2$ integrations, we also show results from q-flux or slab-ocean model (SOM) integrations spanning the range 1-5xCO_2. In these experiments any changes in ocean horizontal heat transport and vertical heat uptake by the deep ocean are not included as the ocean heat flux convergences in the mixed layer ($-\nabla\cdot(vT)$, including both horizontal and vertical heat fluxes) are calculated using preindustrial control values. At the same time, the SOM experiments do capture the mixed layer temperature changes resulting from changes in the net surface heat fluxes (hereafter referred to as "thermodynamic" ocean coupling). As such, contrasting the responses in the FOM and SOM experiments isolates the role of dynamic (i.e. ocean heat flux convergence) coupling on the atmospheric responses in the FOM simulations, consistent with the presentation in Chemke et al. (2022). Note that this approach does not explicitly isolate the contribution of changes in SSTs to the atmospheric circulation response, as the SST response reflects both changes in thermodynamic and dynamic ocean-atmosphere coupling. However, robustly isolating the impact of SSTs can be tricky as previous studies utilizing prescribed SST "warming hole" patterns have shown large sensitivity to how these patterns are prescribed, particularly in relation to SST gradients (see discussion in Gervais et al. (2019)).

b. Temporal Averaging and Spatial Domains

To compare the atmospheric responses from the SSP 2-4.5 simulations with those from the abrupt CO_2 experiments we focus on climatological averaging periods during which the characteristics of the AMOC are similar, i.e., years when the AMOC has recovered in the 2xCO_2 and SSP 2-4.5 R runs, while the AMOC has remained collapsed in the 3xCO_2 and SSP 2-4.5 C experiments. As indicated in Figure 1 (dashed black vertical lines) this corresponds to years beyond which the maximum value of the overturning stream function at 48^{o}N has reached nearly zero, corresponding to years 120-150 and 2400-2500 in the X$\times CO_2$ and SSP 2-4.5 integrations, respectively. We refer to these periods hereafter as the "equilibrated" responses in the model, bearing in mind that the AMOC exhibits multi-centennial instability as was illustrated in an older version of the GISS

climate model (Rind et al. (2018)). Variations on these longer timescales are not addressed in this study.

We begin by presenting differences in climatological means between the SSP 2-4.5 R and C ensembles and between the 2xCO_2 and 3xCO_2 integrations. Statistical significance of the SSP 2-4.5 C-R differences is assessed using a Welch's t-test, given the unequal sample sizes represented by the 8-member R and two-member C ensembles. A two-sample Student's t-test is used when comparing the abrupt CO_2 responses. In addition, when putting the SSP 2-4.5 results in the context of the broader 1-to-5xCO_2 forcing range we define all responses relative to a 150-year average over the preindustrial control simulation from which the abrupt CO_2 experiments are "branched."

For the majority of the analysis considered here we focus on December-January-February (DJF) and over the NH. Our focus on DJF is consistent with the presentation in AR2023, while our focus on the NH is motivated by Mitevski et al. (2021), who showed that the AMOC collapse occurring between 2xCO_2 and 3xCO_2 results in a non-monotonic response in global mean surface temperature, driven primarily by changes occurring in the NH (more precisely, the North Atlantic). We deviate from this convention, however, at two different points in this study. First we use annual mean GMST when evaluating the dynamical sensitivity scaling in Section 3b; second, we present the energy budget analysis in Section 3c using annual means in order to facilitate comparison with previous studies. Some results about the Southern Hemisphere (SH) circulation response are also presented, but only discussed briefly.

Finally, while our main focus is on the "equilibrated" responses defined above, we are also interested in exploiting the evolution of the responses, as in Grise and Polvani (2017) and Chemke and Polvani (2019). As shown in those studies, consideration of the response timescales of different variables affords insight into possible mechanisms governing their evolution.

c. Scaling with Global Mean Surface Temperature (GMST)

We begin by comparing the absolute differences in the atmospheric "equilibrated" responses between the SSP 2-4.5 R and C members (Section 3a1-2) and between the 2-and 3xCO_2 simulations (Section 3a3). When interpreting these differences, however, it is important to note that these could partly be reflective of background differences in the CO_2 forcing. In particular, the CO_2 values in the SSP 2-4.5 extended experiments peak at 643 ppm, or roughly 2.4 times preindustrial values,

and decrease thereafter (Figure 1a in AR2023). It is perhaps not surprising, therefore, that this value of CO_2 lies in between the $2xCO_2$ and $3xCO_2$ levels identified in Mitevski et al. (2021) as the transition point between the AMOC recovering and collapsing under abrupt forcing (Fig. 1b).

Given these differences in CO_2 forcing (further exaggerated when considering the broader suite of 1-5xCO_2 experiments) it may seem most natural to compare the simulations with respect to their associated instantaneous radiative forcing (RF) as in Mitevski et al. (2021). However, another difference between the transient SSP 2-4.5 and abrupt 1-5xCO_2 experiments is the evolution of the forcing. As the AMOC is known to be sensitive to the time history of the forcing, this is important to take into consideration, and so we cast our scaling analysis in Section 3b (in which the SSP 2-4.5 results are compared against the broader 1-5xCO_2 suite) in terms of GMST. This approach is also more in spirit with Ceppi et al. (2018) as it directly addresses the extent to which the dynamical sensitivity captured in the simulations scales with equilibrium climate sensitivity (Q3).

Finally, a related but distinct approach is to normalize by annual mean GMST. KB2021 showed that doing so highlights large differences in temperature gradients and the zonal mean meridional circulation between models in which the AMOC weakens substantially (> 7 Sv), compared to models showing a limited AMOC response (< 7 Sv). However, while this approach is well suited to understanding the multi-model response to the same ($4xCO_2$) forcing, it does not directly afford insight into how dynamical sensitivity scales with GMST. As we have tried both normalizing and not normalizing in this study and draw generally very similar conclusions (not shown), we focus on the unnormalized results.

d. Analysis Approach

1) Hadley Cell and Storm Track Diagnostics

Whereas KB2021 focused on the latitude of the northern midlatitude jet, here we expand their analysis to also include measures of the Hadley Cell (HC) and the storm tracks. Figure 2a highlights how these measures of the HC and midlatitude jet are coupled through eddy momentum fluxes.

To quantify the characteristics of the Hadley Cell we use metrics calculated using the Tropical-width Diagnostics (TropD) code (Adam et al. (2018)) based on fields that were zonally and seasonally averaged before calculation of the metrics. The edge of the HC, ϕ_{UAS}, is defined as the zero-crossing latitude of the surface zonal wind (corresponds to UAS in TropD and is calculated

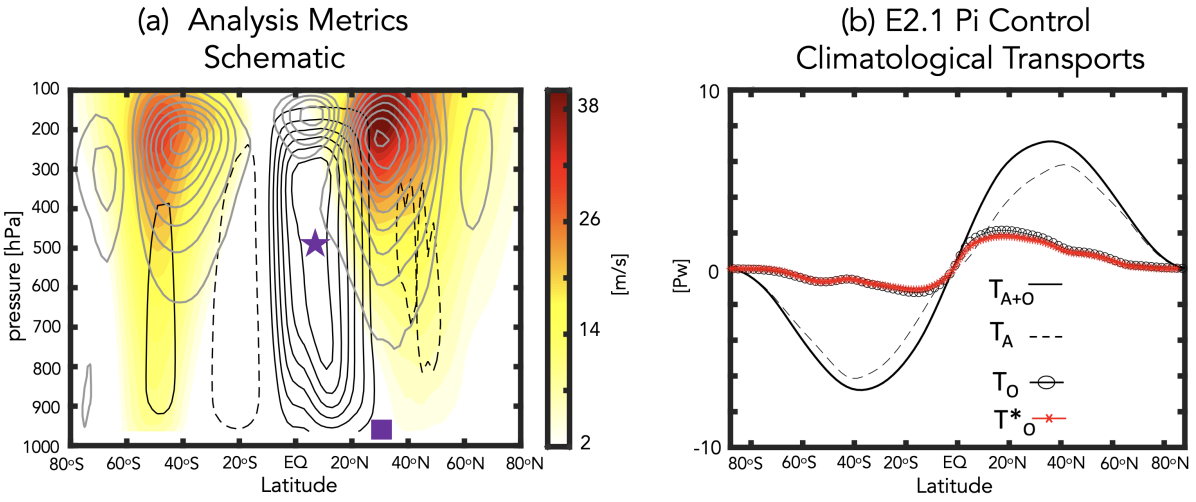

FIG. 2. (a): Schematic of the main zonal mean dynamical metrics considered in this study, illustrated using data from the preindustrial control simulation. The December-January-February (DJF) climatological mean meridional circulation is shown in black contours, with solid and dashed lines denoting clockwise and counterclockwise directions, respectively (contour interval: $3\text{x}10^{10}$ kg/s). The DJF zonally averaged zonal winds are shown in the filled colored contours (only positive values shown; contour interval: 2 m/s) and the DJF eddy momentum fluxes are shown in the grey contours (contour interval: 8 m^2/s^2). The purple star denotes the Northern Hemisphere (NH) Hadley Cell strength, or the maximum value of the mean meridional streamfunction at 500 hPa equatorward of where it crosses zero, while the edge is denoted by ϕ_{UAS} (purple square), or the zero-crossing latitude of the surface zonal wind. (b): Annual mean meridional distributions of the total atmospheric (T_A; black dashed line) and combined atmosphere-ocean (T_{A+O}; black solid line) northward energy transports for the preindustrial control simulation. The implied ocean heat transport (T_O; black circled line), calculated by subtracting T_A from T_{A+O}, exhibits good agreed with online calculations of the ocean transports (T^*_O; red starred line). For more details see Section 2.

using the "zerocrossing" method) (Fig. 2a, purple square). This measure of the HC was shown to correlate well with the latitude at which the mean meridional streamfunction at 500 hPa crosses 0 poleward of its tropical extremum (Waugh et al. (2018)). The value of that tropical extremum (Ψ_{500}) is also examined as a measure of HC strength (Fig. 2a, purple star).

In addition to looking at the Hadley Cell, we also examine its relation to the northern midlatitude jet via the eddy momentum fluxes. This is based on research showing a strong connection between the evolution of the Hadley Cell and the latitude of the maximum eddy momentum fluxes

(Schneider (2006); Chemke and Polvani (2019); Menzel et al. (2019)). The eddy momentum fluxes are calculated as in Chemke and Polvani (2019) as the time mean of [u'v'], where u and v are the zonal and meridional winds, respectively, and primes represent deviations from both the zonal and monthly means. In particular we are interested in the latitude where the eddy momentum flux maximizes (eddy momentum convergence = 0) (Fig. 2a, grey contours). As it is well known that the largest eddy momentum flux convergences are closely collocated with the extratropical storm tracks (e.g., Lau et al. (1978), Lim and Wallace (1991)), we also examine the vertically averaged eddy kinetic energy, calculated using daily output. Connections with static stability and baroclinic eddy generation are also made, where the latter is quantified using $\sim \alpha'\omega'$, where primes denote zonal deviations and α and ω refer to one over the density and vertical velocity in pressure coordinates, respectively.

2) Energetic Analysis

To put the results of the dynamical analysis in an energetic context we evaluate the total meridional heat transport of the coupled ocean-atmosphere transport system, further partitioned into its oceanic and atmospheric contributions. Following Magnusdottir and Saravannan (1999) we estimate the total vertically integrated atmospheric heat flux ($\mathrm{T_A}$) as:

$$\frac{\partial cos\phi}{acos\phi\partial\phi}\overline{[\mathrm{T_A}]} \equiv \frac{\partial cos\phi}{acos\phi\partial\phi}\int_1^0 \overline{(c_pT+gz+Lq)v\rho d\eta}$$

$$= \overline{[-\mathrm{F_T}-\mathrm{F_S}+\mathrm{SHF}+\mathrm{LHF}]} \qquad (1)$$

as well as the vertically integrated meridional heat flux in the combined atmosphere-ocean system ($\mathrm{T_{A+O}}$) as:

$$\frac{\partial cos\phi}{acos\phi\partial\phi}\overline{[\mathrm{T_{A+O}}]} \equiv \overline{[-\mathrm{F_T}]} \qquad (2)$$

where moist static energy density is the sum of dry static energy density (c_pT+gz) and the latent heat density (Lq), ρ and v refer to the mass density and horizontal velocity on η surfaces. Zonal averages and time averages are denoted by square brackets and overbars, respectively. The terms on the RHS of both equations refer to energy fluxes out of the top of the atmosphere and at the

surface: F_T (net upward flux of radiation at the top of the atmosphere, calculated as outgoing longwave radiation (OLR) minus the absorbed solar radiation (ASR)), F_S (net downward flux of radiation at the surface equal to the sum of net downward longwave (LWF) and shortwave (SWF) radiation), and the fluxes of latent and sensible heat at the surface (LHF and SHF).

The resulting annual mean meridional distributions of T_A and T_{A+O}, calculated using the E2.1 150-year preindustrial control simulation, is consistent with the climatological energy transports presented in other studies (e.g., Magnusdottir and Saravannan (1999), Held and Soden (2006)) (Figure 2b). Note that the implied ocean heat transport, calculated by subtracting the first from the second equation above (Fig. 2b, black circled line) is found to exhibit good agreement with online calculations of the ocean transports (Fig. 2b, red starred line). These northward ocean heat transports, simulated in historical integrations using E2.1, have been shown to agree well with 1992-2011 estimates from the ECCO ocean state estimate (Figure 23 in Kelley et al. (2020)). Finally, in addition to examining the compensation between atmospheric and oceanic poleward transports, we also further partition T_A into its moist versus dry contributions using online calculations of the vertically integrated dry static energy and latent heat northward transports (Section 3c).

3. Results

We begin by contrasting the regional SSP 2-4.5 C and R responses in sea surface temperature, sea level pressure, precipitation and zonal winds (Section 3a1) and in the large-scale zonal mean circulation (Section 3a2). Then we compare the SSP 2-4.5 C-R differences to the responses in the $2xCO_2$ and $3xCO_2$ simulations (Section 3a3), followed by a discussion of the full set of abrupt $1\text{-}5xCO_2$ experiments, which we use to examine how the changes in thermodynamics and the circulation scale with changes in global mean surface temperature (Section 3b). To interpret the dynamical scaling results we then examine the compensation that arises between the ocean and atmosphere in response to a decline and eventual collapse of the AMOC (Section 3c).

a. Equilibrated Responses

1) SSP 2-4.5 Collapsed vs. Recovered: Near-Surface Temperatures, Precipitation and Winds

Figure 1 (bottom panels) shows the evolution of annual global mean surface temperature in the SSP 2-4.5 C and R members (Fig. 1c) and the abrupt CO_2 experiments (Fig. 1d). Comparing the collapsed versus recovered SSP 2-4.5 ensemble members reveals global cooling associated with a sustained collapse of the AMOC such that by the time that the AMOC has recovered in the SSP 2-4.5 R members the annual mean global surface temperature is almost one degree warmer, relative to the SSP 2-4.5 C members. In the abrupt CO_2 simulations, the GMST change in the $3xCO_2$ experiment is only ~0.6^{o}C warmer than the $2xCO_2$ simulation, reflective of a clear flattening of the warming trend after years ~60-70. Overall, the changes in GMST are 2.2^{o}C, 2.8^{o}C, 3.0^{o}C, and 2.3^{o}C for the $2xCO_2$, $3xCO_2$ and SSP 2-4.5 recovered and SSP 2-4.5 collapsed ensembles, respectively.

That the cooling associated with a steady decline and eventual collapse of the AMOC acts to mitigate, and partially counteract, other components of the global surface temperature change is reflected in a non-monotonic change in equilibrium climate sensitivity that occurs between $2xCO_2$ and $3xCO_2$ over the broader range of experiments spanning 1-to-5xCO_2 (Figure 1 in Mitevski et al. (2021)). This counteracting of warming due to a weakening of the AMOC has also been shown to occur in 21st century warming simulations (Drijfhout et al. (2012), Caesar et al. (2018), Marshall et al. (2015)).

While the AMOC influence on the climate can occur via its changes in GMST, a reduction in AMOC strength can also influence sea surface temperature patterns. We examine this next, with a focus on DJF, and examine changes in SSTs and associated spatial gradients over the Atlantic and Pacific (Figure 3a). Note that a saturated color bar has been used in order to highlight the structure of SST changes outside of the North Atlantic region.

Examination of the North Atlantic reveals much more cooling in the SSP 2-4.5 collapsed simulations (Fig. 3a) over the subpolar North Atlantic (SPNA), consistent with the results from previous studies. This cooling within the SPNA region is also associated with a large increase in meridional SST gradients over the North Atlantic south of 40^{o}N and enhanced zonal gradients between the

western and eastern Atlantic basins. There is also an indication of a slight increase in SST gradients in the tropics.

The cooler SSTs in the recovered simulations are not only confined to the Atlantic, but also span the Pacific (Fig. 3a), resulting in stronger meridional SST gradients, particularly over middle northern latitudes. Preliminary analysis of the evolution of the SST response (Appendix Figure 1) shows that this cooling over the extratropical Pacific occurs over several centuries and may be related to a deepening and poleward shift of the Aleutian Low (Fig. 3c), resulting in more advection of colder temperatures over the West Pacific (Wu et al. (2008)), although direct thermodynamic advection of colder North Atlantic air may also be occurring. By comparison, the changes in SSTs and associated gradients in the tropical Pacific are much smaller. Unlike some previous studies (Timmermann et al. (2007), Zhang and Delworth (2005)) we find no evidence of an El Niño like response to an AMOC weakening, although the robustness of this response has recently been questioned (KB2021).

In the SH, SSTs warm over the extratropics in the SSP 2-4.5 collapsed integrations, compared to the simulations in which the AMOC recovers. This warming takes several centuries to develop (Appendix Figure 1) and resembles the evolution of the SST pattern documented in Pedro et al. (2018) (their Figure 7). This delayed warming over the SH results in increased SST gradients over the South Atlantic ($\sim 60^{o}$S) in the SSP 2-4.5 C runs, relative to SSP 2-4.5 R, a feature which is not captured in the $3xCO_2$ simulation (discussed more in Section 3a3).

In addition to the changes in SSTs, the response in precipitation in the SSP 2-4.5 collapsed simulations reflects large decreases over the North Atlantic subpolar region, reductions over the Amazon and suggestions of a southward shift of the ITCZ over both the Atlantic and East Pacific basins (Fig. 3b). By comparison, the increased precipitation in the West Pacific is not statistically significant, consistent with previous studies (Vellinga and Wood (2008), KB2021).

Moving next to more dynamical measures, we examine changes in sea level pressure and near-surface zonal winds (Fig. 3c,d). The changes in sea level pressure show differences over the North Atlantic indicative of enhanced (anticyclonic) high level pressure over the subpolar latitudes in the runs in which the AMOC collapses (Fig. 3c). In addition to these SLP changes over the Atlantic, there is also a pronounced dipole of increased and reduced sea level pressure values over the North Pacific middle and high latitudes. While this response was not discussed in KB2021, earlier studies

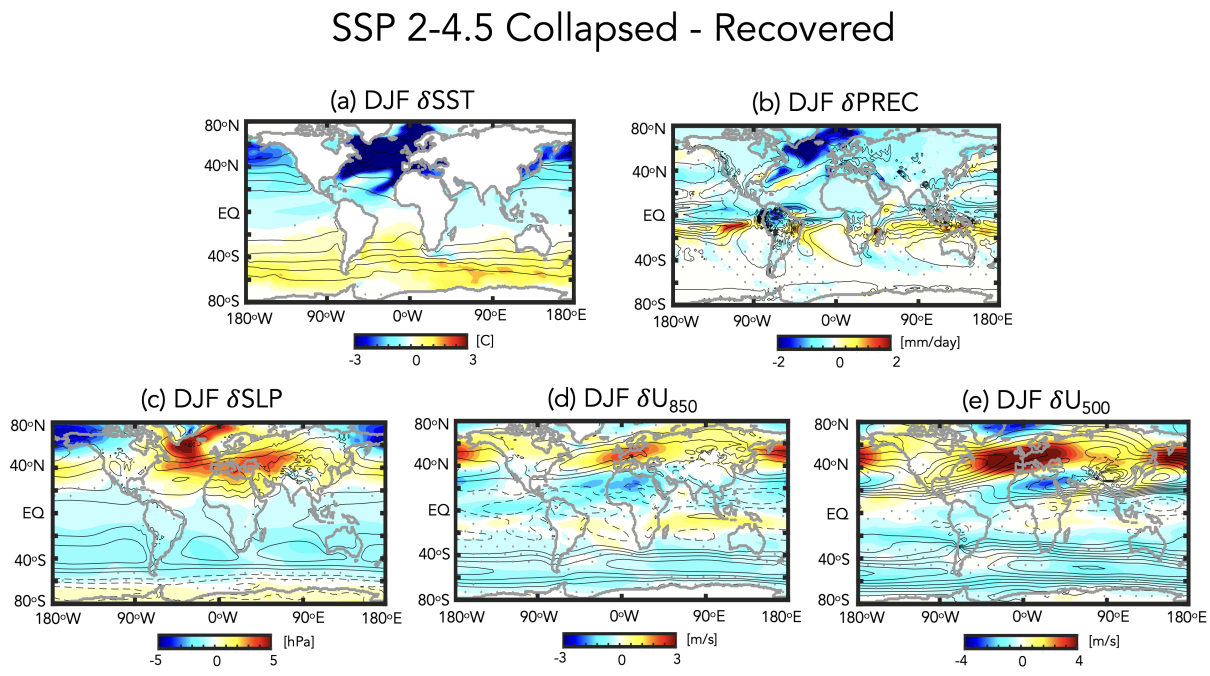

FIG. 3. The difference in the year DJF 2400-2500 climatological mean (a) sea surface temperatures (δSST), (b) precipitation (δPREC), (c) sea level pressure (δSLP), (d) 850 hPa zonal winds (δU_{850}) and (e) 500 hPa zonal winds (δU_{500}) between the SSP 2-4.5 collapsed (C) and recovered (R) ensemble members. Climatological mean values from the preindustrial control simulation are denoted in the black contours (contour intervals: (a) 5°C, (b) 2 mm/day, (c) 5 mb, (d) 3 m/s and (e) 3 m/s). Grey stippling denotes regions where the SSP 2-4.5 C-R differences are not statistically significant.

have shown that a weakening of the AMOC is associated with a deepening of the Aleutian Low (Wu et al. (2008), Liu et al. (2020)).

Consistent with the SLP changes over the North Pacific, there is a strong signature of a weakened AMOC in the near surface zonal winds (850 hPa) (Fig. 3d). These wind changes over the Pacific reflect a poleward shift of the midlatitude jet, whereas over the North Atlantic the jet mainly accelerates and extends further eastward over Europe. This acceleration over the North Atlantic is more pronounced in the mid-troposphere (Fig. 3e), as was also reported in KB2021, who identified a statistically significant strengthening of the midlatitude jet at 250 hPa, but not at 850 hPa, in models featuring a stronger AMOC decline. Finally, in contrast to the NH, there is a uniform weakening of the zonal winds over the SH extratropics. We discuss the vertical coherence of these wind changes in the next section.

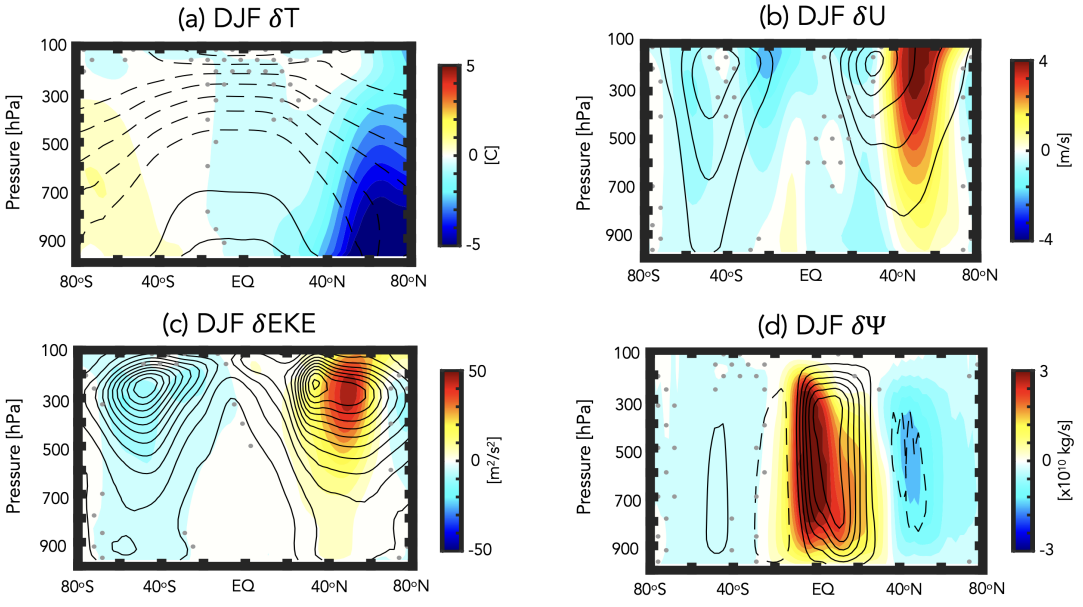

449 FIG. 4. The difference in the year DJF 2400-2500 climatological mean zonal mean (a) temperature (δT), (b)
450 zonal wind (δU), (c) eddy kinetic energy (δEKE) and (d) Eulerian mean stream function ($\delta\Psi$) between the SSP
451 2-4.5 collapsed (C) and recovered (R) ensemble members. Climatological mean values from the preindustrial
452 control simulation are denoted in the black contours (contour intervals: (a) 10°C, (b) 8 m/s, (c) 28 m^2/s^2 and
453 (d) $3x10^{10}$ kg/s). Note that in (d) solid and dashed lines denoting clockwise and counterclockwise directions,
454 respectively. Grey stippling denotes regions where the SSP 2-4.5 C-R differences are not statistically significant.

455 ### 2) SSP 2-4.5 COLLAPSED VS. RECOVERED: VERTICAL STRUCTURE

456 In addition to its impacts on SSTs, changes in the AMOC impact the vertical structure of
457 meridional temperature gradients in the atmosphere. To interpret the zonal wind changes shown in
458 Figure 3 we therefore next examine the zonal mean changes in temperatures, zonal winds and eddy
459 kinetic energy, as well as their coupling to responses in the tropical mean meridional circulation
460 (Figure 4).

465 We begin by examining changes in temperature (Fig. 4a), which show much more cooling over
466 the NH high latitude troposphere in the SSP 2-4.5 collapsed runs. A similar reduction in Arctic
467 warming was reported in the "strongly" collapsed models examined in KB2021 (their Figure S5)
468 and in Liu et al. (2020) (their Figure 6). In addition to the changes over the northern extratropics,

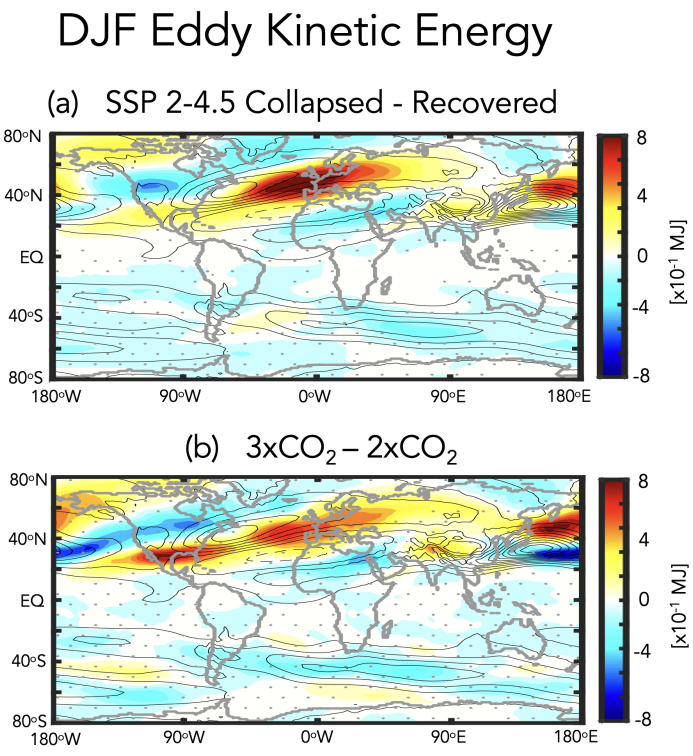

FIG. 5. (a) The difference in the year DJF 2400-2500 climatological mean vertically integrated eddy kinetic energy between the SSP 2-4.5 C and R ensembles. (b) Same as in (a), except showing the year 120-150 difference between the $3xCO_2$ and $2xCO_2$ integrations. Climatological mean values from the preindustrial control simulation are denoted in the black contours (contour interval: $5x10^{-1}$ MJ).

we also find an indication of weak polar amplification characterized by warming throughout the SH middle and high latitudes poleward of 40°S, also seen in the SST differences (Fig. 3a). This warming in the SH is consistent with Liu et al. (2020) (their Figure 6), but inconsistent with KB2021, which likely reflects their focus on shorter (100-150 year) timescales. In addition, KB2021 also identified more warming in the tropical upper troposphere, a feature that is also not evident in the SSP 2-4.5 collapsed runs. Normalization of our results by GMST (not shown) produces an anomalous upper tropical tropospheric warming, suggesting that the results reported in KB2021 are reflective of the normalization performed in that study, not of absolute temperature differences.

Moving next to the zonal winds (Fig. 4b) we find that the reduced warming over NH high latitudes is associated with enhanced meridional temperature gradients, which result in a poleward

shift of the zonal mean northern midlatitude jet in response to a decline and eventual collapse of the AMOC. A similar poleward shift in the NH jet was documented in KB2021 (their Figure 4) and in Liu et al. (2020). In the SH the zonal winds weaken and, if anything shift equatorward, in the SSP 2-4.5 C ensemble members, consistent with the weak polar amplification in that region (Fig. 4a). Again, this wind response is highly consistent with Liu et al. (2020), but opposite to that shown in KB2021, who identified a poleward shift of the SH jet. As that study did not propose a testable mechanism for the SH jet changes, it is not entirely clear what is the driver of the differences between their results and those presented here and in Liu et al. (2020), although both the normalization by GMST as well as the differing integration lengths likely contribute.

In concert with the changes in the zonal winds, the changes in eddy kinetic energy (EKE) over the NH feature increases north of 40°N (Fig. 4c). Note that there is no statistically significant response in the subtropics and only the wind (and EKE) changes poleward of 40°N are robust. Zonally, the increases in EKE are concentrated over the North Atlantic and extend eastward over Europe, as well as over the West Pacific (Fig. 5a), strongly resembling the zonal wind changes at 500 hPa (Fig. 3e). Comparisons with the changes in EKE associated with an AMOC collapse in another model (the Community Earth System Model (CESM-LE)) examined in Mitevski et al. (2021) show very similar anomalies (not shown). Furthermore, a spectral decomposition of these NH EKE changes show increased wave energy over wavenumbers 1-6 in the collapsed SSP 2-4.5 members, relative to the recovered members (also not shown).

Finally, the changes in the mean meridional stream function indicate an overall strengthening of the wintertime NH Hadley circulation in the collaped SSP 2-4.5 simulations (Fig. 4d). This intensification of the NH Hadley circulation in response to an AMOC shutdown has been reported in previous studies (Zhang and Delworth (2005), Orihuela-Pinto et al. (2022)) and generally associated with a southward displacement of the ITCZ, although Brayshaw et al. (2009) also identify a zonally localized enhancement of the Hadley Cell region over the subtropical Atlantic, which they associate with increased meridional SST gradients in that region. Compared to those studies, however, our results also show a poleward displacement of the northern Hadley Cell edge in the lower troposphere (>500 hPa), a result which has not been directly commented on in the literature. These stream function anomalies over the NH extratropical lower troposphere appear to be coupled to a slight strengthening and poleward displacement of the northern Ferrel cell.

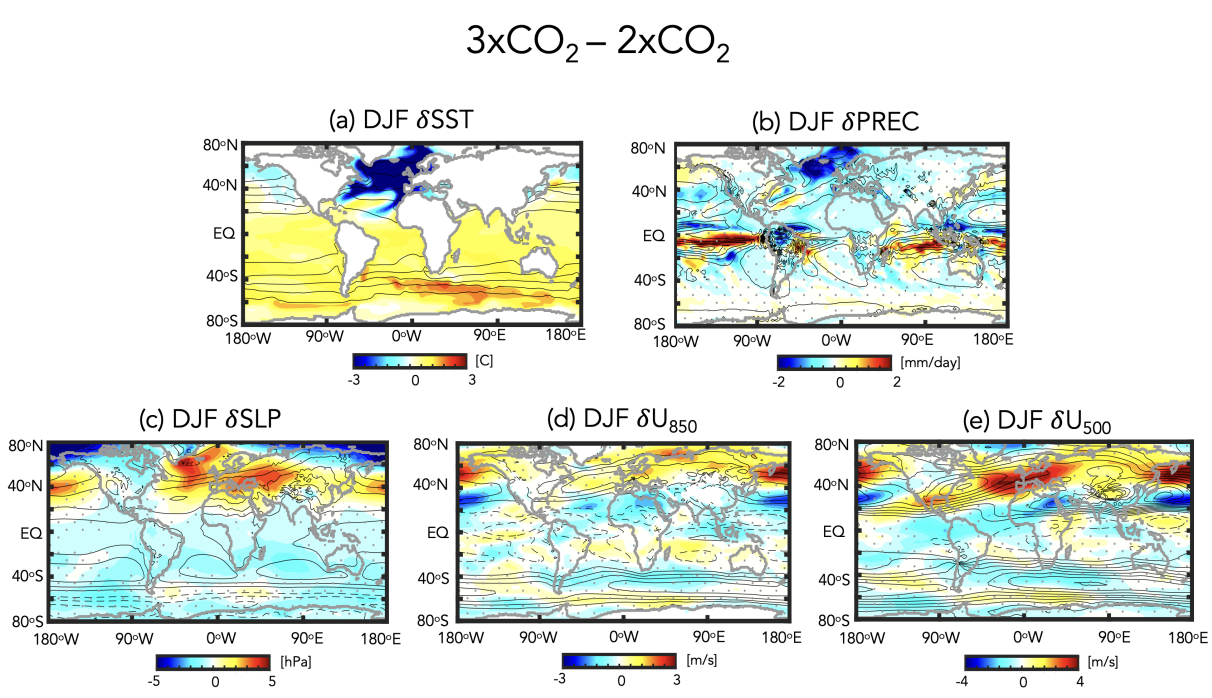

499 FIG. 6. Same as Figure 3, except showing the difference between the year 120-150 climatological mean 3xCO$_2$
500 and 2xCO$_2$ responses.

512 ## 3) COMPARISON WITH 2xCO$_2$ VS 3xCO$_2$

513 Comparisons of the surface and lower tropospheric impacts associated with an AMOC collapse
514 in the SSP 2-4.5 ensemble (Fig. 3) are highly consistent with the responses moving from 2xCO$_2$
515 to 3xCO$_2$ (Fig. 6). In particular, over the North Atlantic the changes moving from 2xCO$_2$ to
516 3xCO$_2$ reflect cooler SSTs (Fig. 6a), reduced precipitation (Fig. 6b) and an anomalous anticylonic
517 circulation over the North Atlantic subpolar gyre region (Fig. 6c), as well as a strengthening and
518 eastward extension of the North Atlantic jet over Europe (Fig. 6d, 6e). The magnitudes of the
519 3xCO$_2$ changes are also similar to the responses in the SSP 2-4.5 collapsed ensemble members,
520 albeit somewhat smaller (Fig. 3).

521 Though the overall responses in the surface temperatures and winds are very similar, there are
522 some important differences worth noting. First, the SSTs in the 3xCO$_2$ simulation show much less
523 cooling over the Pacific northern midlatitudes (> 40°N) compared to the SSP 2-4.5 C simulations,
524 which likely reflects differences in the length of these integrations as this cooling takes centuries
525 to equilibrate (Appendix Figure 1). Second, in response to 3xCO$_2$ there is more warming over the

NH subtropics and tropics, consistent with the higher CO_2 forcing in that simulation. Thus, unlike what happens in the SSP 2-4.5 C ensemble members, there is no SH polar amplification occurring at 3xCO_2.

The different SST gradients over the northern high latitude Pacific and tropics and SH occurring at 3xCO_2 have implications for the jet and precipitation changes in these regions. In particular, over the Pacific northern midlatitudes, where there is much less cooling compared to the SSP 2-4.5 C integrations, the jet response resembles more of a poleward shift, characterized not only by an acceleration north of 40°N, but also reduced winds ~20°N; in the tropical Pacific there is also a much stronger increase in precipitation, relative to the AMOC SSP 2-4.5 C ensemble.

Even over the North Atlantic the SST cooling is slightly weaker and less expansive and the jet response at 850 hPa is not statistically significant at 3xCO_2, in contrast to the SSP 2-4.5 collapsed ensemble members. In the SH, there is also a suggestion of a poleward shift of the midlatitude jet at 3xCO_2, not evident in the SSP 2-4.5 C integrations, although these changes are not statistically significant. These subtle differences aside, however, the overall similarities between Figures 3 and 6 are remarkable and suggest that the climate response that occurs moving from 2xCO_2 to 3xCO_2 is, to first order, determined by the changes in AMOC strength.

Strong consistency is also found when comparing the vertical response of the large-scale circulation between the AMOC SSP 2-4.5 collapsed ensemble (Fig. 4) and the 3xCO_2 integration (Fig. 7). That is, in concert with stronger cooling over the Arctic (Fig. 7a), the 3xCO_2 simulation features a stronger poleward shift of the NH zonal mean jet (Fig. 7b), increased EKE northward of 40°N (Fig. 7c) and a strengthened Hadley Cell (Fig. 7d).

One difference in vertical structure occurs over the Arctic, where the cooling that occurs at 3xCO_2 (Fig. 7a) is much smaller than in the collapsed SSP 2-4.5 ensemble (Fig. 4a), reflecting the higher CO_2 forcing in that simulation. There is also stronger warming occurring within the tropics and over southern latitudes. Despite these differences in absolute temperature, however, the increase in meridional temperature gradients that occurs is similar to what happens when comparing the SSP 2-4.5 C and R ensemble members. As such, the zonal mean NH jet response is quite similar in the 3xCO_2 simulation (Fig. 7b) compared to SSP 2-4.5 C (Fig. 4b) and is also coupled to an EKE increase on the poleward flank of the jet (Fig. 7c). Maps of the EKE response show that at 3xCO_2 much of this increased EKE reflects changes over the Atlantic (Fig. 5b), as in the SSP 2-4.5 C en-

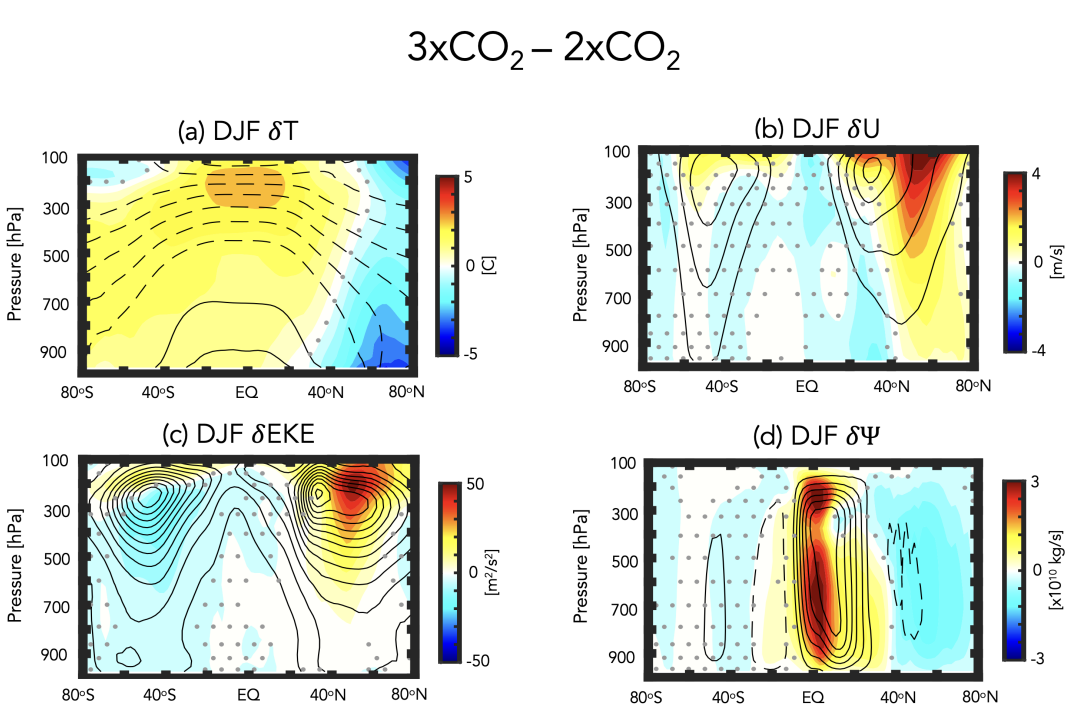

FIG. 7. Same as Figure 4, except showing the difference between the year 120-150 climatological mean 3xCO$_2$ and 2xCO$_2$ responses.

semble (Fig. 5a), although there is also increased EKE over the western Pacific and North America.

To summarize: In response to a collapse of the AMOC, our results show widespread cooling over the Arctic and stronger meridional temperature gradients over the NH. This increase in temperature gradients is associated with a poleward shift of the midlatitude jet (and associated eddy energy) as well as a strengthening of the NH Hadley Cell. In the lower troposphere (> 600 hPa) the NH Hadley cell is displaced poleward.

Over the Northern Hemisphere the response to an increase from 2xCO$_2$ to 3xCO$_2$ is remarkably similar to the differences between the SSP 2-4.5 R and C simulations, in terms of both the magnitude and spatial patterns of these changes. Some exceptions, however, include the near surface (850 hPa) wind response over the North Atlantic, which is not statisically significant at 3xCO$_2$, as well as in the tropics, where precipitation increases strongly over the Pacific. There is also more warming in the tropical upper troposphere and SH in the 3xCO$_2$ simulation. Overall, this close

correspondence suggests that the collapse of the AMOC is the dominant driver of the large-scale circulation changes moving from 2xCO_2 to 3xCO_2 in our model.

b. Scaling of Equilibrated Thermodynamic and Dynamic Responses with Global Mean Surface Temperature (GMST)

One question (Q3) not addressed in the previous sections relates to how changes in the climate response to an eventual collapse of the AMOC scale with changes in GMST. To this end, here we expand our analysis to include the results of additional (4xCO_2 and 5xCO_2) FOM abrupt CO_2 runs, as well as the results from the SOM abrupt CO_2 integrations.

1) Global Thermodynamic Changes

Figure 8a shows the annual global mean surface temperature response among all of the simulations, plotted as a function of associated instantaneous radiative forcing (RF), where RF is calculated from the expression 5.35ln (NxCO_2/1xCO_2) (Byrne and Goldblatt (2014)) and, for each run, N is the CO_2 multiple of the PI value (2.4, for the case of all SSP 2-4.5 ensemble members). The changes in GMST across this broader range of CO_2 forcing show the nonlinear behavior between the 2xCO_2 and 3xCO_2 FOM simulations (blue circles) that was first identified in Mitevski et al. (2021) (their Figure 1). By comparison, the results from the SOM experiments (aqua circles) show no evidence of a nonlinearity. This result was also documented in Mitevski et al. (2021) and suggests that the changes in ocean horizontal and vertical heat fluxes not included in the q-flux experiments are primarily responsible for the nonlinear changes in GMST occurring in the FOM experiments.

Building on Mitevski et al. (2021), here we also include the results from the SSP 2-4.5 R and C ensemble members (red circles, cyan and blue outlines) which are seen to align respectively with the SOM (solid cyan) and FOM (solid blue) scalings. This suggests that the GMST differences between the collapsed (C) versus recovered (R) SSP 2-4.5 ensemble members are primarily associated with the changes in ocean heat convergence occurring in the former. Note that the SSP 2-4.5 results are plotted with respect to the peak CO_2 level achieved (i.e. 643 ppm), which occurs at year 2200 (not at the values occurring during years 2400-2500, which are lower (579-598 ppm)) (Meinshausen et al. (2020)).

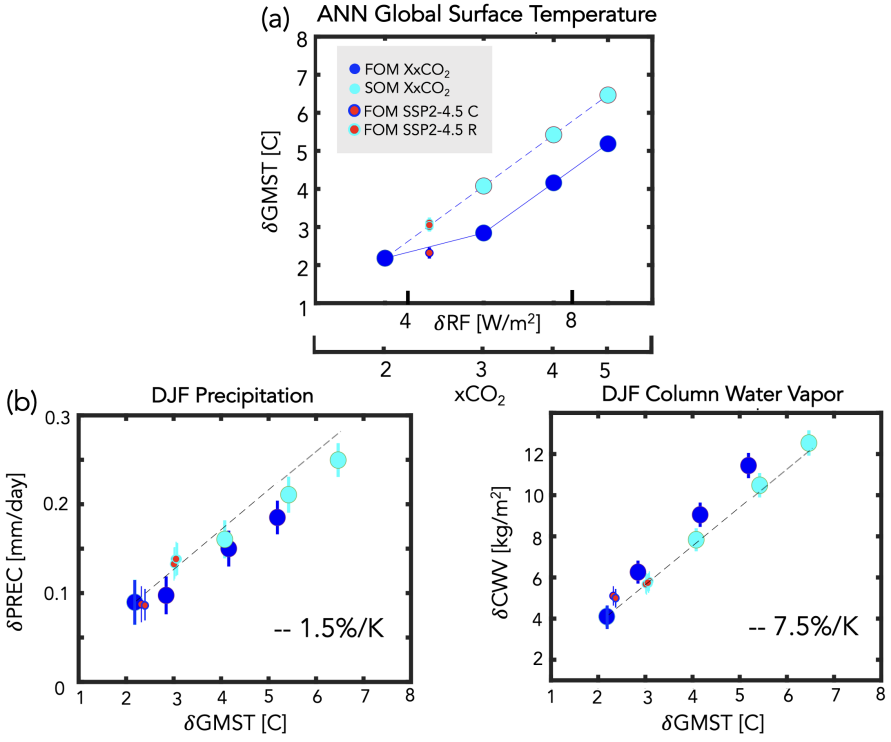

591 FIG. 8. Top: Changes in annual mean global mean surface temperature (GMST), plotted as a function of the
592 associated radiative forcing (RF), calculated from the expression 5.35ln ($NxCO_2/1xCO_2$) (Byrne and Goldblatt
593 (2014)) where, for each run, N is the CO_2 multiple of the PI value (2.4, for the case of the SSP 2-4.5 ensemble
594 members), consistent with the presentation in Mitevski et al. (2021). Bottom: Changes in DJF global mean
595 precipitation (left) and atmospheric column water vapor (right). Changes in precipitation and column water
596 vapor are plotted relative to the annual mean GMST changes in (a). Results from the abrupt 2-5xCO_2 fully
597 coupled atmosphere-ocean model (FOM) and slab ocean model (SOM) results are shown in the blue and cyan
598 filled circles. The FOM SSP 2-4.5 recovered (R) and collapsed (C) results are also shown in the red circles
599 (cyan and blue outlines, respectively). Interannual variability for each metric is indicated by the vertical bars.
600 Note that in all panels the SOM 2xCO_2 results have been adjusted to match the FOM 2xCO_2 results in order to
601 facilitate comparison of the FOM and SOM scalings with CO_2 and GMST, not on the absolute magnitude of the
602 responses.

611 Next we examine how changes in first-order thermodynamic variables scale with these (nonlinear)
612 changes in GMST. As with GMST, the changes in global mean precipitation and integrated column
613 water vapor (CWV) also vary nonlinearly with respect to radiative forcing in the FOM simulations
614 moving from 2xCO_2 to 3xCO_2 (Appendix Figure 2). As expected from the GMST changes, this

behavior is absent in the SOM integrations and the SSP 2-4.5 C and R members again align with the FOM and SOM scalings, respectively.

However, plotting the precipitation and CWV DJF changes relative to annual mean GMST, reveals that the nonlinear scaling with RF more-or-less disappears (Fig. 8b). This demonstrates that, while the first order global scale hydrological cycle is sensitive to the collapse of the AMOC, this sensitivity occurs primarily through changes in GMST. It is also interesting to note that the lower precipitation values occurring in the SOM integrations, for a given values of GMST, are consistent with the direct effect of greenhouse gases, which tend to suppress global mean precipitation (Samset et al. (2016)).

Finally, we note that the scaling of precipitation and CWV with GMST roughly follow the predictions from Held and Soden (2006), who identified a Clausius-Clapeyron (CC) scaling of integrated column water vapor (dashed black line denoting 7.5%/K, Fig. 8b, right) and a significantly sub-CC scaling of global mean precipitation (1.5%/K, Fig. 8b, left). While some additional nonlinearity in precipitation is also evident at higher CO_2 levels, as this is not immediately relevant to the SSP 2-4.5 ensemble, we reserve further discussion for future work.

2) Northern Hemisphere Dynamical Changes: A Regime Shift

Moving next to the dynamical response, we find that several measures of the NH DJF zonal mean dynamical circulation behave nonlinearly (and even non-monotonically) with respect to radiative forcing in the FOM simulations (Appendix Figure 3). Unlike precipitation and CWV, however, this non-linear behavior in the NH surface wind-based Hadley cell edge (Fig. 9a), Hadley Cell strength (Fig. 9b), northern midlatitude EKE (Fig. 9c), latitude of maximum eddy momentum fluxes (Fig. 9d) and northern midlatitude static stability (Fig. 9e) also occurs after plotting as a function of GMST. Overall, these results suggest that there is no clear (certainly not linear) relationship between the northern Hadley Cell (strength and lower tropospheric edge) and midlatitude jet behavior with GMST in simulations ($3xCO_2$ and SSP 2-4.5 C) in which the AMOC eventually collapses.

Rather, the changes in both the NH Hadley Cell edge and strength reflect an abrupt poleward shift and increase, respectively, moving from $2xCO_2$ to $3xCO_2$ and between the SSP 2-4.5 R and SSP 2-4.5 C ensemble members. This abrupt poleward shift and strengthening saturates at $3xCO_2$ and even decreases at higher CO_2 values for certain metrics, despite continued increases in GMST (Fig.

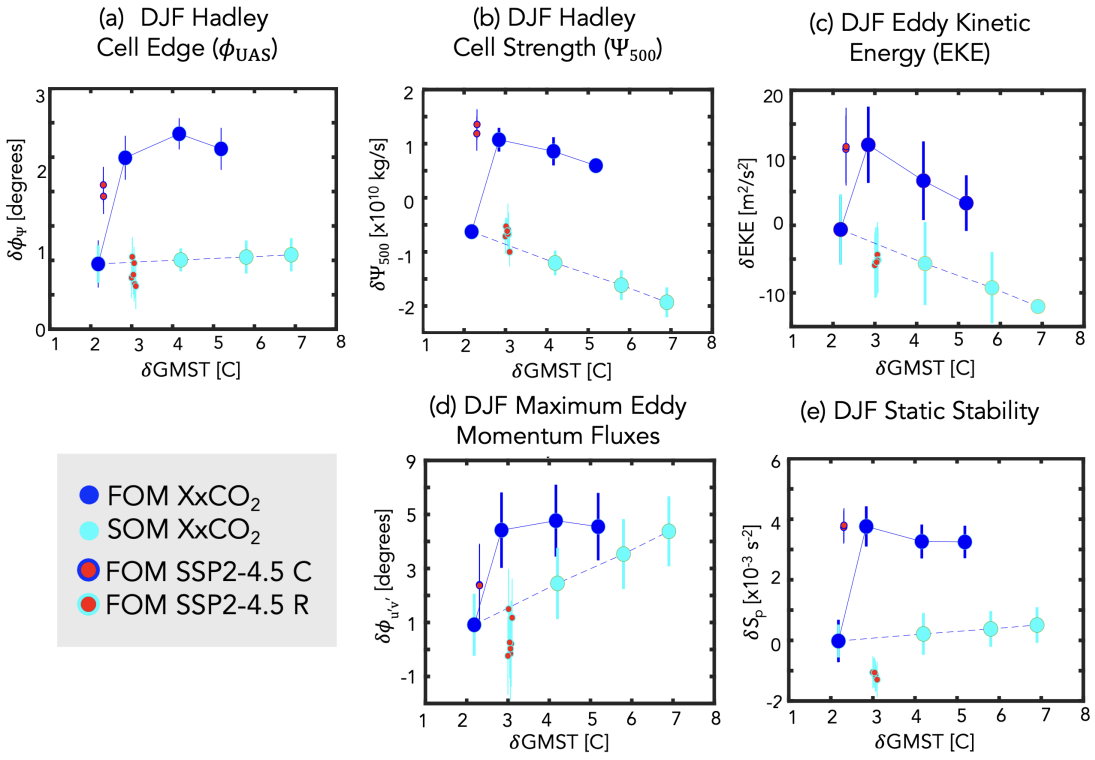

640 FIG. 9. Changes in various DJF Northern Hemisphere (NH) dynamical metrics, plotted as a function of GMST.
641 Specifically, shown are the Hadley Cell edge (ϕ) (a), Hadley Cell strength (Ψ_{500}) (b), NH column eddy kinetic
642 energy (EKE) (c), latitude of the maximum NH eddy momentum fluxes (d) and NH midlatitude dry static stability
643 (e). The quantities in (a), (b) and (d) are defined in Section 2, while the zonally averaged EKE and static stability
644 changes have both been averaged over 300-1000 hPa and 30°N-60°N. Results from the abrupt 2-5xCO_2 fully
645 coupled atmosphere-ocean model (FOM) and slab ocean model (SOM) results are shown in the blue and cyan
646 filled circles. The FOM SSP 2-4.5 recovered (R) and collapsed (C) ensemble members are shown in the red
647 circles (cyan and blue outlines, respectively). Interannual variability for each metric is indicated by the vertical
648 bars. As in Figure 8 the SOM 2xCO_2 results have been adjusted to match the FOM 2xCO_2 results.

653 9b, 9c). As such, this saturation in the NH circulation is indicative of a "regime" shift in our model,
654 consistent with the use of the term in Caballero and Langen (2005), albeit for the low-gradient,
655 high temperature regime identified in their study using a more idealized model (see discussion in
656 Section 4). In particular, our results suggest that the AMOC collapse is associated with a regime
657 shift in our model between a climate state in which the Hadley Cell is substantially weaker and

displaced equatorward (strong AMOC) and a state in which the Hadley Cell and midlatitude EKE is stronger and displaced poleward (weak AMOC).

Note that, while the increases in Hadley Cell strength (Fig. 9b) have been well documented, the poleward shift in the northern Hadley Cell edge has been less examined (Fig. 9a). Our examination of the Hadley Cell edge, as gauged using the surface zonal winds, is partly motivated by the results presented in Figure 3d, which show increased SLP over the North Pacific and Atlantic high latitudes. That is, the SLP increases over the North Atlantic extend as far south as 40^{o}N and thus, together with the Pacific response, reflect a pattern which is consistent with the SLP pressure signature of an expanded northern edge of the Hadley cell (Schmidt and Grise (2017)). Another motivation comes from KB2021, who suggest that, in addition to reduced warming over the Arctic, stronger tropical heating and a related expansion of the HC may contribute to the poleward shift of the northern jet, although this was never explicitly shown.

The fact that changes in the Hadley Cell and midlatitude eddy-driven jet are linked is consistent with recent studies showing that the HC edge is strongly linked to the latitude of maximum eddy momentum fluxes, such that a poleward shift of the jet is associated with HC expansion (Chemke and Polvani (2019), Waugh et al. (2018), Menzel et al. (2019)). As discussed in those studies, this connection is likely associated with changes in the latitude of the maximum eddy momentum fluxes and the vertical potential temperature gradient (i.e., the static stability, $S_p = -(\frac{T}{\Theta})(\frac{\partial \Theta}{\partial P})$) over northern midlatitudes, which also exhibit regime shifts in the NH (Fig. 9 d-e). The sensitivity of the extratropical tropospheric eddy response to even modest changes in isentropic slope, resulting both from changes in baroclinicity and static stability, is well known (Thompson and Birner (2012)) and previous studies have shown that increases in static stability at higher CO_2 forcing can increase subtropical baroclinicity, causing the HC edge and subtropical eddy fields to shift poleward (Chemke and Polvani (2019); Menzel et al. (2019)). Note that the changes in EKE and static stability are shown averaged over 300-1000 hPa and over 30^{o}N-60^{o}N; similar results are found averaging over the entire hemisphere poleward of 20^{o}N.

Another interesting feature highlighted in Figure 9 is that for some variables even the *sign* of the response is different than would otherwise be predicted from the SOM experiments which ignore changes in ocean heat convergence. This applies both to the changes in Hadley Cell strength (Fig. 9b) and tropospheric column averaged EKE (Fig. 9c) which otherwise decrease in response to

increasing CO_2. This role of the ocean in the behavior of projected changes in northern EKE is consistent with Chemke et al. (2022), who showed that changes in ocean heat convergence are essential for correctly capturing the sign of the projected response in future storm track changes over the North Atlantic.

To further relate the changes in the Hadley Cell to the changes in midlatitude eddies, Figure 10 shows the evolution of the response in northern HC strength (a), EKE (b), baroclinic eddy generation (c), and midlatitude static stability (d). While the HC strengthening may be more directly linked to the southward shift of the ITCZ as proposed in previous studies (Zhang et al. (2010)), the increases in dry static stability in the 3xCO_2 and SSP 2-4.5 simulations evolve on a similar time scale as the changes in northern midlatitude tropospheric baroclinic eddies. The similar behavior among those variables suggests that they are mechanistically related. Furthermore, while changes in tropopause height have also been invoked to interpret future changes in the midlatitude jet stream (Cronin and Jansen (2016), Held (1993), Vallis et al. (2015)) and edge of the Hadley Cell (Lu et al. (2007)), we do not observe a consistent response in tropopause height between the 3xCO_2 and SSP 2-4.5 C integrations (not shown), suggesting that tropopause height changes alone are not the primary drivers of the Hadley Cell and jet behaviors exhibited in these runs.

Note that the similar evolution of the HC strength and midlatitude eddy changes suggested in Figure 10 may seem at odds with the findings in Menzel et al. (2019), who showed a strong disconnect between the strength of the subtropical jet and the edge of the Hadley Cell. However, there are some subtle differences in the evolution of those responses; furthermore, that study inferred this disconnect based on interannual variability and the response to an abrupt 4xCO_2 forcing, which both yield a weakening and poleward shift of the Hadley Cell. By comparison, in connection with a southward shifted ITCZ a collapse of the AMOC is associated with a strengthened Hadley Cell (Zhang and Delworth (2005); Orihuela-Pinto et al. (2022)).

c. Energetic Analysis: Bjerknes Compensation in Response to an AMOC Shutdown

The previous section showed that, unlike the global mean thermodynamic response, several measures of NH dynamical sensitivity do not scale linearly with changes in global mean surface temperature. Rather, a collapsed AMOC in our model is accompanied by an abrupt strengthening and northward shift of the Hadley Cell and northern midlatitude jet. To better understand why these

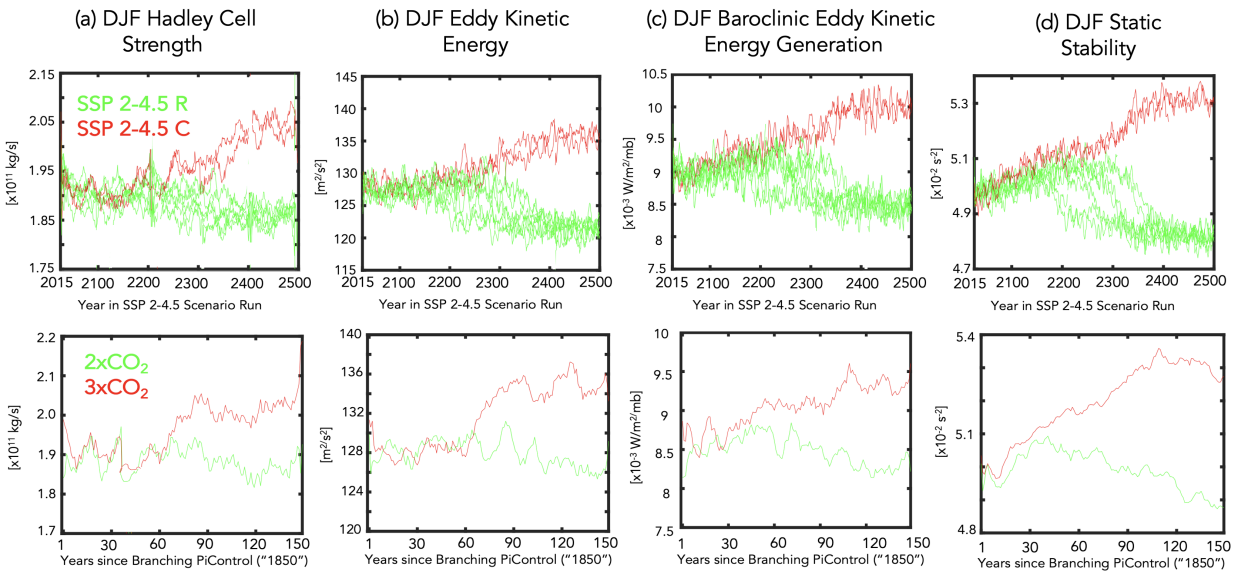

FIG. 10. Evolution of DJF Northern Hemisphere Hadley Cell strength (a), eddy kinetic energy (b), baroclinic eddy kinetic energy generation (c) and midlatitude dry static stability (d). The baroclinic eddy generation has been averaged over the same region (300-1000 hPa, 30°N-60°N) as the EKE and static stability fields, consistent with Figure 9. Comparisons among the SSP 2-4.5 recovered (R) and collapsed (C) ensemble members (top panels) and between the $2xCO_2$ and $3xCO_2$ runs (bottom panels) are shown in the green and red lines, respectively. A 5-year moving average has been applied to all time series.

variables exhibit this regime shift we examine the changes in energetics – and their partitioning between the atmosphere and ocean – that arise moving from $2xCO_2$ to $3xCO_2$ and between the SSP 2-4.5 R and SSP 2-4.5 C members.

1) Ocean and Atmosphere Compensation

Figure 11 shows the response in the annual mean northward total (atmosphere + ocean), oceanic and atmospheric transports, relative to the preindustrial control simulation. Between $2xCO_2$ and $3xCO_2$ and between the SSP 2-4.5 R and SSP 2-4.5 C members there is a large decrease/increase in T_O/T_A over northern latitudes with a peak located at ~30-40°N. This behavior is reflective of an abrupt Bjerknes compensation that emerges in the model, wherein large anomalies in heat transported by the atmosphere increase to approximately balance large reductions in northward ocean transport (Bjerknes (1964)). More precisely, the reduction in northward ocean heat transport in the SSP 2-4.5 C ensemble members and at $3xCO_2$ is approximately 1 PW (Fig. 11), representing

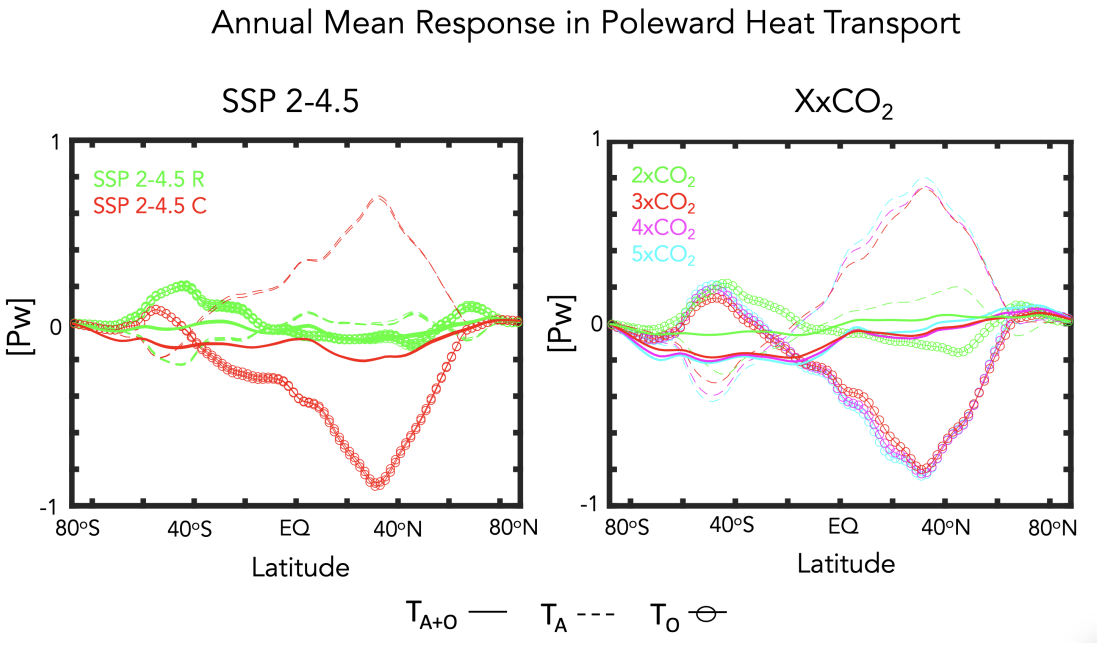

741 FIG. 11. Changes in the annual mean atmospheric (T_A), oceanic (T_O) and total (atmospheric + oceanic, T_{A+O})
742 northward energy transport, relative to the preindustrial control simulation. Results from the SSP 2-4.5 ensemble
743 members and the 2-5xCO_2 simulations are shown in the left and right panels. The simulations in which the
744 AMOC collapses (3xCO_2, SSP 2-4.5 C) versus recovers (2xCO_2, SSP 2-4.5 R) are highlighted in the red and
745 green lines, respectively.

735 a ~50% decrease relative to preindustrial values (Fig. 2b). Magnusdottir and Saravannan (1999)
736 attributed this compensatory response in the atmosphere to high dynamical efficiency of atmo-
737 spheric eddy transport. Note that the annual mean is shown here to facilitate comparison with the
738 annual mean results presented in previous studies (e.g., Figure 1 in Zhang and Delworth (2005)
739 and Figure 5 in Zhang et al. (2010)). We note in passing that the responses in the boreal winter
740 transports look very similar (not shown).

746 What Figure 11 makes clear is that the changes in ocean heat transport are dominated by the
747 changes in the AMOC, as reflected in the magnitude of the compensation occurring at 3xCO_2
748 (similar to the compensation occurring in the SSP 2-4.5 C ensemble) which saturates, despite
749 further increases in CO_2 (and GMST). This helps to explain the behavior of the dynamical indices
750 discussed in the previous section (Fig. 9), which also saturate at 3xCO_2 and do not increase
751 (rather, decrease) moving to higher CO_2 forcings. A dramatic reduction in poleward ocean heat

transport at ~30-40°N was also noted in the CMIP5 historical models in association with strong air-sea interactions within the midlatitude storm tracks (Outten et al. (2018)) and in several future climate integrations performed using the CMIP5 version of the GISS climate model (E2) Rind et al. (2018). In the latter case, however, the near cessation of the AMOC severely limited, but did not entirely shut off, poleward heat transport, which was partly maintained through the ocean subtropical gyre contribution. Our results also show stronger compensation occurring over SH high latitudes poleward of 40°S.

While the changes in T_O and T_A reflect near entire compensation, this compensation is nonetheless not perfect and slightly negative, resulting in a net reduction in the total northward combined atmospheric and oceanic energy transport. This reduction in net poleward energy transport was also found in Liu et al. (2020), who showed that a weakened AMOC caused a larger energy change at the Earth's surface than at the TOA (their Figure S.5). In particular, over the NAWH region they found that more energy was taken from the atmosphere through surface turbulent heat fluxes, resulting in a situation where the NH atmosphere loses more energy at the surface compared to the energy that is gained at the TOA (through reduced OLR). In the GISS model we also find that there is more energy loss at the surface compared to changes at the TOA and that these are primarily associated with reduced latent heat fluxes (Appendix Figure 4). The reductions in surface latent heat fluxes occur over the North Atlantic and are strongly shaped by changes in evaporation (not shown). The exact extent and nature of this compensation, however, is likely shaped strongly by cloud feedbacks (Zhang et al. (2010)) as discussed more in Section 4b.

2) Moist vs. Dry Atmospheric Transports

To better understand the nature of the compensation occurring in the GISS model, Figure 12 further decomposes the changes in T_A into changes in the northward transports of latent heat (Fig. 12a) and dry static energy (Fig. 12b). Over the SH the changes in dry and moist static energy nearly compensate in all simulations, resulting in weakly negative northward atmospheric transports poleward of ~40°S in both the $XxCO_2$ and SSP 2-4.5 runs. Equatorward of ~40°S, however, this behavior transitions in the SSP 2-4.5 C members to net positive northward atmospheric transport from the SH subtropics towards and across the equator (which compensates the reduction in oceanic equatorward heat transport in that region evident in Figure 11). This behavior over the SH

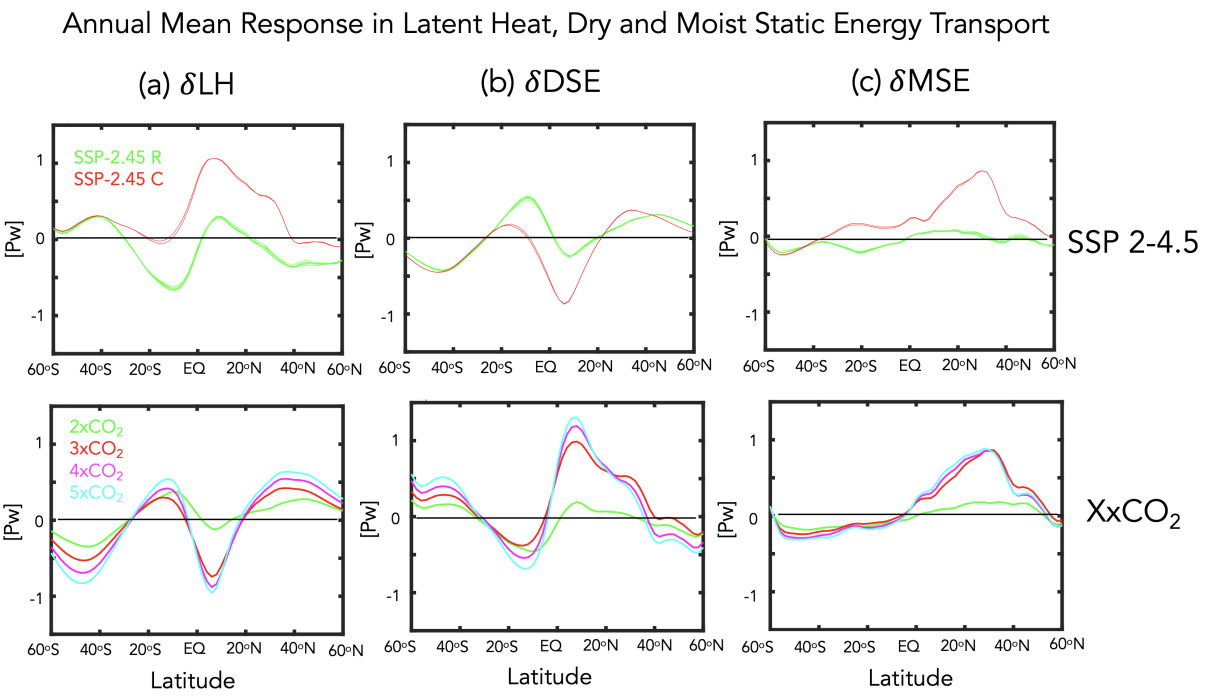

788 FIG. 12. Changes in the annual mean atmospheric latent heat (a), dry static energy (b) and total moist static
789 energy (c) northward transports, relative to the preindustrial control simulation. Results from the SSP 2-4.5
790 ensemble members and the 2-5xCO_2 simulations are shown in the top and bottom panels. The simulations in
791 which the AMOC collapses (3xCO_2, SSP 2-4.5 C) versus recovers (2xCO_2, SSP 2-4.5 R) are highlighted in the
792 red and green lines, respectively.

781 subtropics is distinct from what occurs in the XxCO_2 simulations, in which there is overall reduced
782 northward atmospheric transport (and less compensation by the oceanic transports). The fact that
783 the oceanic compensation in this region is weaker at 3xCO_2 (relative to the SSP 2-4.5 C members)
784 may reflect the differences in simulation length between the abrupt CO_2 and SSP 2-4.5 integrations
785 or the fact that at 3xCO_2 there is increased water vapor in the atmosphere in the warmer climate and
786 hence increased poleward latent heat transport. Notably, however, the AMOC response in all runs
787 has little effect on extratropical latent heat transport over the Southern Hemisphere extratropics.

793 Aside from the subtle differences between the 3xCO_2 and SSP 2-4.5 C runs that occur over the
794 SH subtropics, the fact that the changes in dry static energy (DSE) and latent heat transport nearly
795 compensate over southern and tropical latitudes in all runs is consistent with the expectation from
796 Held and Soden (2006). Interestingly, however, this compensation does not occur over northern
797 latitudes spanning ~10°N to ~40°N, resulting in a net increase in poleward moist static energy

transport (Fig. 12c). Over these latitudes the increased atmospheric energy transport resulting from an AMOC collapse is almost entirely due to changes in dry static energy, not latent heat transport. In particular, DSE transport exhibits a "jump" between 2xCO_2 and 3xCO_2 (also evident in the differences between the SSP 2-4.5 C and SSP 2-4.5 R members) (Fig. 12b); a similar jump is only evident in the latent heat transports equatorward of 20^{o}N (which, if anything, enhances energy transport equatorward, not poleward). The jump in DSE transport over the northern extratropics saturates for forcings greater than 3xCO_2. Further analysis of the evolution of the dry static energy transports at different latitudes in the northern hemisphere (not shown) reveals that these changes in DSE transport first emerge between 30^{o}N-40^{o}N and propagate thereafter to higher latitudes.

The fact that the abrupt increase in atmospheric poleward transport derives primarily from changes in DSE transport helps in interpreting why a similar shift emerges in the Hadley Cell and eddy-driven jet, since the Hadley cell fluxes dry static energy poleward (Frierson et al. (2007)). Indeed, previous energetic definitions of the storm track have appealed directly to DSE (e.g. latitude of maximum vertically-integrated dry static energy flux (Hoskins and Valdes (1990)). More recently, Lachmy and Shaw (2018) show that the vertically integrated eddy potential energy flux shifts in same sense as the vertically integrated eddy DSE flux. They then use the Eliassen-Palm flux relation to connect these changes in energy fluxes to changes in the eddy momentum fluxes. Therefore, the fact that these features all shift in concert with each other in our runs should perhaps not be too surprising.

4. Discussion

a. Caveats Concerning Model Biases

One important caveat with our results relates to known biases in vertical mixing in the ocean component of the GISS model, as discussed in Miller et al. (2021). This biased mixing is likely related to why E2.1 exhibits a more sensitive AMOC response to a quadrupling of CO_2, compared to some other CMIP6 models (KB2021). In addition, Rind et al. (2020) showed that the parameterization of rainfall evaporation associated with moist convective precipitation has a strong influence on the AMOC sensitivity to greenhouse gas forcing in the E2.1 (and higher top E2.2) models, likely via its effect on moisture loading in the atmosphere. Thus, in addition to oceanic processes, atmospheric parameterizations could also be influencing this result.

Along with biases in vertical mixing, the ocean component of E2.1 is also low resolution (one degree). This likely has direct implications for the stability of the AMOC, as discussed in AR2023 (see references therein). In particular, the stability of the AMOC will differ between low resolution climate models, which exhibit a negative salt-advection feedback (leading to salinification of the subpolar gyre and AMOC recovery), and eddy-permitting models, which tend to exhibit a stable AMOC-off state. We emphasize here, however, that throughout we have focused on the response of the atmospheric circulation given a collapse in the AMOC. Thus, while the particular mechanisms by which the AMOC is weakened (and subsequently recovers) in E2.1 may be model-specific, our focus has been on quantifying the atmospheric changes. We also note that Mitevski et al. (2021) showed that the behavior of the AMOC in E2.1 was similar to the response in CESM-LE; furthermore that model also featured a nonlinear response in GMST related to a collapse of the AMOC, albeit one occurring at the transition between 3xCO_2 and 4xCO_2.

b. Bjerknes Compensation: Cloud Feedbacks and Dry Versus Moist Energy Transports

A key result from our study is that a collapse of the AMOC results in a regime shift in various components of the NH large-scale circulation and this shift is reflective of an abrupt Bjerknes compensation that emerges at 3xCO_2 and in the SSP 2-4.5 C ensemble members. There are several aspects of this compensation, however, that require closer examination. Among others, these include:

1) Influence of Cloud Feedbacks

Mitevski et al. (2022) showed that nonlinearity in ECS occurring between 2xCO_2 and 3xCO_2 in our model was related to nonlinear variations in the atmospheric feedback parameter and not to changes in radiative forcing. At the same time, the strength of the Bjerknes compensation in our model will likely depend on cloud feedbacks, as the right-hand-side of Equation (1) makes clear (via the F_T and F_S terms). For example, Zhang et al. (2010) showed a strong sensitivity of the tropical climates' response to a freshwater hosing forcing to changes in cloud feedbacks, showing that in a model with no cloud feedbacks the tropical response to the weakening of the AMOC (including its southward ITCZ shift) was much smaller. Thus, while the overall Bjerknes compensation occurring in our model is generally consistent (in its meridional distribution and

amplitude) with the results from other similar studies, the exact details of how compensation occurs is likely to be sensitive to local climate feedbacks which may be model-dependent and/or poorly constrained by observations. Future work will focus on better understanding how changes in cloud feedbacks modulate the response of the atmosphere to a weakened AMOC in our model.

2) Atmospheric Dry vs. Moist Compensation

One interesting result from this study is that the large compensation in poleward atmospheric transport that occurs as the AMOC collapses is primarily related to increases in the northward transport of dry static energy poleward of 20^{o}N (coincident with the edge of the non-monotonically shifting HC edge) (Fig. 12). This result is initially surprising as it downplays the compensation that occurs through changes in latent heat transport over northern midlatitudes. Thus, while our results do show a compensatory latent heat transport occurring in the tropics, this does not occur over the NH extratropics and is therefore not fundamentally associated with the non-monotonic behavior in the NH Hadley Cell edge and midlatitude eddy-driven jet.

The diminished importance of the latent heat transports over northern midlatitudes is initially surprising, given that warming in response to increased CO_2 results in an overall increase in atmospheric water vapor. Upon further reflection, however, this effect of enhanced global warming needs to be considered in the context of both the reduced Arctic warming and poleward shifted EKE evident in Figure 4. The former can, via cooling, reduce the total moisture available for northward transport, while the latter would impact the efficiency with which subtropical moisture is transported poleward to higher latitudes. In our results it appears that these changes compensate, resulting in no net AMOC imprint on the latent heat transports over northern extratropical latitudes (Fig. 10a, bottom). While disentangling these contributions is beyond the scope of this study, we do comment on the consistent results shown in Figure S5 of Mitevski et al. (2021), who identified a much stronger non-monotonicity present in the edge of the dry zone (P-E) compared to NH specific humidity. While this suggests that the circulation changes are themselves responsible for the behavior of the latent heat transports (and not vice versa), more work is needed to understand the underlying mechanism present in our model and whether this behavior is also exhibited in other models (or the real atmosphere).

5. Conclusions

Here we have documented the atmospheric response to a CO_2-induced AMOC collapse using the CMIP6 version of the NASA GISS climate model (E2.1). Using simulations from an identically forced (SSP 2-4.5) ensemble in which the AMOC collapses and recovers in two and eight members, respectively, we have isolated the atmospheric response to a spontaneous collapse of the AMOC in the context of a warming climate, absent any external perturbations that may interfere with the model's internal dynamics. By comparison, previous studies have all needed to employ (negative) freshwater flux perturbations or similar AMOC "locking" methods (Liu et al. (2020), Orihuela-Pinto et al. (2022)). We then placed the atmospheric response in the SSP 2-4.5 simulations in the broader context of a set of integrations in which CO_2 is abruptly increased, run both using fully coupled atmosphere-ocean (FOM) and slab-ocean (SOM) configurations, in which changes in ocean heat flux convergences are respectively included and neglected.

Our main results are as follows:

1. In our model a sustained decline and eventual collapse of the AMOC results in a strengthening of the NH Hadley cell and the northern midlatitude jet, as well as an abrupt northward shift of the Hadley Cell edge in the lower troposphere. Quite remarkably, these features dominate the large-scale atmospheric circulation response that occurs in the NH moving from $2xCO_2$ to $3xCO_2$.

2. For certain variables (i.e., HC strength, EKE) an ultimate collapse of the AMOC produces changes that are *opposite* in sign to the response to increased CO_2 forcing occurring in the absence of ocean circulation changes.

3. The regime shift in the NH large-scale circulation reflects an abrupt Bjerknes compensation that emerges in the $3xCO_2$ and collapsed SSP 2-4.5 C simulations. This compensation is located further south (~40^oN) of what is often considered to be the main region of maximum ocean-atmosphere compensation (70^oN) (Shaffrey and Sutton (2006)) and reflects a key role for the midlatitude storm tracks in the coupled system's response to a warmer climate.

4. The impact of the AMOC on the large-scale NH circulation occurs mainly through its influence on mean free-tropospheric temperature gradients, not GMST. This finding reinforces growing evidence that the climate's "dynamical sensitivity" does not scale with equilibrium climate sensitivity (Grise and Polvani (2016), Ceppi et al. (2018)), particularly in the presence of a collapsed AMOC .

The regime shift in NH dynamics resulting from an AMOC collapse in our model is, to the best of our knowledge, the first time that such behavior has been documented for a CMIP class model. While previous studies have also reported nonlinear behaviors in Hadley Cell strength (Levine and Schneider (2011), O'Reilly et al. (2016)) these studies have employed mainly idealized models. In addition to the changes in the Hadley Cell we also identify a regime shift in the behavior of the northern storm tracks. This result brings to mind the findings from Caballero and Langen (2005), who showed that poleward energy transport increases over a range of increasing surface temperature but saturates in the low-gradient, high temperature regime. As in our study, they attribute this "low-gradient" paradox to increasing tropospheric static stability and the poleward migration of the storm tracks. However, they too employed a highly idealized (aquaplanet) model and find that this saturation in storm track behavior is related to a saturation of latent heat transport. Our results, by comparison, highlight the role of compensatory dry static energy transports and suggests that studies accounting for dynamic ocean-atmospheric coupling (i.e., changes in vertical and horizontal ocean heat fluxes) may come to different conclusions about the nature of compensation in the atmosphere.

In addition to contributing to improved understanding of the coupled atmosphere-ocean response to a weakening of the AMOC, our results also have a practical implication for the purpose of developing storylines of atmospheric circulation changes (Zappa and Shepherd (2017)) and for interpreting model differences in projected storm tracks. In particular, while the use of "global warming levels" applied throughout the IPCC AR6 report may suffice for understanding the global hydrological cycle (Hausfather et al. (2022)) here we have shown that this does not hold true for projections of the NH jet stream and Hadley Cell edge. This underscores the need to understand

the direct impact of the AMOC on meridional temperature gradients and not only on surface temperature.

Finally, preliminary analysis of the high-top GISS climate model (E2.2 (Rind et al. (2020), Orbe et al. (2020)) suggests a different sensitivity of the AMOC compared to E2.1 (occurring between $3xCO_2$ and $4xCO_2$). Understanding these differences and how they are reflected in different Bjerknes compensations will be described in a follow-up paper.

Acknowledgments. C.O. thanks Ivan Mitevski for processing the zonally varying eddy kinetic energy fields that were used as part of this analysis. Climate modeling at GISS is supported by the NASA Modeling, Analysis and Prediction program, and resources supporting this work were provided by the NASA High-End Computing (HEC) Program through the NASA Center for Climate Simulation (NCCS) at Goddard Space Flight Center.

Data availability statement. The CMIP6 SSP 2-4.5 data used in this study is available from the Earth System Grid Federation (ESGF) (`https://esgf-node.llnl.gov/search/cmip6/`) or from the NASA Center for Climate Simulations (NCCS) (`https://portal.nccs.nasa.gov/datashare/giss/cmip6/`). The specific simulations used here are a subset of the historical r[1-10]i1p1f2 (`doi:87010.22033/ESGF/CMIP6.7127`) and SSP 2-4.5 r[1-10]i1p1f2 (`doi:10.22033/ESGF/CMIP6.7415`) runs. The $XxCO_2$ data used to produce the figures in the study is publicly available in a Zenodo repository at `https://doi.org/10.5281/zenodo.3901624`. The authors acknowledge the World Climate Research Programme's Working Group on Coupled Modeling and we thank all climate modeling groups for making available their model output. All GISS ModelE components are open source and available at `https://www.giss.nasa.gov/tools/modelE/`.

APPENDIX

Appendix Figures

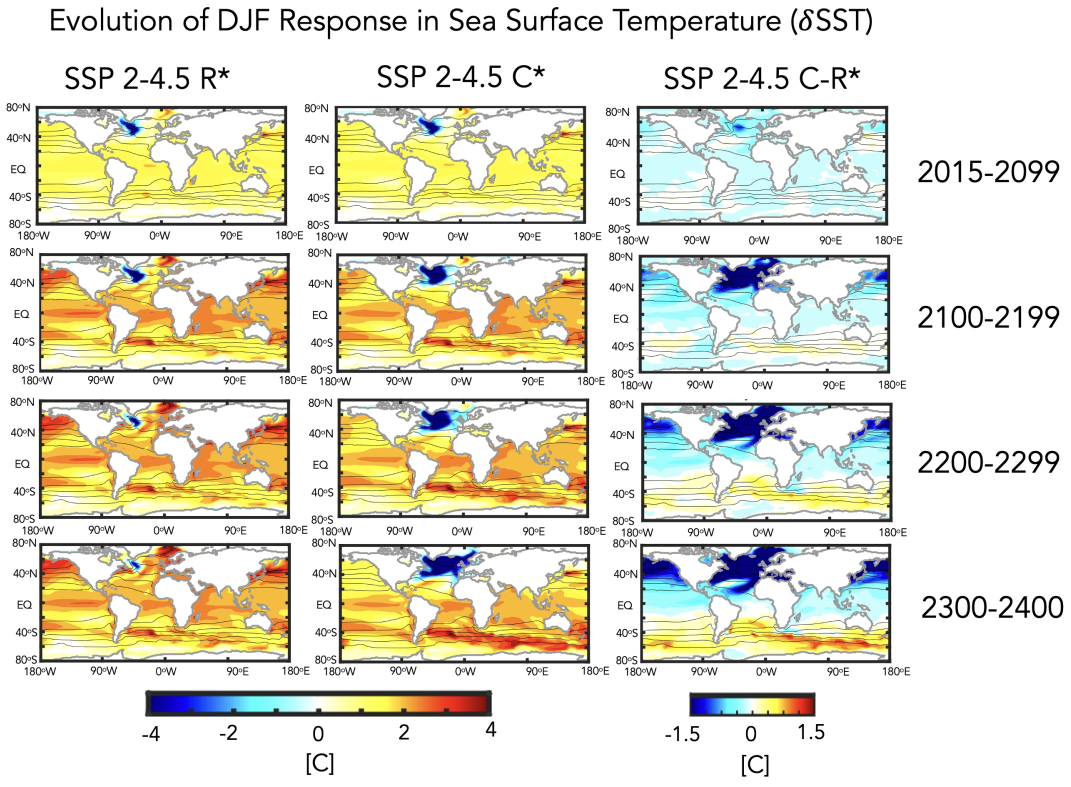

FIG. A1. The evolution of the DJF sea surface temperature difference, relative to the preindustrial control simulation, in one of the SSP 2-4.5 recovered (R) (left) and collapsed (C) ensemble members (middle). The difference between the SSP 2-4.5 recovered and collapsed ensemble members is also shown (right). Note that only one ensemble member is used due to the different recovery times of the AMOC among the "recovered" ensemble members prior to year 2400. Climatological mean values from the preindustrial control simulation are denoted in the black contours.

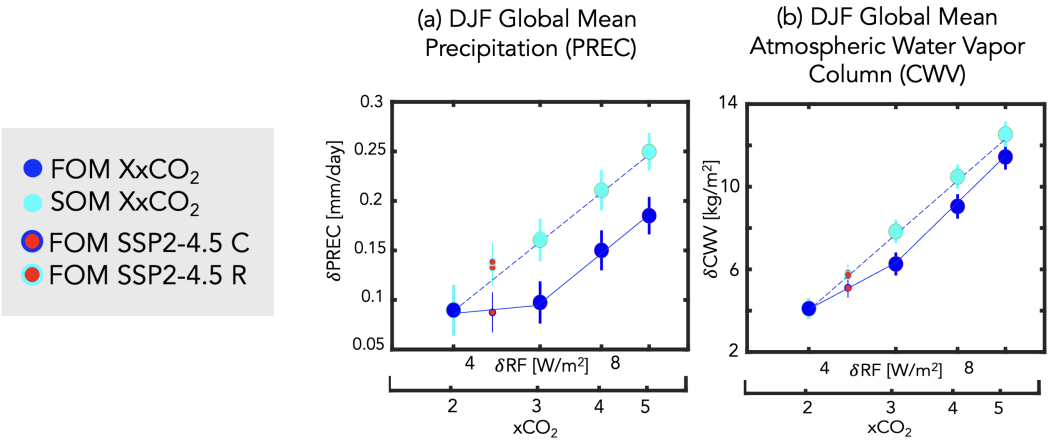

973 FIG. A2. Changes in DJF global mean precipitation (a) and atmospheric column water vapor (b), plotted as a
974 function of the associated radiative forcing (RF), calculated from the expression 5.35ln ($NxCO_2/1xCO_2$) (Byrne
975 Goldblatt (2014)) where, for each run, N is the CO_2 multiple of the PI value (2.4, for the case of the SSP 2-4.5
976 ensemble members). Results from the abrupt 2-5xCO_2 fully coupled atmosphere-ocean model (FOM) and slab
977 ocean model (SOM) results are shown in the blue and cyan filled circles. The FOM SSP 2-4.5 recovered and
978 collapsed ensemble members are also shown in the red circles (cyan and blue outlines, respectively). Interannual
979 variability for each metric is indicated by the vertical bars.

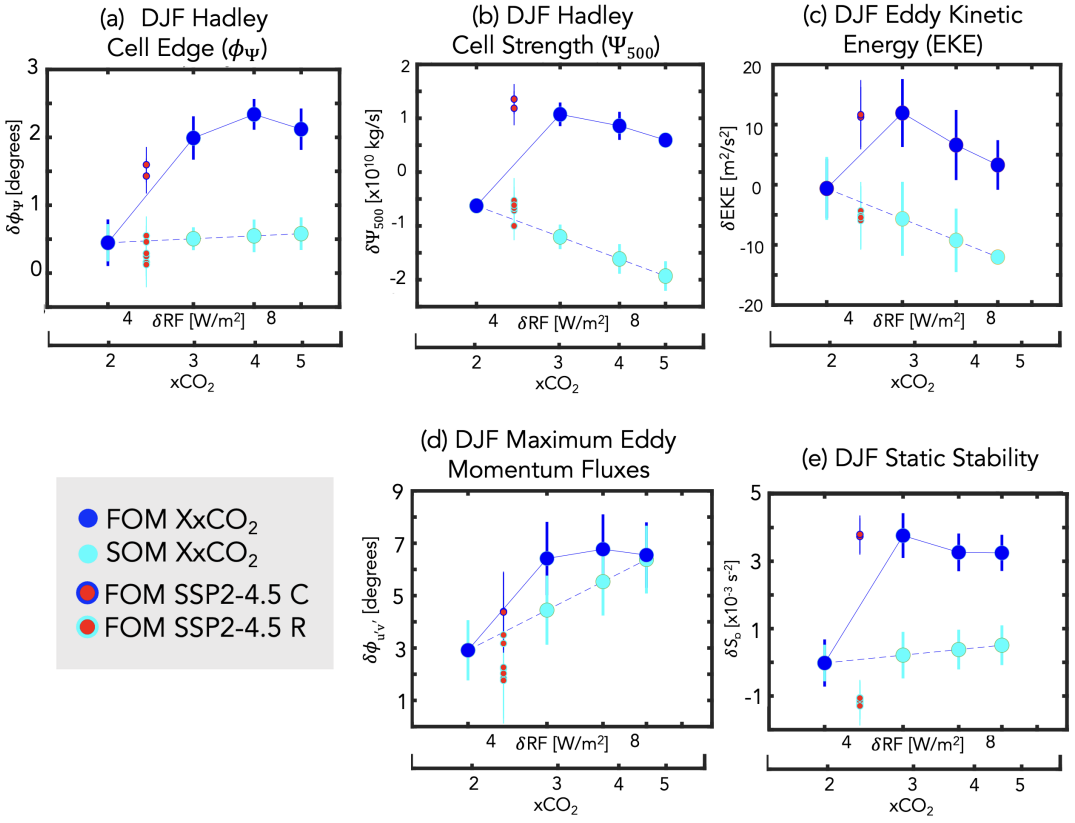

FIG. A3. Changes in various DJF Northern Hemisphere (NH) dynamical metrics, plotted as a function of associated radiative forcing. Specifically, shown are the Hadley Cell edge (ϕ_{UAS}) (a), Hadley Cell strength (Ψ_{500}) (b), NH column eddy kinetic energy (EKE) (c), latitude of the maximum NH eddy momentum fluxes (d) and NH midlatitude dry static stability (e). The quantities in (a), (b) and (d) are defined in Section 2, while the zonally averaged EKE and static stability changes have both been averaged over 300-1000 hPa and 30°N-60°N. Results from the abrupt 2-5xCO$_2$ fully coupled atmosphere-ocean model (FOM) and slab ocean model (SOM) results are shown in the blue and cyan filled circles. The FOM SSP 2-4.5 recovered and collapsed ensemble members are shown in the red circles (cyan and blue outlines, respectively). Interannual variability for each metric is indicated by the vertical bars.

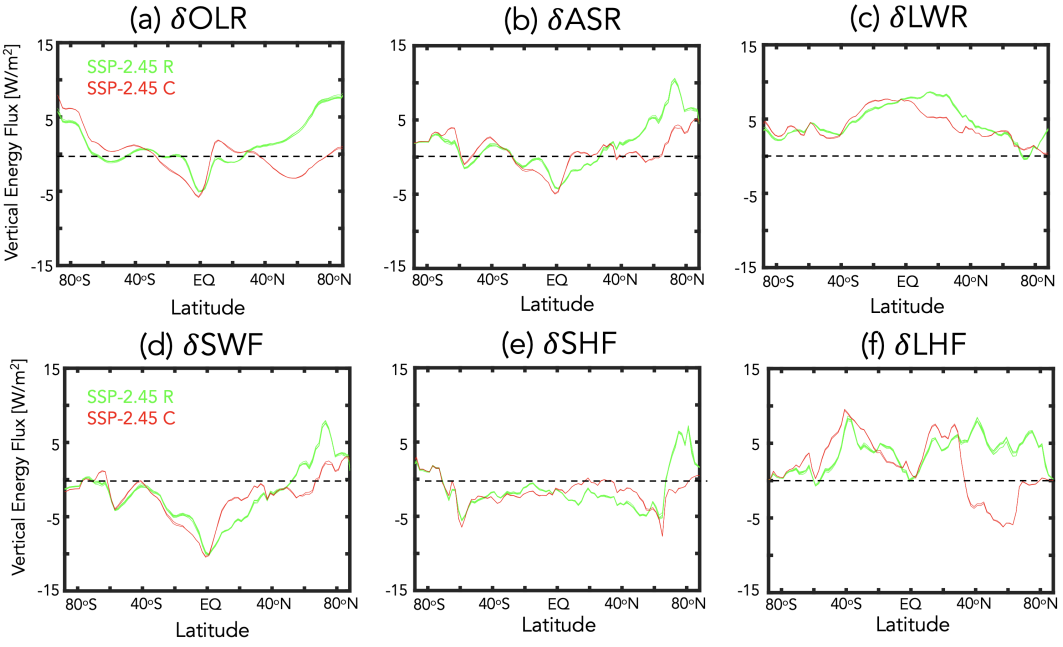

FIG. A4. Changes in the annual mean top of the atmosphere outgoing longwave radiation (OLR) (a) and absorbed shortwave radiation (ASR) (b) and the downward fluxes of radiation at the surface, decomposed into longwave (LWF) (c) and shortwave (SWF) (d) components. The fluxes of latent and sensible heat at the surface (LHF and SHF) are shown in (e) and (f), respectively. All changes are shown for the SSP 2-4.5 collapsed (C) (red) and SSP 2-4.5 recovered (R) (green) ensemble members and are defined relative to the preindustrial control simulation.

References

Adam, O., and Coauthors, 2018: The TropD software package (v1): standardized methods for calculating tropical-width diagnostics. *Geoscientific Model Development*, **11 (10)**, 4339–4357.

Bellomo, K., M. Angeloni, S. Corti, and J. von Hardenberg, 2021: Future climate change shaped by inter-model differences in Atlantic meridional overturning circulation response. *Nature Communications*, **12 (1)**, 1–10.

Bjerknes, J., 1964: Atlantic air-sea interaction. *Advances in geophysics*, Vol. 10, Elsevier, 1–82.

Brayshaw, D. J., T. Woollings, and M. Vellinga, 2009: Tropical and extratropical responses of the North Atlantic atmospheric circulation to a sustained weakening of the MOC. *Journal of Climate*, **22 (11)**, 3146–3155.

Byrne, B., and C. Goldblatt, 2014: Radiative forcing at high concentrations of well-mixed greenhouse gases. *Geophysical Research Letters*, **41 (1)**, 152–160.

Caballero, R., and P. L. Langen, 2005: The dynamic range of poleward energy transport in an atmospheric general circulation model. *Geophysical Research Letters*, **32 (2)**.

Caesar, L., S. Rahmstorf, A. Robinson, G. Feulner, and V. Saba, 2018: Observed fingerprint of a weakening Atlantic ocean overturning circulation. *Nature*, **556 (7700)**, 191–196.

Ceppi, P., G. Zappa, T. G. Shepherd, and J. M. Gregory, 2018: Fast and slow components of the extratropical atmospheric circulation response to CO_2 forcing. *Journal of Climate*, **31 (3)**, 1091–1105.

Chemke, R., and L. M. Polvani, 2019: Exploiting the abrupt $4\times$ CO_2 scenario to elucidate tropical expansion mechanisms. *Journal of Climate*, **32 (3)**, 859–875.

Chemke, R., L. Zanna, C. Orbe, L. T. Sentman, and L. M. Polvani, 2022: The future intensification of the North Atlantic winter storm track: the key role of dynamic ocean coupling. *Journal of Climate*, **35 (8)**, 2407–2421.

Cheng, W., J. C. Chiang, and D. Zhang, 2013: Atlantic meridional overturning circulation (AMOC) in CMIP5 models: RCP and historical simulations. *Journal of Climate*, **26 (18)**, 7187–7197.

Cronin, T. W., and M. F. Jansen, 2016: Analytic radiative-advective equilibrium as a model for high-latitude climate. *Geophysical Research Letters*, **43 (1)**, 449–457.

Deser, C., and A. S. Phillips, 2009: Atmospheric circulation trends, 1950–2000: The relative roles of sea surface temperature forcing and direct atmospheric radiative forcing. *Journal of Climate*, **22 (2)**, 396–413.

Drijfhout, S., G. J. Van Oldenborgh, and A. Cimatoribus, 2012: Is a decline of AMOC causing the warming hole above the North Atlantic in observed and modeled warming patterns? *Journal of Climate*, **25 (24)**, 8373–8379.

Frierson, D. M., I. M. Held, and P. Zurita-Gotor, 2007: A gray-radiation aquaplanet moist GCM. Part II: Energy transports in altered climates. *Journal of the Atmospheric Sciences*, **64 (5)**, 1680–1693.

Gervais, M., J. Shaman, and Y. Kushnir, 2019: Impacts of the North Atlantic warming hole in future climate projections: Mean atmospheric circulation and the North Atlantic jet. *Journal of Climate*, **32 (10)**, 2673–2689.

Grise, K. M., and L. M. Polvani, 2014: The response of midlatitude jets to increased co2: Distinguishing the roles of sea surface temperature and direct radiative forcing. *Geophysical Research Letters*, **41 (19)**, 6863–6871.

Grise, K. M., and L. M. Polvani, 2016: Is climate sensitivity related to dynamical sensitivity? *Journal of Geophysical Research: Atmospheres*, **121 (10)**, 5159–5176.

Grise, K. M., and L. M. Polvani, 2017: Understanding the time scales of the tropospheric circulation response to abrupt co2 forcing in the southern hemisphere: Seasonality and the role of the stratosphere. *Journal of Climate*, **30 (21)**, 8497–8515.

Haarsma, R., F. Selten, and S. Drijfhout, 2015: Decelerating Atlantic meridional overturning circulation main cause of future west european summer circulation changes. *Environmental Research Letters*, **10 (9)**.

Hausfather, Z., K. Marvel, G. A. Schmidt, J. W. Nielsen-Gammon, and M. Zelinka, 2022: Climate simulations: Recognize the 'hot model'problem. Nature Publishing Group.

Held, I. M., 1993: Large-scale dynamics and global warming. *Bulletin of the American Meteorological Society*, **74 (2)**, 228–242.

Held, I. M., and B. J. Soden, 2006: Robust responses of the hydrological cycle to global warming. *Journal of climate*, **19 (21)**, 5686–5699.

Hoskins, B. J., and P. J. Valdes, 1990: On the existence of storm-tracks. *Journal of Atmospheric Sciences*, **47 (15)**, 1854–1864.

Jackson, L., R. Kahana, T. Graham, M. Ringer, T. Woollings, J. Mecking, and R. Wood, 2015: Global and european climate impacts of a slowdown of the AMOC in a high resolution GCM. *Climate Dynamics*, **45 (11)**, 3299–3316.

James, R., R. Washington, C.-F. Schleussner, J. Rogelj, and D. Conway, 2017: Characterizing half-a-degree difference: a review of methods for identifying regional climate responses to global warming targets. *Wiley Interdisciplinary Reviews: Climate Change*, **8 (2)**, e457.

Josey, S. A., J. J.-M. Hirschi, B. Sinha, A. Duchez, J. P. Grist, and R. Marsh, 2018: The recent Atlantic cold anomaly: Causes, consequences, and related phenomena. *Annual Review of Marine Science*, **10**, 475–501.

Kelley, M., and Coauthors, 2020: GISS-E2. 1: Configurations and climatology. *Journal of Advances in Modeling Earth Systems*, **12 (8)**, e2019MS002 025.

Lachmy, O., and T. Shaw, 2018: Connecting the energy and momentum flux response to climate change using the Eliassen-Palm relation. *Journal of Climate*, **31 (18)**, 7401–7416.

Lau, N.-C., H. Tennekes, and J. M. Wallace, 1978: Maintenance of the momentum flux by transient eddies in the upper troposphere. *Journal of Atmospheric Sciences*, **35 (1)**, 139–147.

Levine, X. J., and T. Schneider, 2011: Response of the Hadley circulation to climate change in an aquaplanet GCM coupled to a simple representation of ocean heat transport. *Journal of the Atmospheric Sciences*, **68 (4)**, 769–783.

Lim, G. H., and J. M. Wallace, 1991: Structure and evolution of baroclinic waves as inferred from regression analysis. *Journal of Atmospheric Sciences*, **48 (15)**, 1718–1732.

Liu, W., A. V. Fedorov, S.-P. Xie, and S. Hu, 2020: Climate impacts of a weakened Atlantic Meridional Overturning Circulation in a warming climate. *Science Advances*, **6 (26)**, eaaz4876.

Lu, J., G. A. Vecchi, and T. Reichler, 2007: Expansion of the Hadley cell under global warming. *Geophysical Research Letters*, **34 (6)**.

Magnusdottir, G., and R. Saravannan, 1999: The response of atmospheric heat transport to zonally-averaged SST trends. *Tellus A: Dynamic Meteorology and Oceanography*, **51 (5)**, 815–832.

Marshall, J., J. R. Scott, K. C. Armour, J.-M. Campin, M. Kelley, and A. Romanou, 2015: The ocean's role in the transient response of climate to abrupt greenhouse gas forcing. *Climate Dynamics*, **44 (7)**, 2287–2299.

Meinshausen, M., and Coauthors, 2020: The shared socio-economic pathway (SSP) greenhouse gas concentrations and their extensions to 2500. *Geoscientific Model Development*, **13 (8)**, 3571–3605.

Menary, M. B., and R. A. Wood, 2018: An anatomy of the projected North Atlantic warming hole in CMIP5 models. *Climate Dynamics*, **50 (7)**, 3063–3080.

Menzel, M. E., D. Waugh, and K. Grise, 2019: Disconnect between Hadley cell and subtropical jet variability and response to increased CO_2. *Geophysical Research Letters*, **46 (12)**, 7045–7053.

Miller, R. L., and Coauthors, 2021: CMIP6 historical simulations (1850–2014) with GISS-E2. 1. *Journal of Advances in Modeling Earth Systems*, **13 (1)**, e2019MS002 034.

Mitevski, I., C. Orbe, R. Chemke, L. Nazarenko, and L. M. Polvani, 2021: Non-monotonic response of the climate system to abrupt CO_2 forcing. *Geophysical Research Letters*, **48 (6)**, e2020GL090 861.

Mitevski, I., L. M. Polvani, and C. Orbe, 2022: Asymmetric warming/cooling response to CO_2 increase/decrease mainly due to non-logarithmic forcing, not feedbacks. *Geophysical Research Letters*, **49 (5)**, e2021GL097 133.

Nazarenko, L. S., and Coauthors, 2022: Future climate change under SSP emission scenarios with GISS-E2. 1. *Journal of Advances in Modeling Earth Systems*, e2021MS002871.

Orbe, C., and Coauthors, 2020: GISS model E2. 2: A climate model optimized for the middle atmosphere—2. Validation of large-scale transport and evaluation of climate response. *Journal of Geophysical Research: Atmospheres*, **125 (24)**, e2020JD033 151.

O'Reilly, C. H., M. Huber, T. Woollings, and L. Zanna, 2016: The signature of low-frequency oceanic forcing in the Atlantic Multidecadal Oscillation. *Geophysical Research Letters*, **43 (6)**, 2810–2818.

Orihuela-Pinto, B., M. H. England, and A. S. Taschetto, 2022: Interbasin and interhemispheric impacts of a collapsed Atlantic Overturning Circulation. *Nature Climate Change*, 1–8.

Outten, S., I. Esau, and O. H. Otterå, 2018: Bjerknes compensation in the CMIP5 climate models. *Journal of Climate*, **31 (21)**, 8745–8760.

Pedro, J. B., M. Jochum, C. Buizert, F. He, S. Barker, and S. O. Rasmussen, 2018: Beyond the bipolar seesaw: Toward a process understanding of interhemispheric coupling. *Quaternary Science Reviews*, **192**, 27–46.

Rahmstorf, S., J. E. Box, G. Feulner, M. E. Mann, A. Robinson, S. Rutherford, and E. J. Schaffernicht, 2015: Exceptional twentieth-century slowdown in Atlantic Ocean overturning circulation. *Nature climate change*, **5 (5)**, 475–480.

Riahi, K., and Coauthors, 2011: RCP 8.5—A scenario of comparatively high greenhouse gas emissions. *Climatic Change*, **109**, 33–57.

Rind, D., G. A. Schmidt, J. Jonas, R. Miller, L. Nazarenko, M. Kelley, and J. Romanski, 2018: Multicentury instability of the Atlantic meridional circulation in rapid warming simulations with GISS ModelE2. *Journal of Geophysical Research: Atmospheres*, **123 (12)**, 6331–6355.

Rind, D., and Coauthors, 2020: GISS Model E2. 2: A climate model optimized for the middle atmosphere—Model structure, climatology, variability, and climate sensitivity. *Journal of Geophysical Research: Atmospheres*, **125 (10)**, e2019JD032 204.

Robson, J., P. Ortega, and R. Sutton, 2016: A reversal of climatic trends in the North Atlantic since 2005. *Nature Geoscience*, **9 (7)**, 513–517.

Romanou, A., and Coauthors, Under Review: Stochastic bifurcation of the North Atlantic circulation under a mid-range future climate scenario with the NASA-GISS ModelE. *Journal of Climate*.

Samset, B., and Coauthors, 2016: Fast and slow precipitation responses to individual climate forcers: A PDRMIP multimodel study. *Geophysical Research Letters*, **43 (6)**, 2782–2791.

Santer, B. D., T. M. Wigley, M. E. Schlesinger, and J. F. Mitchell, 1990: Developing climate scenarios from equilibrium GCM results.

Schmidt, D. F., and K. M. Grise, 2017: The response of local precipitation and sea level pressure to Hadley cell expansion. *Geophysical Research Letters*, **44 (20)**, 10–573.

Schneider, T., 2006: The general circulation of the atmosphere. *Annu. Rev. Earth Planet. Sci.*, **34**, 655–688.

Shaffrey, L., and R. Sutton, 2006: Bjerknes compensation and the decadal variability of the energy transports in a coupled climate model. *Journal of Climate*, **19 (7)**, 1167–1181.

Shaw, T., and A. Voigt, 2015: Tug of war on summertime circulation between radiative forcing and sea surface warming. *Nature Geoscience*, **8 (7)**, 560–566.

Shepherd, T. G., 2014: Atmospheric circulation as a source of uncertainty in climate change projections. *Nature Geoscience*, **7 (10)**, 703–708.

Smith, D. M., R. Eade, N. J. Dunstone, D. Fereday, J. M. Murphy, H. Pohlmann, and A. A. Scaife, 2010: Skilful multi-year predictions of Atlantic hurricane frequency. *Nature Geoscience*, **3 (12)**, 846–849.

Tebaldi, C., and J. M. Arblaster, 2014: Pattern scaling: Its strengths and limitations, and an update on the latest model simulations. *Climatic Change*, **122 (3)**, 459–471.

Thompson, D. W., and T. Birner, 2012: On the linkages between the tropospheric isentropic slope and eddy fluxes of heat during Northern Hemisphere winter. *Journal of the Atmospheric Sciences*, **69 (6)**, 1811–1823.

Timmermann, A., and Coauthors, 2007: The influence of a weakening of the Atlantic meridional overturning circulation on ENSO. *Journal of Climate*, **20 (19)**, 4899–4919.

Vallis, G. K., P. Zurita-Gotor, C. Cairns, and J. Kidston, 2015: Response of the large-scale structure of the atmosphere to global warming. *Quarterly Journal of the Royal Meteorological Society*, **141 (690)**, 1479–1501.

Vellinga, M., and R. A. Wood, 2008: Impacts of thermohaline circulation shutdown in the twenty-first century. *Climatic Change*, **91 (1)**, 43–63.

Vial, J., C. Cassou, F. Codron, S. Bony, and Y. Ruprich-Robert, 2018: Influence of the Atlantic meridional overturning circulation on the tropical climate response to CO_2 forcing. *Geophysical Research Letters*, **45 (16)**, 8519–8528.

Waugh, D. W., and Coauthors, 2018: Revisiting the relationship among metrics of tropical expansion. *Journal of Climate*, **31 (18)**, 7565–7581.

Weijer, W., W. Cheng, O. A. Garuba, A. Hu, and B. Nadiga, 2020: CMIP6 models predict significant 21st century decline of the Atlantic meridional overturning circulation. *Geophysical Research Letters*, **47 (12)**, e2019GL086 075.

Woollings, T., J. M. Gregory, J. G. Pinto, M. Reyers, and D. J. Brayshaw, 2012: Response of the North Atlantic storm track to climate change shaped by ocean–atmosphere coupling. *Nature Geoscience*, **5 (5)**, 313–317.

Wu, L., C. Li, C. Yang, and S.-P. Xie, 2008: Global teleconnections in response to a shutdown of the Atlantic meridional overturning circulation. *Journal of Climate*, **21 (12)**, 3002–3019.

Zappa, G., and T. G. Shepherd, 2017: Storylines of atmospheric circulation change for european regional climate impact assessment. *Journal of Climate*, **30 (16)**, 6561–6577.

Zhang, R., and T. L. Delworth, 2005: Simulated tropical response to a substantial weakening of the Atlantic thermohaline circulation. *Journal of Climate*, **18 (12)**, 1853–1860.

Zhang, R., and T. L. Delworth, 2006: Impact of Atlantic multidecadal oscillations on India/Sahel rainfall and Atlantic hurricanes. *Geophysical Research Letters*, **33 (17)**.

Zhang, R., S. M. Kang, and I. M. Held, 2010: Sensitivity of climate change induced by the weakening of the Atlantic meridional overturning circulation to cloud feedback. *Journal of Climate*, **23 (2)**, 378–389.